Title
A LOW FREQUENCY ELECTROMAGNETIC PROSPECTING SYSTEM

Author
Jain, B.K.

Publication Date
1978-04-01

LBL-7042

A LOW FREQUENCY ELECTROMAGNETIC PROSPECTING SYSTEM

Birendra Kumar Jain
(Ph. D. thesis)

April 1978

Prepared for the U. S. Department of Energy
under Contract W-7405-ENG-48

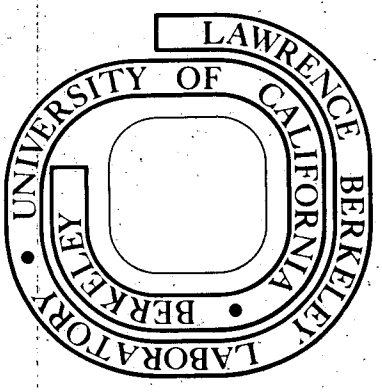

LBL-7042

DISCLAIMER

A Low Frequency Electromagnetic Prospecting System

By

Birendra Kumar Jain

Lawrence Berkeley Laboratory
University of California
Berkeley, California 94720

Work performed under the auspices of the U.S. Department of Energy.

ABSTRACT

A prototype portable electromagnetic sounding system was assembled and depth sounding survey was conducted in Grass Valley, Nevada, as a part of a program to evaluate geophysical techniques in geothermal exploration. A horizontal loop transmitter of radius 50 meters operating between .01 Hz and 100 Hz was used in conjunction with a SQUID magnetometer. A digital synchronous detector was used for on site processing of magnetometer output. This detector allowed useful data acquisition with transmitter-receiver separation of up to 2 km with power requirements of less than 72 watts.

Conductive sediments (1-10 ohm-m) of thicknesses of up to 1.5 km were well resolved with this system and the interpreted sections compared very well with d.c. resistivity measurements made with much heavier equipment and larger arrays in the same area.

This work is dedicated
to my wife,
Lata.

ACKNOWLEDGEMENTS

The work herein reported has been supported by the U.S. Energy Research and Development Adminstration through the University of California - Lawrence Berkeley Laboratory. I sincerely wish to express my gratitude to Prof. H. F. Morrison and Dr. A. Dey for their valuable guidance leading to the conclusion of this work.

TABLE OF CONTENTS

INTRODUCTION

In 1973 the University of California at Berkeley and the Lawrence Berkeley Laboratory jointly undertook a program for the assessment of geothermal reservoirs. This program had three main goals:

1) To evaluate, on the basis of detailed geological, geochemical and geophysical data, the geothermal reservoirs in the mid Basin and Range Geologic province.
2) To compare and evaluate geophysical techniques used in the exploration and delineation of these reservoirs.
3) To develop the new techniques and instrumentation that are specifically required for deep penetration in geothermal investigations.

The work discussed in this dissertation concerns the application of a controlled source frequency domain electromagnetic method for determining the subsurface electrical conductivity. The application of any geophysical method, other than thermal, in geothermal exploration is based on the fact that the physical properties of the rock being measured are affected to some degree by an increase in temperature (Birch and Clarke, 1940; Birch, 1943; Hochstein and Hunt, 1970; Murase and McBirney, 1973; Spencer and Nur, 1976). The increase in the electrical conductivity of wet porous rocks with temperature is the basis of the application of electrical and electromagnetic methods for subsurface resistivity mapping in geothermal exploration. It must be borne in mind that the variation in electrical conductivity may be due to changes in porosity or salinity rather than the temperature and

there is no unique relationship between the temperature and the indirectly obtained electrical conductivity of the subsurface. Any inference made about the existence of a geothermal reservoir must, therefore, include other geological or geophysical data.

Subsurface conductivity distribution can be mapped by natural source methods (e.g. tellurics, or magnetotellurics) or controlled source methods (e.g. direct current resistivity, loop source electromagnetic methods). Application of natural source methods in geothermal exploration has been the subject of study of many authors (Beyer, 1977; Beyer et al., 1975; Combs and Wilt, 1975; Cormy and Muse, 1975; Hermance et al., 1975; Hoover and Long, 1975; Whiteford, 1975). Such methods have the advantage of requiring no artificial "source," which reduces the field logistics considerably. However, the telluric method has been proved only to be a qualitative tool (Beyer, 1977) and the magnetotelluric method suffers from the fact that a large scatter in the measured data is generally observed, this resulting in the degradation of the model resolution (Ward, 1977).

Amongst the controlled source methods, direct current resistivity methods have been most widely used in geothermal exploration (Beyer, 1977; Beyer et al., 1975; Garcia, 1975; Gupta et al., 1975; Hochstein, 1975; Jiracek et al., 1975; Keller et al., 1975). A severe practical problem in the use of such a method, however, is that large transmitter-receiver separations are needed to achieve deep penetration. Beyer (1977) reports using a spacing of up to 10 km in order to map a conductive basin of a thickness of the order of 1 km in his dipole-dipole survey in Grass Valley, Nevada. The use of such large separations not only requires a large power supply, but also makes

data interpretation extremely difficult because of the presence of lateral inhomogeneities. Moreover, these direct current electrical methods are impractical in areas where it is difficult to inject current into the ground because of a highly resistive surface layer.

Another controlled source method of mapping subsurface resistivity, the electromagnetic method, has been used to a limited extent in geothermal exploration and is the subject of discussion in this dissertation. Applications of this method have been reported by Keller and Rapolla (1976), Harthill (1976), Jackson and Keller (1973), Ghosh and Hallof (1973), and Keller (1970). Electromagnetic methods have a fundamental advantage over the direct current resistivity methods. In the direct current resistivity techniques the depth of exploration is controlled only by the separation between the transmitter and receiver; in electromagnetic methods the depth of exploration is controlled both by the frequency of the source current and the separation between transmitter and receiver. It is therefore possible to probe the ground to a comparable depth with transmitter-receiver separations which are considerably shorter than those possible in a direct current resistivity survey. Another advantage of the electromagnetic method is that by employing a loop source to energize the ground and by measuring only magnetic fields, direct contacts with the ground are eliminated. These contacts often cause problems in direct current resistivity surveys.

Despite the many advantages of electromagnetic methods over direct current resistivity techniques, electromagnetic methods have been less extensively used in geothermal exploration, mainly because of the unavailability of lightweight, easily deployable field equipment

necessary in such a survey, and also due to the fact that the techniques of interpretation of electromagnetic data are comparatively less developed and more complex than those of direct current resistivity methods. However, because of recent advances in the design of low-powered digital data processing units and with the availability of highly sensitive magnetic field sensors, attention has been focussed on designing and developing a lightweight, efficient,electromagnetic system, which then could play its much needed role in geothermal exploration.

A frequency domain electromagnetic sounding system has been designed and built which operates in a frequency band of .01 Hz to 100 Hz and has been successfully tested in a potential geothermal area. Conductive sediments (2-10 ohm-m) of thicknesses of up to 1.5 km were well resolved with this system and the interpreted structure compared very well with d.c. resistivity measurements made with much heavier equipment and larger arrays in the same area.

The system consists of a multiturn horizontal current loop as the transmitter and a 3-axis Josephson-effect superconducting magnetometer as the receiver. A phase sensitive digital synchronous signal averager processes the signal, real time, on location and provides the necessary phase and amplitude information. The increased sensitivity of the superconducting magnetometer over the conventional induction coil receivers (100 times more sensitive at 10^{-2} Hz) and synchronous stacking of the signal by the digital signal averager, resulted in a significant improvement in the signal to noise ratio of the measured magnetic field and this in turn allowed the use of much larger transmitter-receiver separations with a relatively smaller power

source than would have been possible using a conventional receiver.

The equipment was assembled during 1975-76 and field measurements were made in the summer of 1976. The design aspects of the electromagnetic sounding system and its application in mapping resistivity structures are described in this dissertation.

Since the theory of horizontal loop electromagnetic sounding has been thoroughly discussed before (e.g. Wait, 1962; Grant and West, 1965, Keller and Frischknecht, 1966; Ward, 1967; Ryu et al., 1970), it will not be presented here. In Chapter I, the design criteria of a loop transmitter will be discussed. In Chapter II, the description of the electromagnetic sounding system as built will be given and the result of the sounding survey in Grass Valley, Nevada, will be discussed.

CHAPTER I

DESIGN OF AN ELECTROMAGNETIC TRANSMITTER

1. Introduction

The application of electromagnetic sounding techniques for geothermal surveys has the requirement that a depth conductivity profile of up to 5-10 km of the upper crust of the earth's surface be obtained. To achieve this depth of penetration, a source-receiver separation of up to 10-20 km would be necessary. Since the strength of the signal at the receiver is directly proportional to the dipole moment M of the transmitter coil (M = NIA, where N is the number of turns, I is the r.m.s. current, and A is the area of the transmitter coil) M has to be made sufficiently large for the signals to be detectable at the receiver site. As M depends upon the coil geometry and the power supply, a careful analysis of these parameters is necessary for an optimum design of the transmitter.

In geophysical literature, design formulas for electromagnetic sensing coils have been given before (e.g. Becker, 1967) but design formulas for transmitter coils have never appeared. The purpose of this chapter of the thesis is to fill this gap, and provide charts for rapid calculation of all of the parameters involved in designing an electromagnetic transmitter.

2. Design Considerations

The questions to be answered in designing an electromagnetic transmitter of moment M are:

a) What should be the radius of the transmitter loop?

b) How many turns should be used?

c) What should be the size of the wire?

d) How much power is needed?

Another important parameter to be considered in the design of the transmitter is the effect of the self-inductance of the loop on the transmitter performance. The total load, as seen from the power-supply source, consists of a resistive ohmic load, due to the ohmic resistance of the loop, and a reactive load, due to the inductance of the loop. This is given as the vector sum of the two loads. Since the reactive part of the load depends upon the frequency of the current, the total load increases with increases in frequency, and this results in a lowering of the current in the transmitter loop, which in effect reduces the moment M. This apparent loss of power can be offset by series tuning the coil with a capacitor but this would only be practicable with the availability of suitable capacitors. Additionally, high reactive voltages are developed across the coil, and this could be a limiting factor in operating the coil beyond a certain frequency. The power supply for driving the coil must, therefore, be selected with the above considerations in mind.

The requirements for an optimum design, then, would be to

a) minimize the weight of the loop

b) minimize the inductance of the loop

c) minimize the power supply

d) minimize the radius of the loop

3. Design Parameters

i) Weight of transmitter coil:

The weight, W, of the transmitter coil (neglecting the weight of the insulation material) is given as

$$W = N \times 2\pi a \times \pi r^2 \times D \text{ kg} \qquad \text{(I-1)}$$

where

N = number of turns in the coil

a = radius of coil in meters

r = radius of the wire in meters, and

D = density of the wire material in kg/m^3.

ii) Ohmic power supply:

The power, P, needed to drive the coil is given as

$$P = I^2R \text{ watts} \qquad \text{(I-2)}$$

where I is r.m.s. current in amperes, and R is ohmic resistance of the coil in ohms. Expressing R in terms of parameters of the coil, P could be written as

$$P = I^2 \times \frac{2NA\rho}{r^2} \text{ watts} \qquad \text{(I-3)}$$

where ρ = resistivity of the wire in ohm-meters. Eliminating I, equation (I-3) could be modified as

$$P = \frac{2M^2\rho}{\pi^2 r^2 a^3 N} \text{ watts} \qquad \text{(I-4)}$$

where M is the dipole moment of the transmitter.

iii) Inductance of the transmitter coil:

The inductance, L, of a circular coil (Terman, 1943, p. 63) is given approximately as

$$L = 1.256 \times 10^{-6}\, aN^2 \left(2.303 \log_{10} \frac{8a}{\sqrt{N}r} - 1.75\right) \text{ henries} \quad \text{(I-5)}$$

4. Optimum Transmitter Design

The most important parameters in designing an electromagnetic transmitter are the weight of the coil and the power of the current supply. Both of these quantities should be selected with the goal of easy field portability. Instead of treating them separately, it is advantageous to study the weight-power product as a new design parameter. This quantity may be directly obtained from equations (I-1) and (I-4) to read:

$$W \times P = \frac{4M^2 D\rho}{a^2} \text{ kg-watts} \quad \text{(I-6)}$$

This is an important relation, as it dictates the necessary power requirement for a given weight of the coil or vice versa for a desired M/R ratio. Taking the values of density, D, and resistivity, ρ, of copper as 8.90×10^3 kg/meter^3 and 1.724×10^{-8} ohm-meters respectively (Handbook of Chemistry and Physics, 47th edition, p. F-110), the product of D and ρ for copper wire is 1.5326×10^{-4}. For aluminum wire, it is 0.7551×10^{-4}. Thus the choice of aluminum wire over copper wire would result in halving the value of WP. This is an important factor to consider in designing a rigid transmitter coil. But for transporting the coil in the field, a flexible transmitter coil would be more appropriate. The greater tendency of aluminum to become brittle upon repeated bending makes the use of this metal prohibitive in such a case. In our design, copper wire would be preferred and therefore equation

(I-6) becomes:

$$W \times P = 6.137 \times 10^{-4} \times \frac{M^2}{a^2} \quad \text{kg-watts} \qquad \text{(I-7)}$$

From the above relation, we can conclude that the single most important parameter design is the coil radius. The larger the radius of coil selected, the smaller will be the product WP needed for the same dipole moment M. However, the maximum possible value of the radius is governed by field logistics considerations.

Once the radius of the loop has been selected, the only other variable remaining to be fixed is N or I. Selection of a small or large N dictates a small or large value of the inductance of the transmitter coil, as is seen from equation (I-5). However, it is important to note that the reactive power in the coil at a particular frequency is independent of the manner in which N or I is chosen for a given coil radius 'a' and dipole moment 'M'. It is only the reactive voltage across the coil which is governed by the selection of a small or large I (correspondingly a large or small N). The expressions for the reactive power, P', and the reactive voltage V', across the coil, are given as

$$P' = I^2 \times \omega \times L \quad \text{VAR} \qquad \text{(I-8)}$$

$$V' = I \times \omega \times L \quad \text{volts} \qquad \text{(I-9)}$$

where ω is the angular frequency.

Substituting the expressions for L from equation (I-5) and rearranging the terms, we get

$$P' = 1.256 \times 10^{-6} \frac{M^2 \omega}{\pi^2 a^3} \left(2.303 \log_{10} \frac{8a}{\sqrt{N}\, r} - 1.75\right) \text{VAR} \qquad \text{(I-10)}$$

$$V' = 1.256 \times 10^{-6} \frac{M^2 \omega}{I \pi^2 a^3} \left(2.303 \log_{10} \frac{8a}{\sqrt{N}\, r} - 1.75\right) \text{volts} \qquad \text{(I-11)}$$

From the above two expressions, it is clear that, in order to minimize P' and V', a large radius loop should be selected. This same consideration was arrived at earlier when we were considering design parameters for W and P. Another conclusion to be drawn from equation (II-11) is that the value of current I should be selected as maximum (thus, a minimum number of turns) in order that the reactive voltage across the coil be kept to a minimum. An excessive reactive voltage could cause the insulation breakdown of the coil wire and also could cause damage to the power-supply driving the loop. A proper selection of maximum tolerable voltage is therefore an important criterion in the transmitter design and dictates up to what maximum frequency a transmitter could be operated for a desired moment M under the constraint of a maximum permissible loop radius, a.

In conclusion, the design of the electromagnetic loop transmitter of moment M should proceed as follows:

a) select the radius 'a' of loop as large as is practical.

b) select the weight W of the coil as heavy as is practical.

c) calculate the minimum necessary power (considering ohmic losses only) required to drive the coil from equation (I-7).

d) Select the maximum value of current, I, which could be safely

delivered from the power-supply source. The resistance, R, of the coil then could be found from equation $P = I^2R$. Nearest wire size conforming to the resistance R and weight W of the coil then could be found from a reference table or from the chart provided later in this chapter.

e) N is then computed from equation M = NIA.

f) Inductance of such a coil could then be found from equation (I-5).

5. Transmitter Design Chart

In the above discussions, expressions had been presented regarding the various parameters involved in an electromagnetic transmitter design. For rapid evaluations of different designs, charts have been prepared to facilitate the selection of different parameters, and also to evaluate the effect of inductance in design considerations. The following is a list of the various charts:

a) Weight-power calculation chart (Figure I-1)

b) Number of turns-current calculation chart (Figure I-2)

c) Ohmic power calculation chart (Figure I-3)

d) Wire size calculation chart (Figure I-4)

e) Inductance calculation chart (Figure I-5)

f) Reactance calculation chart (Figure I-6)

g) Tuning capacitance calculation chart (Figure I-7)

The use of these charts is explained in the following design example.

6. Design Example

It is required to design a transmitter to operate in a frequency band of .01 Hz to 1000 Hz with a moment of 10^6 M.K.S.A. units.

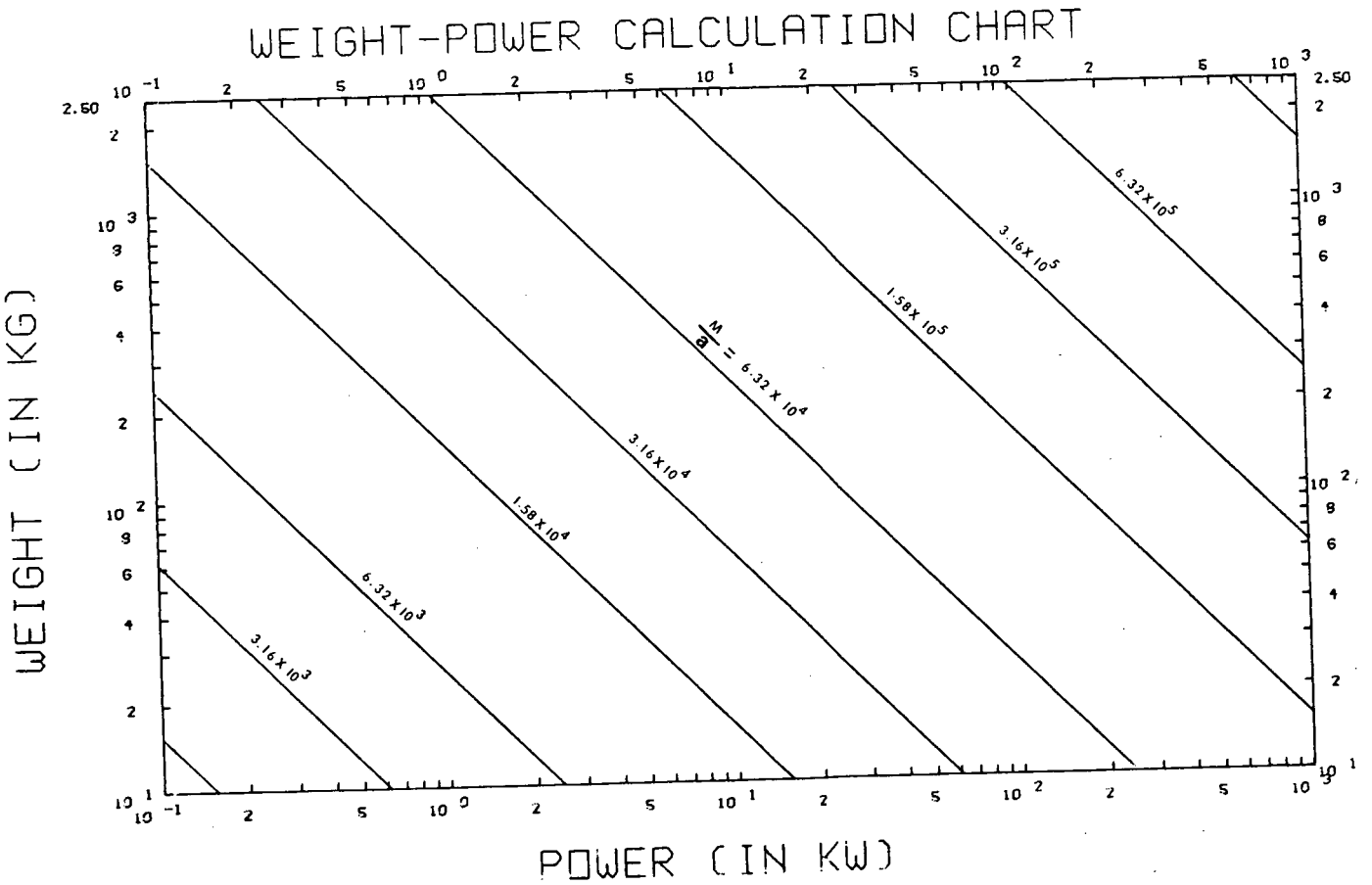

Figure I-1. Weight - Power calculation chart.

XBL 784-8051

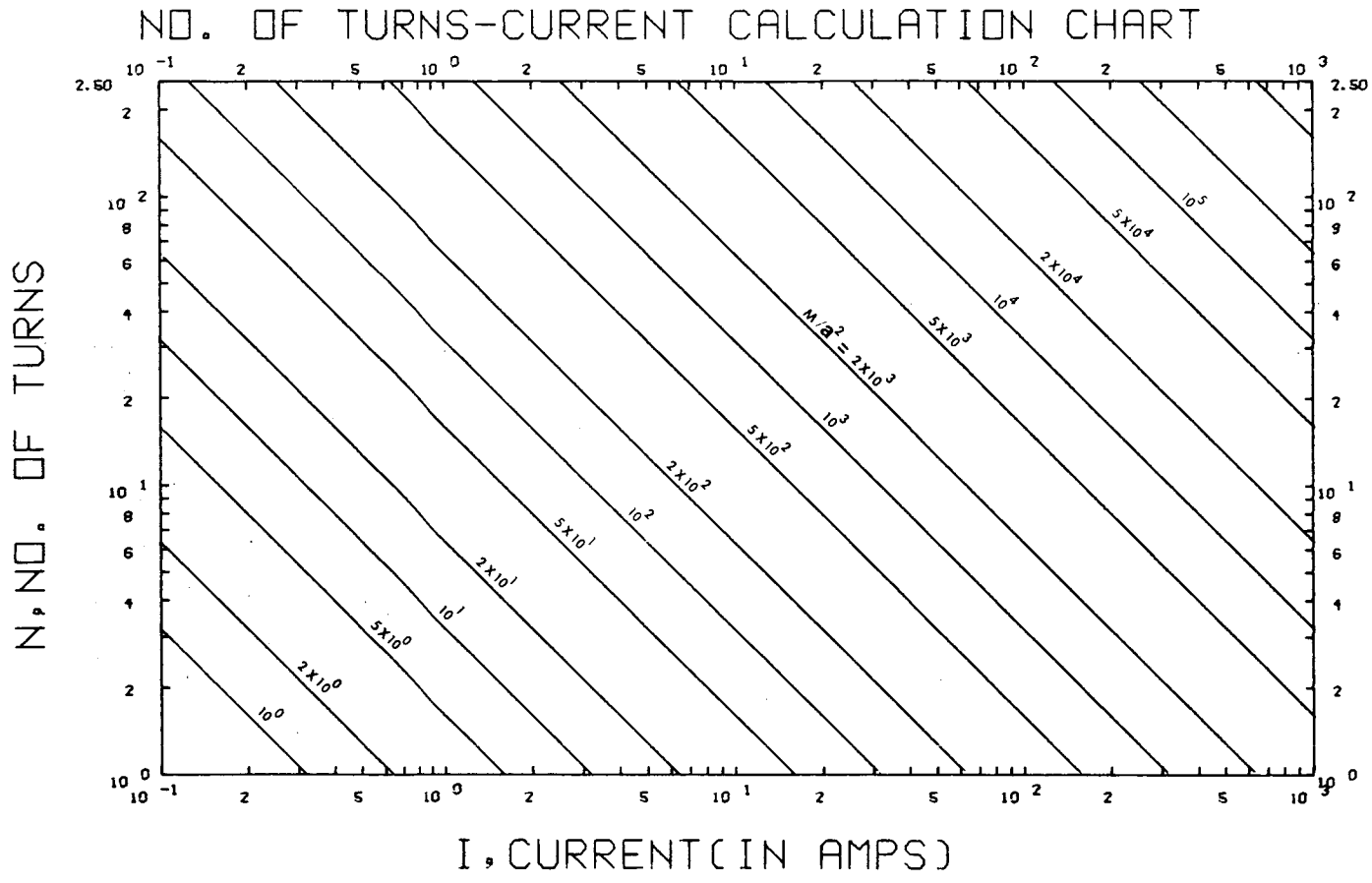

Figure I-2. Number of Turns - Current calculation chart.

XBL 784-8050

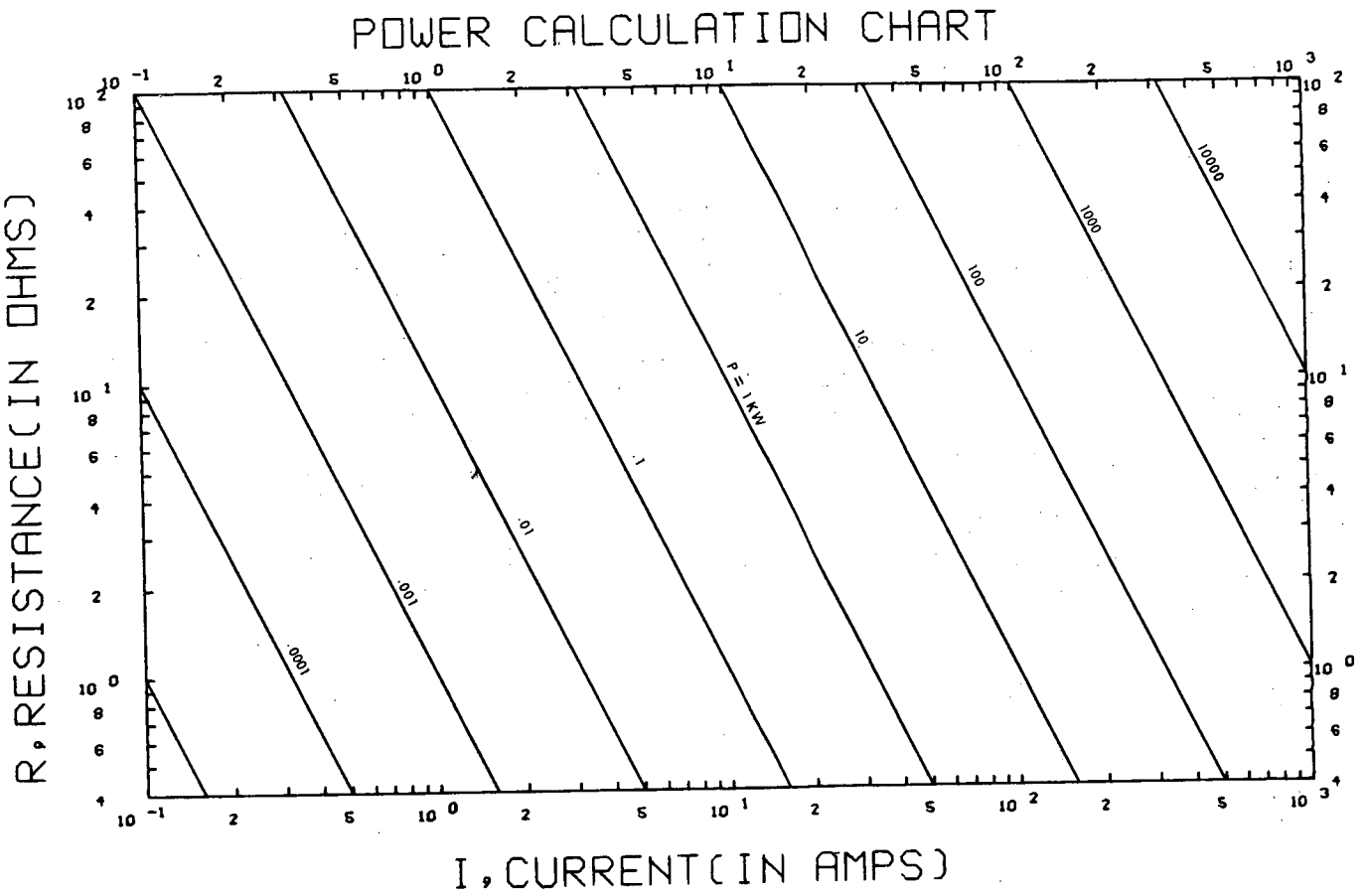

Figure I-3. Power calculation chart

XBL 784-8057

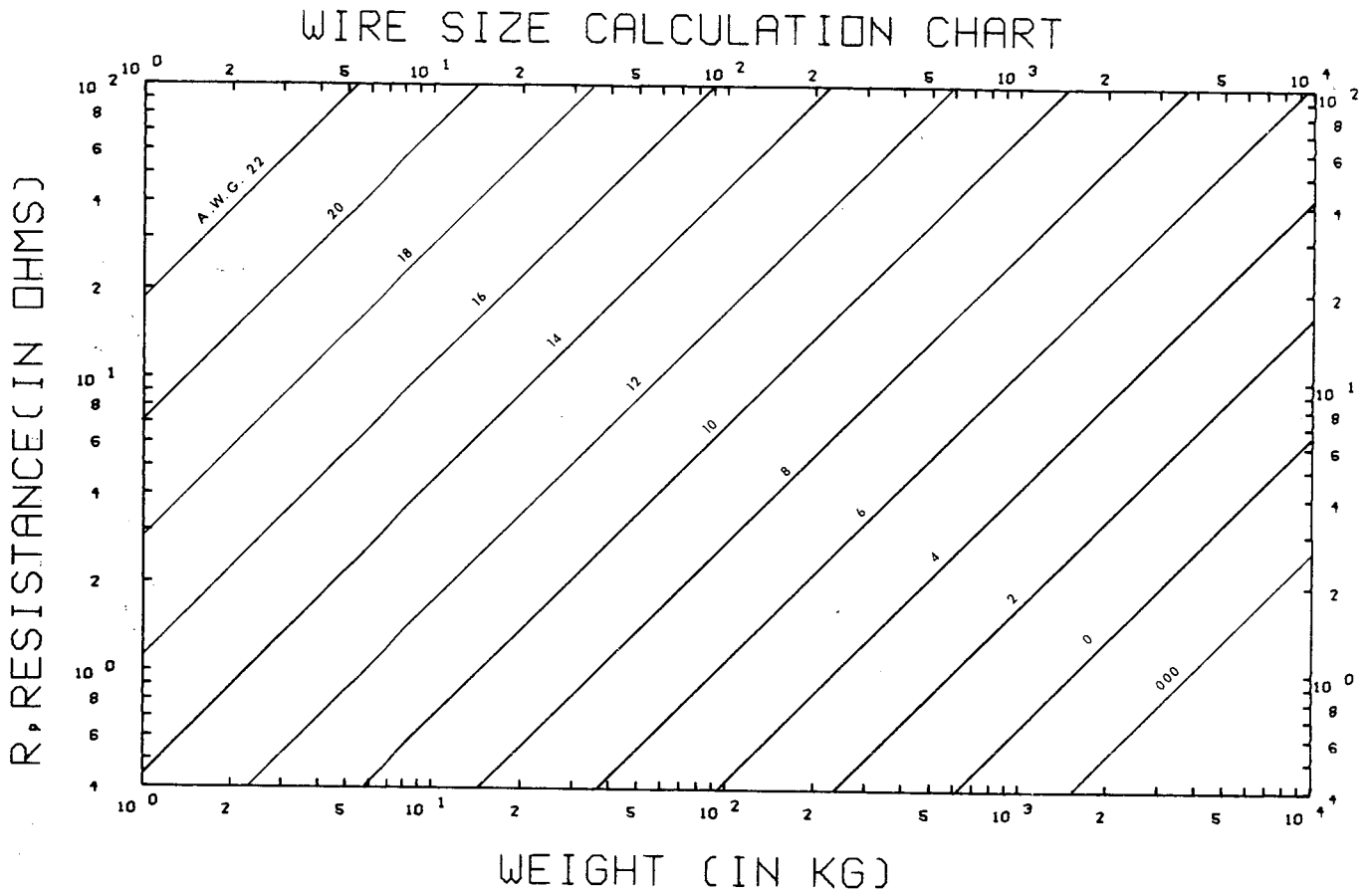

Figure I-4. Wire Size calculation chart.

XBL 784-8049

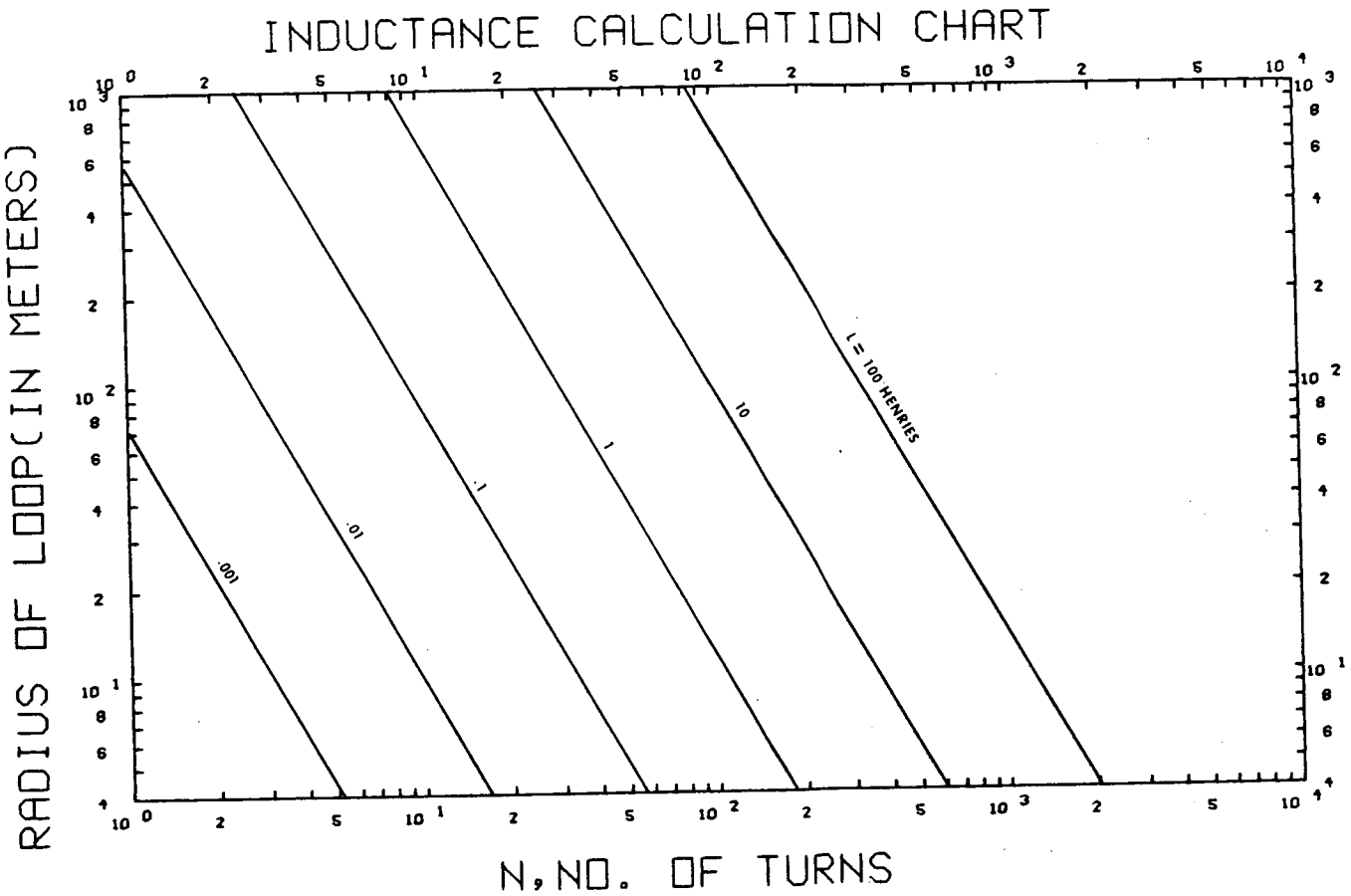

Figure I-5. Inductance calculation chart.

XBL 784-8030

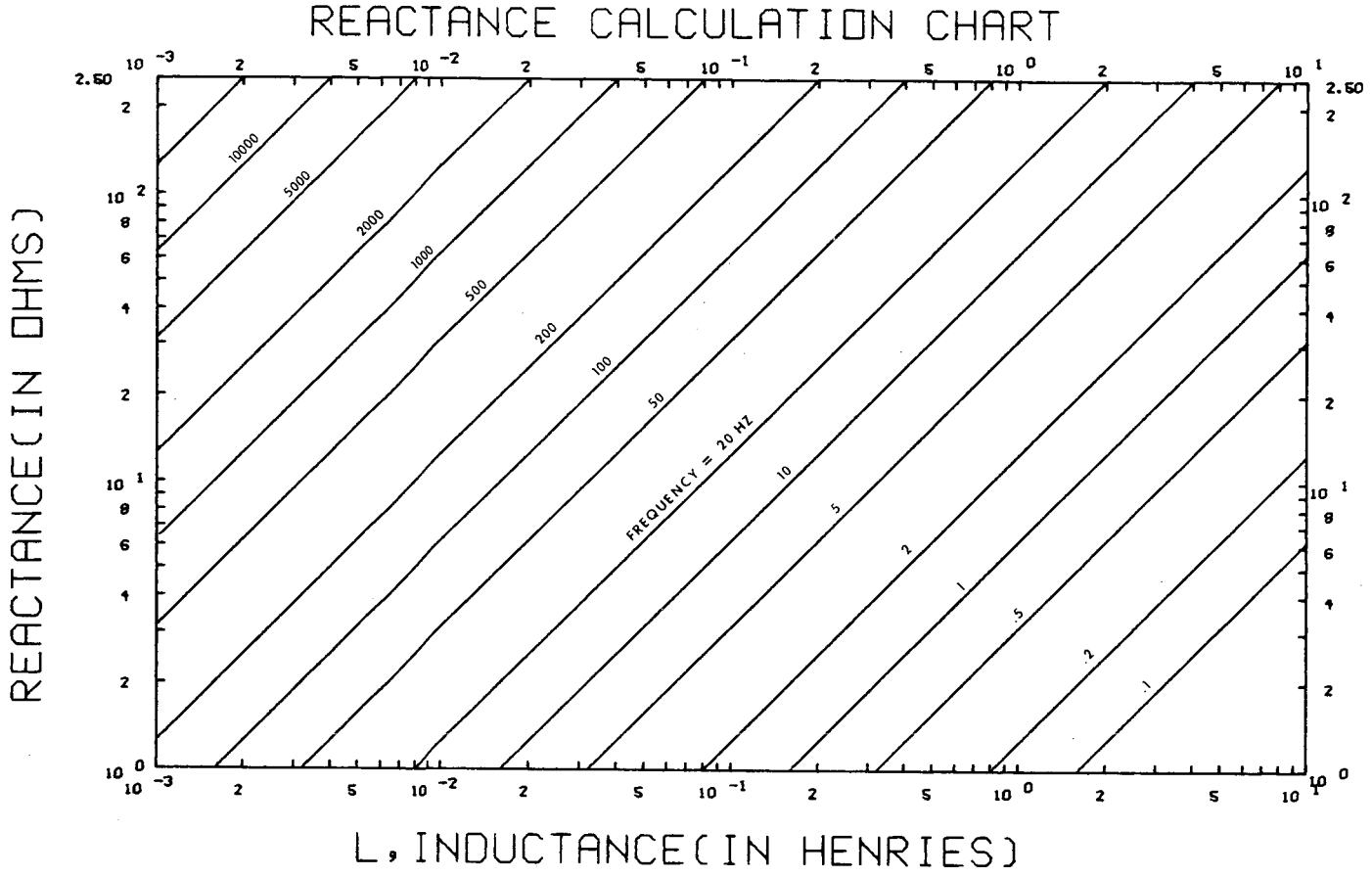

Figure I-6. Reactance calculation chart.

XBL 784-8052

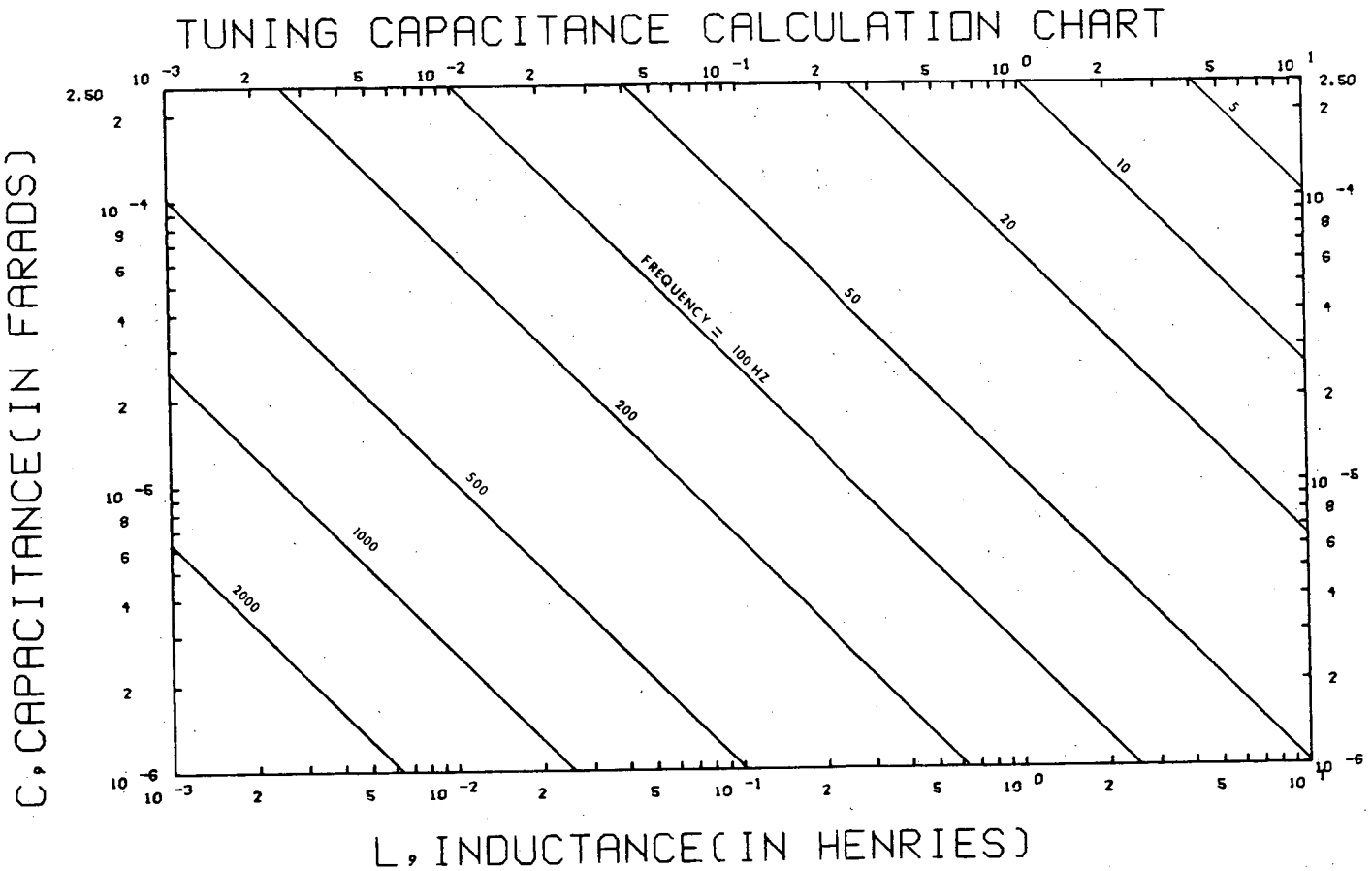

Figure I-7. Tuning Capacitance calculation chart.

XBL 784-8055

From field considerations, the radius of the loop is selected to be 50 meters and the weight of the coil is taken to be 100 kg. In the following, then, we will calculate the other design parameters.

From Figure I-1, noting that $M/a = 2 \times 10^4$ and W = 100 kg, we get P = 2.5 KW. Suppose the available power-supply source has a maximum current rating of 25 amps, then the resistance of the coil should be 4 ohms. For this particular resistance and weight of the loop, the nearest wire size is found to be that of A.W.G. #9 wire from Figure I-4 and total number of turns in the loop, noting that $M/a^2 = 400$, would be 5 from Figure I-2. Figure I-5 is an approximate inductance calculation chart, and is plotted for A.W.G. #4 wire. From this chart, we find the inductance of the designed loop to be approximately 15 mhenry.

To sum up, then, the various parameters of the designed transmitter are:

a = 50 meters

w = 100 kg

P = 2.5 KW

N = 5 turns

I = 25 amps

R = 4 ohms

L = 15 mh

wire size = A.W.G. # 9

7. Design of a power supply source

In order to attain a moment of the order of 10^6 M.K.S. units, total power dissipation in the coil, was noted to be of the order of 2.5 KWatts in the previous design example. Assuming that different coil parameters may have to be selected in view of differing field conditions and also to accommodate even higher moment, the power of the current supply source should ideally be of the order of 5 to 10 KVA. A linear power amplifier, which would be an ideal power source, is not available in this range since the heat dissipation becomes enormous at the low frequency range. So, a most practical design of a power source for such an application would be a switching bridge (Figure I-8a), which alternately connects the load to two d.c. power supply sources (of opposite polarity) producing a bipolar square wave. The design of such a bridge is considered here. Moreover, driving the loop with a square wave source rather than a sine wave source would offer the following advantages:

a) The transmitter controller design is obviously simpler for square waves than for sine waves.

b) A signal processor, such as a cross-correlator, can readily recover the fundamental component and higher harmonics so that the possibility for measuring more than one frequency at a time exists.

c) Given a certain maximum value of current (typical limitation of power supply) the component of the fundamental in a square wave is 1.27 times the fundamental in a sine wave.

The large power sources used in d.c. resistivity surveys are also basically switching power supplies. These designs use SCRs to control the switching, since up till now these were the only

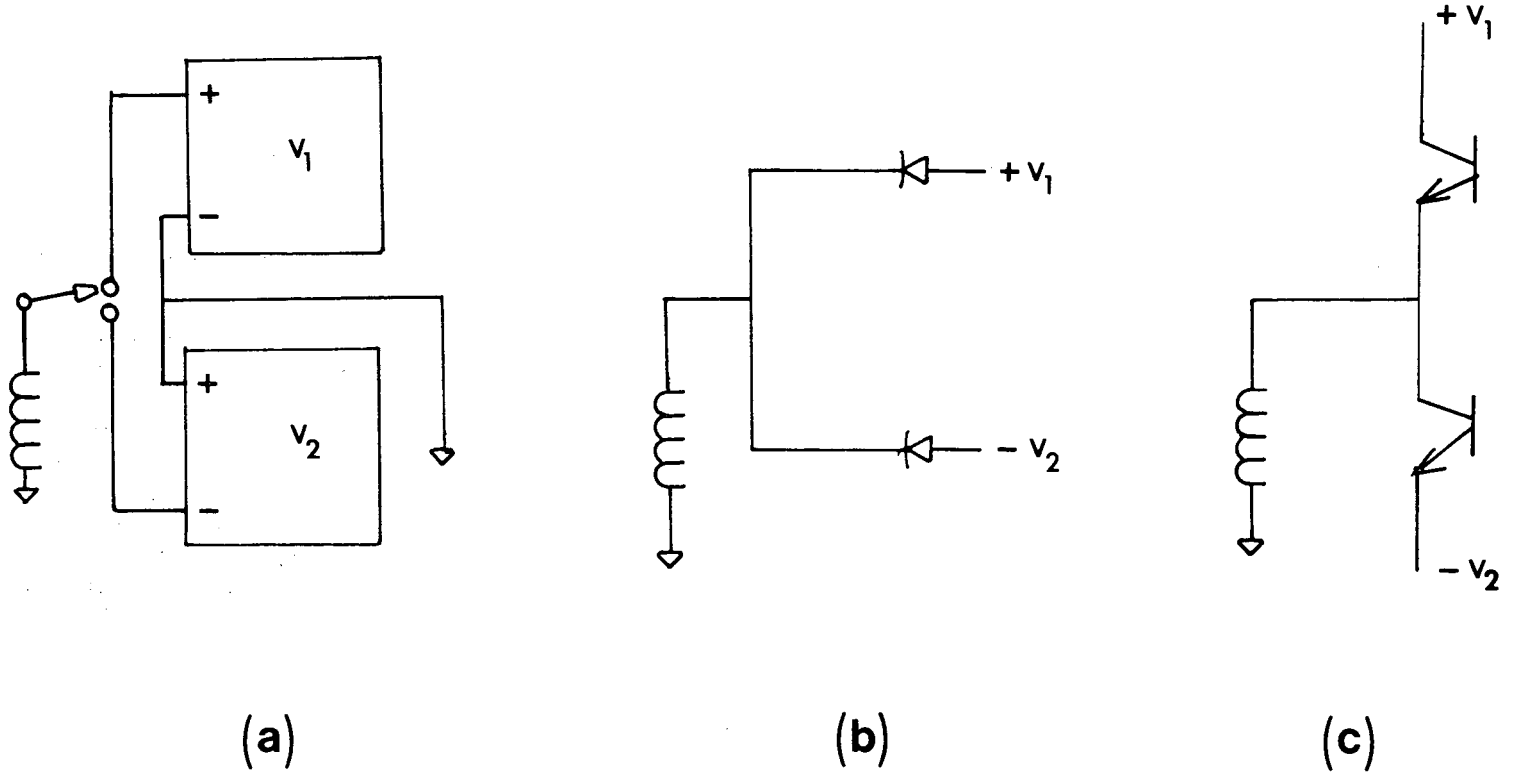

Figure I-8. Schematic of Switching Bridge.

devices available which could handle large currents. The characteristics of SCRs, however, make such power supplies unsuitable in driving the loop transmitter, especially at high frequencies, because of the inductive nature of the load. The phase reversal in a SCR controlled switching is accomplished (Figure I-8b) by turning 'off' one SCR which was conducting during the positive half cycle and then turning 'on' the other SCR which then conducts during the negative half cycle and thus a bipolar square wave is obtained. However, before one SCR is turned on, the other SCR must have stopped conducting, otherwise damage to the SCR would result. One of the properties of SCRs is that they would be turned on instantly by applying a gate control signal, but they could not be turned off until the current in the circuit has dropped to zero. In an inductive load, the current is maintained even after the applied voltage has been taken off because of the stored magnetic energy, and the time this current takes to decay is dependent on the L/R time constant of the circuit. Hence, a finite amount of dead time is required between the phase reversal of the current using a SCR switch. This dead time could be reduced somewhat by appropriately designing the circuit, but could not be eliminated altogether. Thus, an SCR controlled power supply could only be successful in driving the loop at rather low frequencies.

A solution to the problem is to use transistors to accomplish the switching as described in Figure I-8c. Unlike SCRs, transistors could be turned 'on' and 'off' by control signals, thus a switching frequency in excess of 1 KHz could be obtained. High power

transistors are now available to be used in the design of a 10 KW or larger power source to drive transmitting loops. Such a transmitter is currently being developed at the Lawrence Berkeley Laboratory for a second generation electromagnetic system.

CHAPTER II

ELECTROMAGNETIC DEPTH SOUNDING IN GRASS VALLEY, NEVADA

1. Introduction

The objective of this study was to investigate the capability of an active source electromagnetic sounding system using a horizontal current loop in defining the subsurface resistivity distribution in a geothermal area. A prototype electromagnetic sounding system has been built and electromagnetic soundings have been carried out at Grass Valley, Nevada. The results of this survey are presented and discussed in this chapter. The Grass Valley area was chosen for the study, since extensive geological and geophysical data for this area are available from investigations by the University of California, Berkeley, and the Lawrence Berkeley Laboratory. A detailed summary of the investigation of the UCB-LBL joint project has been given by Beyer et al. (1976).

2. Geology of Grass Valley

Grass Valley (Leach Hot Springs) is located in northcentral Nevada, and lies within an area of higher than normal heat flow, the Battle Mountain high heat flow area (Sass et al., 1971) as shown on Figure II-1. Beyer et al. (1976) have given the following account of the geological setting of Grass Valley area:

> The Leach Hot Springs area is located in Grass Valley, Nevada approximately 50 km south of Winnemucca. The Sonoma and Tobin Ranges bound the valley on the east, while the valley is constricted south of the hot springs by the Goldbanks Hills, locus of earlier mercury mining. Grass Valley is bounded on the west by the basalt-capped East Range. The distribution of major lithologic units in the region is illustrated on the geologic map (Figure II-2) and their stratigraphic relationships on the cross section (Figure II-3). The intrictate fault and lineament pattern, based strongly on photo interpretation (Noble, 1975) is shown on a seperate map, (Figure II-4). Paleozoic siliceous clastic rocks and greenstones are the oldest bedrock types in the region. In places in the Sonoma and Tobin Ranges, the Paleozoics are in thrustfault contact with Triassic siliceous clastic and carbonate rocks. The Paleozoic and Triassic rocks have been intruded by granitic rocks of probable Triassic age in the Goldbands Hills; elsewhere the granitics are probably of Cretaceous age. Though not exposed in the Leach Hot Springs area, Oligocene-Miocene rhyolitic tuffaceous rocks are probably present in the subsurface. They are overlain by a sequence of interbedded sandstone, fresh water limestone and altered tuffs, which are in turn over-lain by coarser conglomeratic sediments (fanglomerates) derived from mountain range fronts steepened by the onset of basin and range faulting. The fanglomerates are opalized in places by siliceous hydrothermal activity associated with fault zones; occasionally the locus of mercury mineralization. Opalization of mercury deposits in the Goldbanks hills and East Range closely resembles the opalized sinter at Leach Hot Springs. The Tertiary sedimentary sequence is overcapped by predominantly basaltic volcanic rocks whose ages, dated by the potassium-argon method, range from 14.5 to 11.5 million years.
>
> Characteristic of the hot spring systems observed in northern Nevada, Leach Hot Springs is located on a fault, strongly expressed by a 10 to 15 m high scrap trending NE. Normal faulting since mid-Tertiary has offset rock units vertically several tens to several hundred meters (idealized cross section, Figure II-3). As shown on the fault and lineament map (Figure II-4) the present-day hot springs occur at the zone of intersection of the NE trending fault and the NNW-SSE trending lineaments.

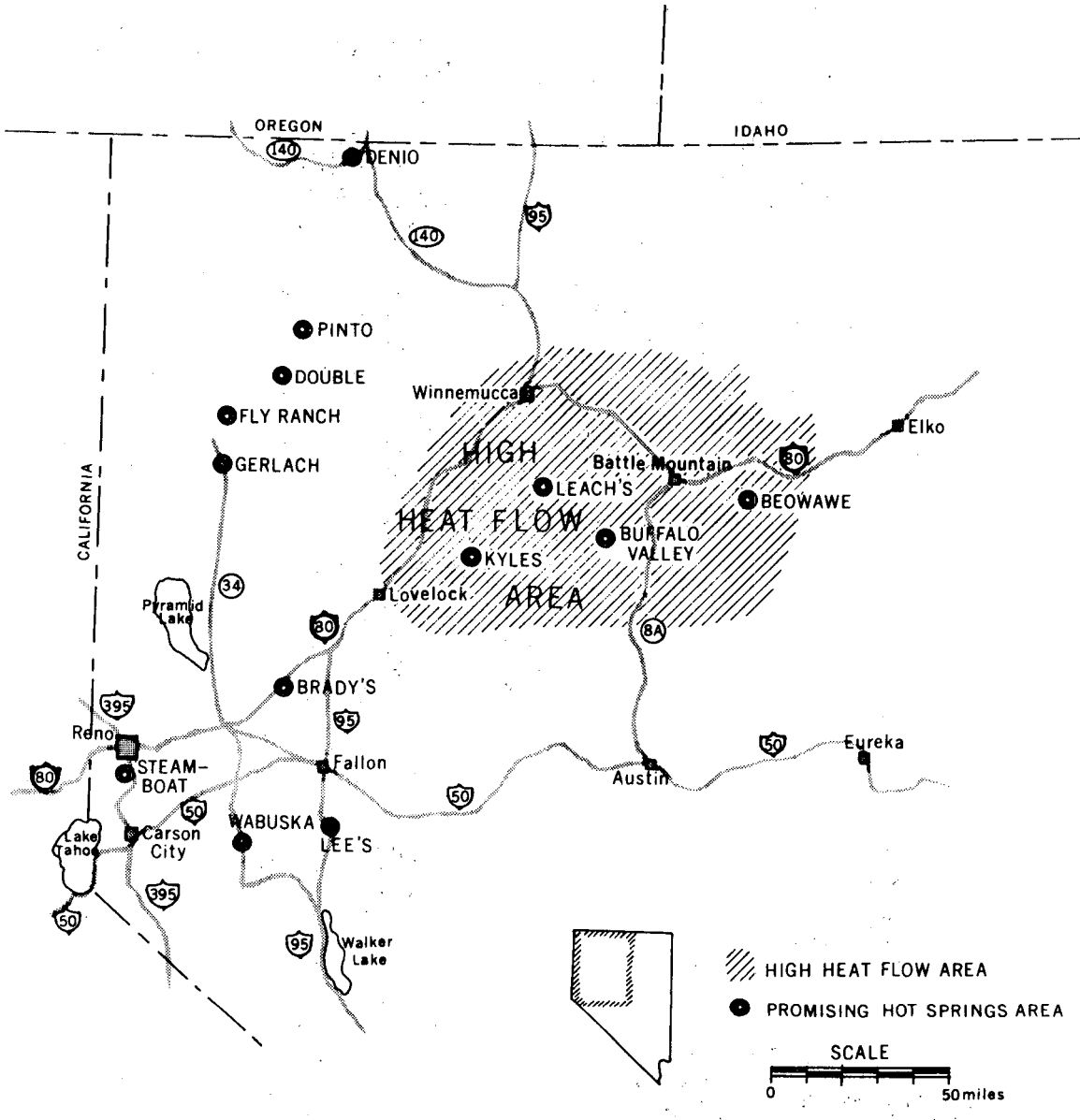

Hot Springs in Northwestern Nevada

XBL 735 676

Figure II-1. Location map, northwestern Nevada, showing prominent thermal spring areas within and outside of the Battle Mountain high heat flow region(After Sass et al., 1971).

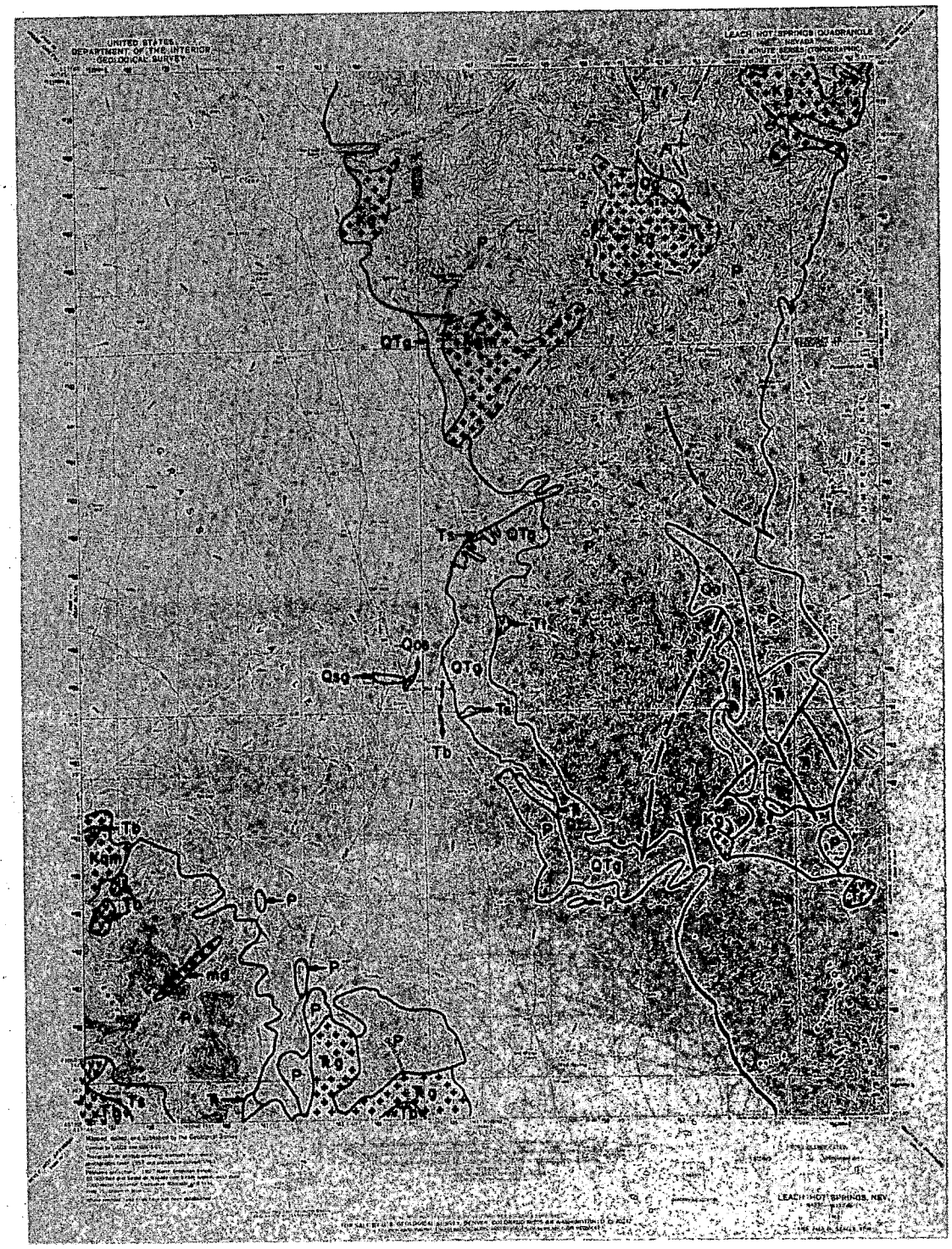

C&B 751-49

Figure II-2. Lithologic map, Leach Hot Springs area. Qal: alluvium, Qos: older sinter deposits, Qsg: sinter gravels, QTg: Quaternary -Tertiary gravels and fanglomerates, Tb: Tertiary basalt, Tr: Tertiary rhyolite, Tt: tuff, Ts: Tertiary sedimentary rocks, Kqm: quartz monzonite, Kg: granitic rock, md: mafic dike, TRg: Triassic granitic rocks, TR: undifferentiated Triassic sedimentary rocks, P: undifferentiated paleozoic sedimentary rocks (After Beyer et al., 1976).

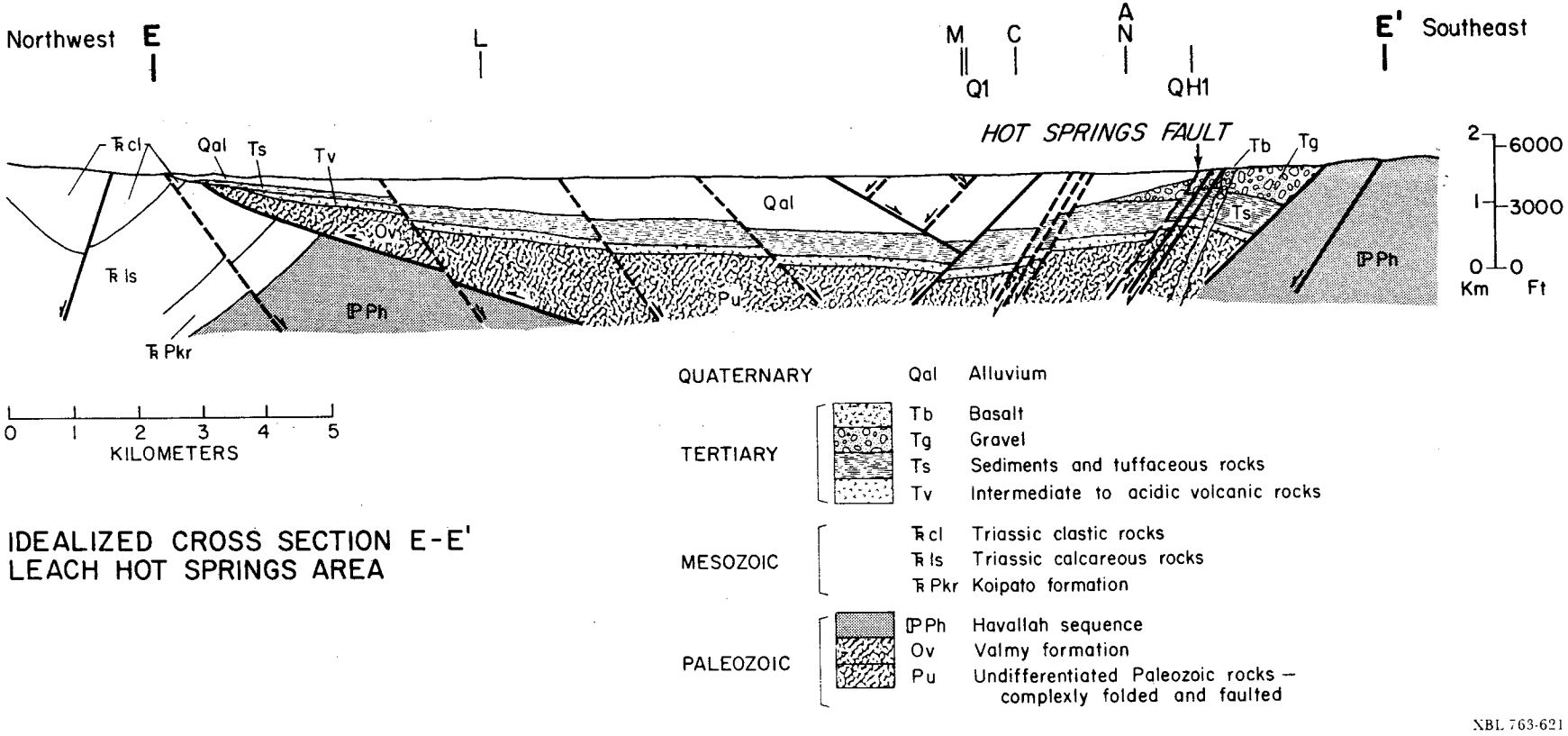

IDEALIZED CROSS SECTION E-E'
LEACH HOT SPRINGS AREA

Figure II-3. Idealized geologic cross section (After Beyer et al., 1976) along Line E-E' (Figure II-5).

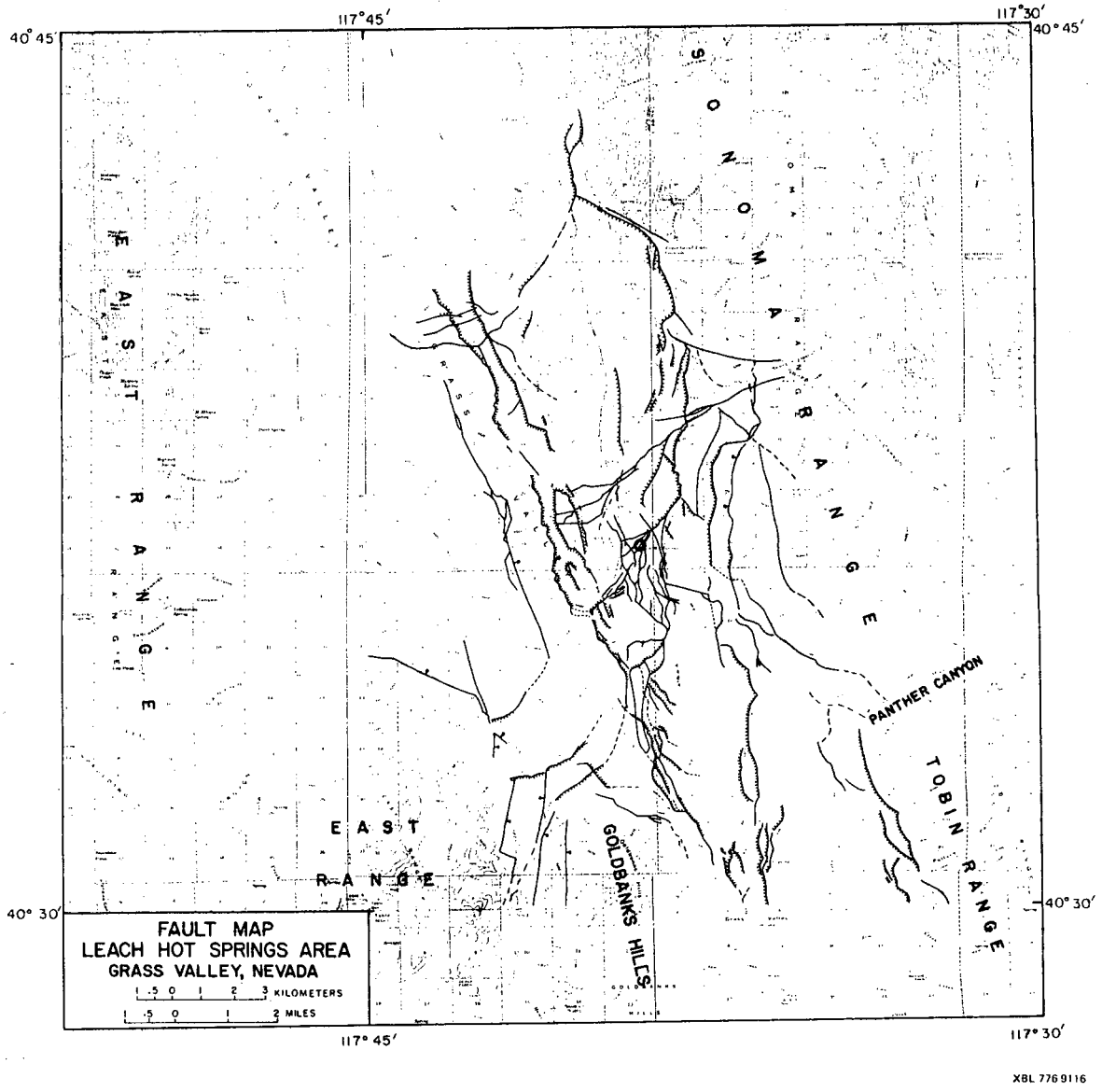

Figure II-4. Fault map of the Leach Hot Springs area. Hachured lines indicate down-faulted sides of scarplets; ball symbol indicates downthrust side of other faults (After Beyer et al., 1976).

3. Location of the Survey Line

Extensive geophysical surveys have been carried out in Grass Valley with the goal of locating and delineating the source of geothermal activity seen in this area. A total of 16 survey lines mainly trending N-S and E-W were laid out as shown in Figure II-5. Geophysical methods that were used included gravity, magnetic, self-potential, direct current resistivity, tellurics, magnetotellurics, microearthquakes, ambient microseism (ground noise), and reflection and refraction seismic surveys. Not all methods, however, were necessarily tried on each line. The results of this exploration effort have not been followed up by drilling and so the implications with respect to the geothermal potential remain unproven. However, because of the availability of so much geophysical and geological data Grass Valley served as an ideal location for the evaluation of the electromagnetic experiment. Since it was strictly a technique evaluation experiment, and since the available time to complete the survey was short, attempts were made only to obtain a resistivity vs. depth profile of the central part of the valley, along line EE' (Figure II-5). Other evidence suggested a sediment thickness on the order of 1000-1500 m in this part of the valley.

A total of nine depth soundings were obtained from two transmitter locations, marked as T3 and T7 on line EE' (Figure II-6), with transmitter-receiver separations of 1 and 2 kilometers covering a total distance of 8.75 line kilometers. All but one receiver stations were located on line EE', as shown on Figure II-6. Receiver station R3' was located one km north of transmitter T3, on a line perpendicular to EE'. Receiver positions R9' was located at 8.75 W on line EE', because of a nearby fence at 9W.

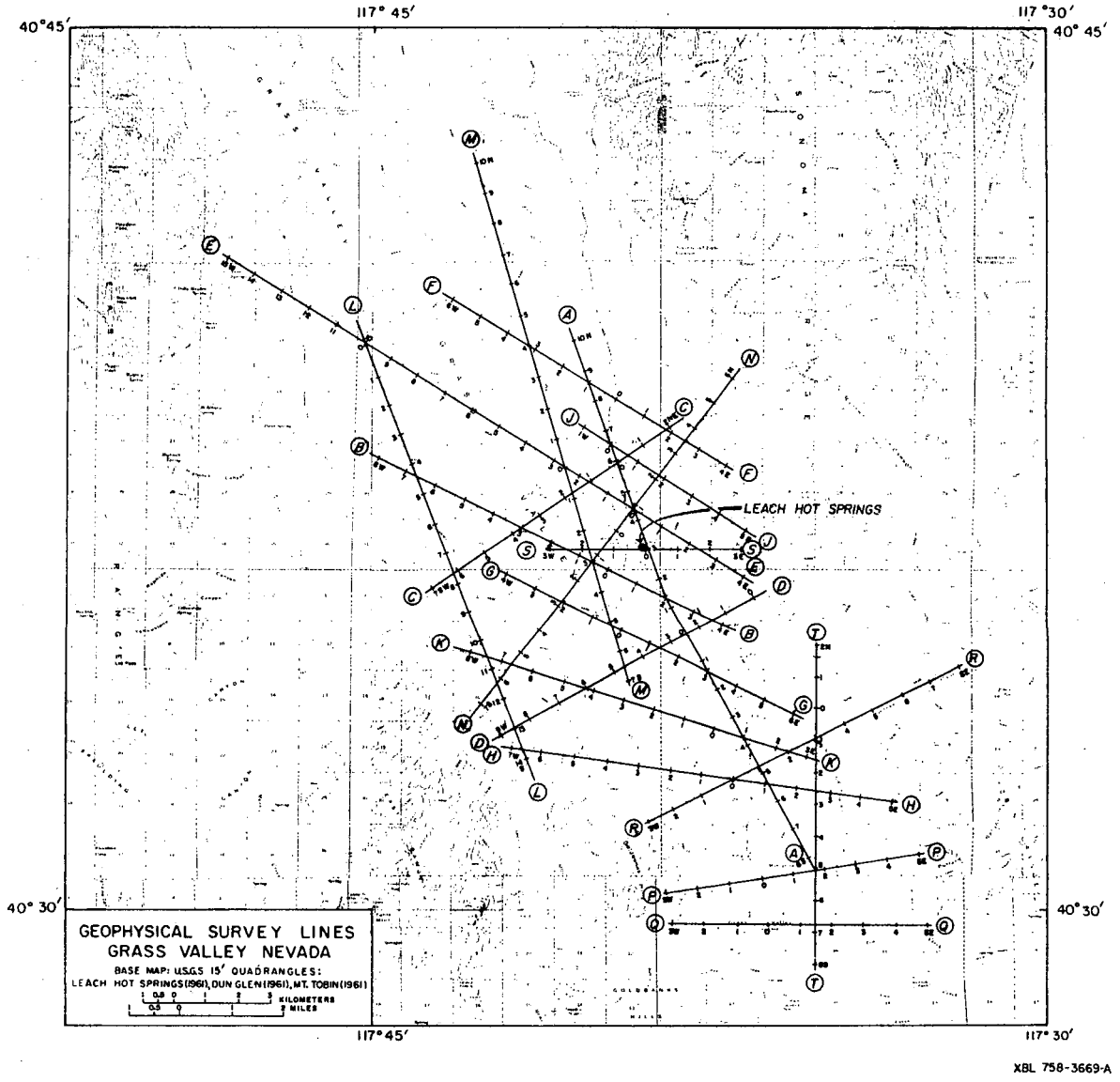

Figure II-5. Location of geophysical survey lines (After Beyer et al., 1976).

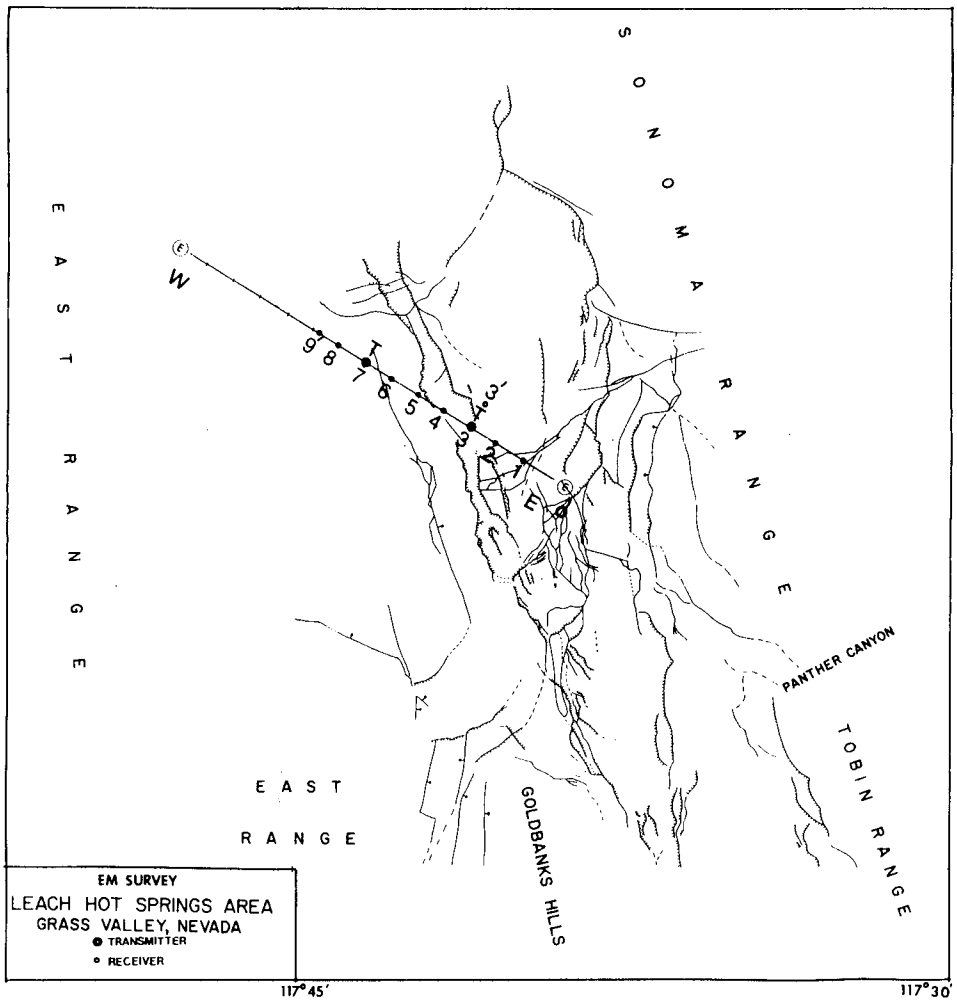

Figure II-6. Electromagnetic Transmitter and Receiver locations.

XBL 784-8035

4. Field program

The field procedure for an inductive frequency domain EM depth sounding is fairly standard: a loop source to energize the ground is deployed and a receiver is set up at a distance roughly equal to the depth to which information about the subsurface conductivity distribution is desired. Alternating current is then driven into the loop at a particular frequency and the resulting electromagnetic fields are measured at the receiver. Such measurements are made at several discrete frequencies covering a range of induction numbers of interest (from .1 to 20), where the induction number is defined as the ratio of transmitter-receiver separation to the skin depth in the first layer of the subsurface.

If the ground consisted of homogeneous, isotropic layers, the resulting electromagnetic fields due to a horizontal loop source are completely described by the two components of magnetic fields (horizontal magnetic field H_r and vertical magnetic field, H_z) and one component of electrical field (tangential electrical field E_θ), all of which have an in-phase and quadrature components with respect to the current in the loop source. Measurement of these three complex field quantities are required in an EM survey to interpret the layered earth's electrical parameters.

In the EM survey at Grass Valley, however, only magnetic fields were measured as the field deployment of a magnetic field detector is considerably simpler and faster than the emplacement of electrodes with connecting cables for the measurement of electrical fields. Because of the expected thicknesses (1~1.5 km)

and conductivities (1-10 Ω-m) of the sedimentary section in the center of Grass Valley, measurement frequencies were selected in the range .01 to 100 Hz. Separations of 1 and 2 km between the transmitter and receiver were chosen for the variable frequency measurements to emphasize shallower and deeper boundaries and to study any lateral variations in the resistivities. An even larger spacing would have been desirable, but was limited by signal to noise considerations.

5. Instrumentation

The equipment for this survey comprised of a transmitting unit and a receiving unit. Telephone wire links were provided between the transmitter and receiver to carry the phase reference. The equipment was built up with available standard components and with some special equipment made available for the survey. The biggest handicap during the experiment was the lack of a large enough power supply to drive the reactive load of the loop. An attempt to adapt a 20 kw (SCR) switching amplifier, graciously loaned to the university by the Chevron Reasearch Corporation, proved futile because of the limitations of such a power supply in driving the reactive load of the loop, reasons for which have been presented earlier.

A much smaller power supply (350 watts) was eventually used and heavy reliance was placed in the improvement of signal to noise ratio by signal averaging techniques. A brief description of the transmitting and receiving unit used in the survey is given below.

A. Transmitting unit: The transmitting unit consisted of a loop antenna, a custom made function generator and a linear power amplifier. A block diagram of the unit is shown on Figure II-7 and a detailed description is given in the following.

i) Transmitting loop antenna: The antenna consisted of a horizontal circular loop of 100 meters in diameter. The loop had 20 turns of A.W.G. #10 wire giving an effective NA of 1.57×10^5 turn-meter^2. It had a d.c. resistance of 24 ohms and an inductance of 200 millihenrys. The loop parameters were selected principally in accordance with the earlier discussion on the transmitter design.

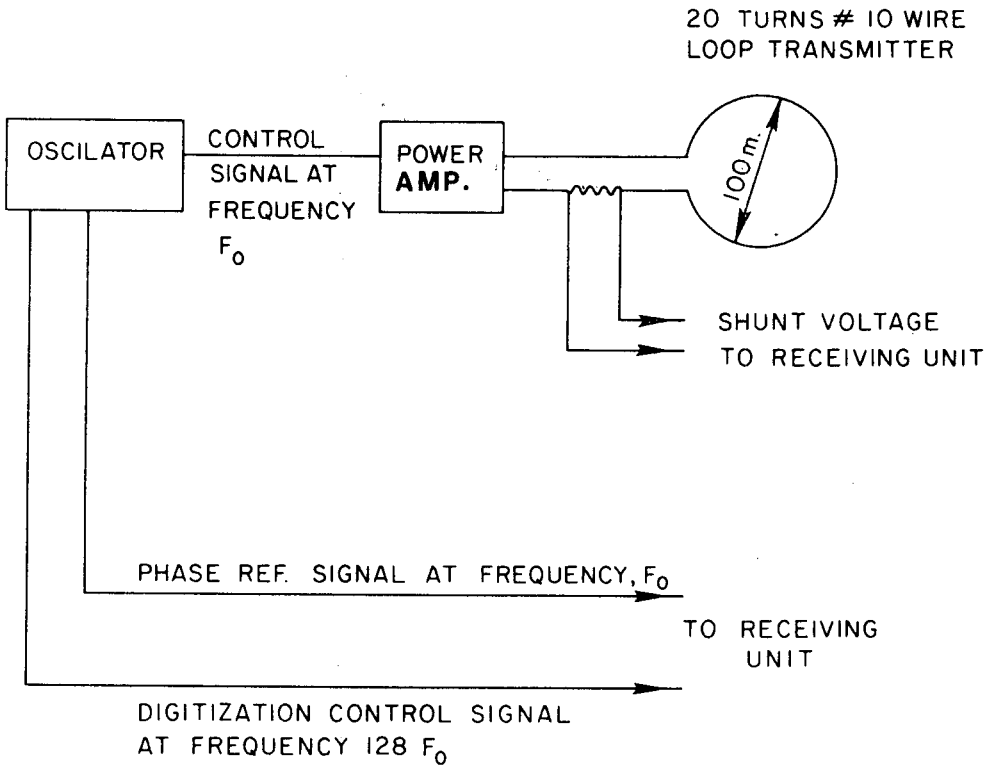

Figure II-7. Schematic of Transmitting Unit.

The wire was stored on the reel in a trailer and it took approximately two hours for two men to lay it in the form of a circular loop on the ground.

ii) Function Generator: The function generator serves three purposes; a) it provides an input sine wave at a frequency, F_0, to the power amplifier; b) it provides a square wave at a frequency, F_0, to serve as a standard phase reference, and c) it provides a square wave pulse at frequency, $128F_0$ (128 times F_0) to serve as a masterclock for the Signal Averager, which is described later in this section. These three signals are derived from a digital frequency dividing circuit--a 12 stage binary counter (4040M5) which is driven by a variable frequency oscillator (Figure II-8). At the various output stages (from 1 to 12) of this binary counter, pulses whose periods are in steps of power of 2 (from 2^1 to 2^{12}) of the input signal are available. The $128F_0$ signal and the F_0 reference signal are thus directly obtained from the proper output stages of this binary counter. The sinusoidal signal, however, is approximated by combining and properly weighting the various stages of the binary counter so that a staircase type waveform (a total of 256 steps in a period) as shown in Figure II-8 is obtained. This waveform is then further filtered by a sine shaper circuit.

iii) Power source: The power source used to drive the loop was 350 Watt direct coupled solid state power amplifier (Phase Linear Model 700). This power amplifier has a frequency response from 0 to 20 Khz and runs on 110V-50 Hz power supply. A maximum of 1.7 amps (r.m.s.) current was delivered to the load with this power supply. The dipole moments of the antenna at various frequencies

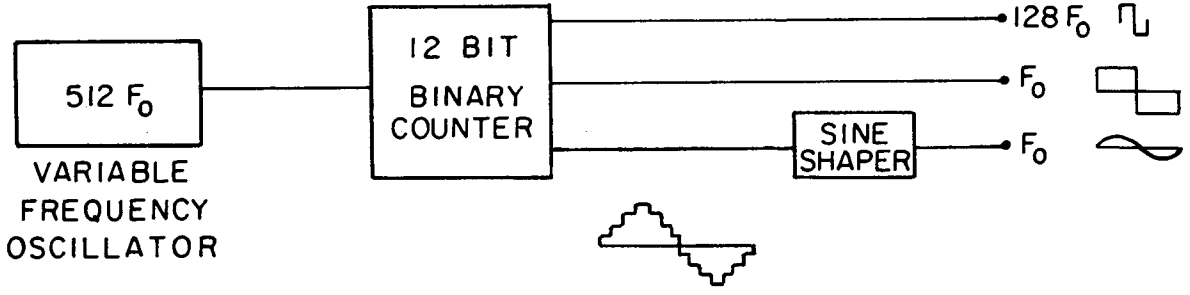

XBL 784-8031

Figure II-8. Schematic of Function Generator

are listed in Table II-1. The current is monitored by placing a shunt in series with the loop.

B. Receiving unit: The receiving unit consisted of a magnetic field detector and a signal processing unit. A pictorial view of the unit is shown in Plate II-1 and a block diagram of it is presented in Figure II-9. A detailed description of the unit is given below.

i) Magnetic field detector: The magnetic field detector used in this survey was a SQUID magnetometer (Develco model 8230). Such magnetometers are now in routine use in magnetotelluric surveys, but this is the first reported use of one in an active source electromagnetic survey. An excellent description of the working principle of SQUID magnetometers has been presented by Clarke (1974) and a comparative study of it with other types of magnetometers has been presented by Zimmerman and Campbell (1975).

The magnetometer has three mutually orthogonal sensors. However, for this survey only two sensors were used; one to measure H_r (radial toward center of the transmitting loop) and the other to measure H_z (vertical). The magnetometer is lightweight and tripod mounted. A collar and sleeve arrangement make it easy to orient in the desired direction, once it is in place and leveled. Its dewar has a capacity of 5 liters of liquid helium and a hold time of 2 days. According to manufacturers' specifications, it has a sensitivity of $10^{-5}\gamma/\sqrt{Hz}$ and a flat frequency response from d.c. to several KHz. The magnetometer sensor was separated from its electronics box by 30 meters. A distance of 30m was necessary between the magnetometer and the vehicle containing the electronics to reduce the noise caused by vibration of the vehicle. The output

Frequency (Hz)	$I_{r.m.s.}$ (amps)	Dipole Moment (NIA)
63.0	0.513	0.806×10^5
40.0	0.766	1.203×10^5
25.0	1.072	1.684×10^5
12.5	1.510	2.372×10^5
4.0	1.702	2.674×10^5
1.0	1.203	1.889×10^5
0.5	1.115	1.752×10^5
0.25	1.123	1.764×10^5
0.1	1.128	1.771×10^5
0.02	1.121	1.760×10^5
0.01	1.115	1.751×10^5

Table II-1. Dipole moment of electromagnetic transmitter at various frequencies.

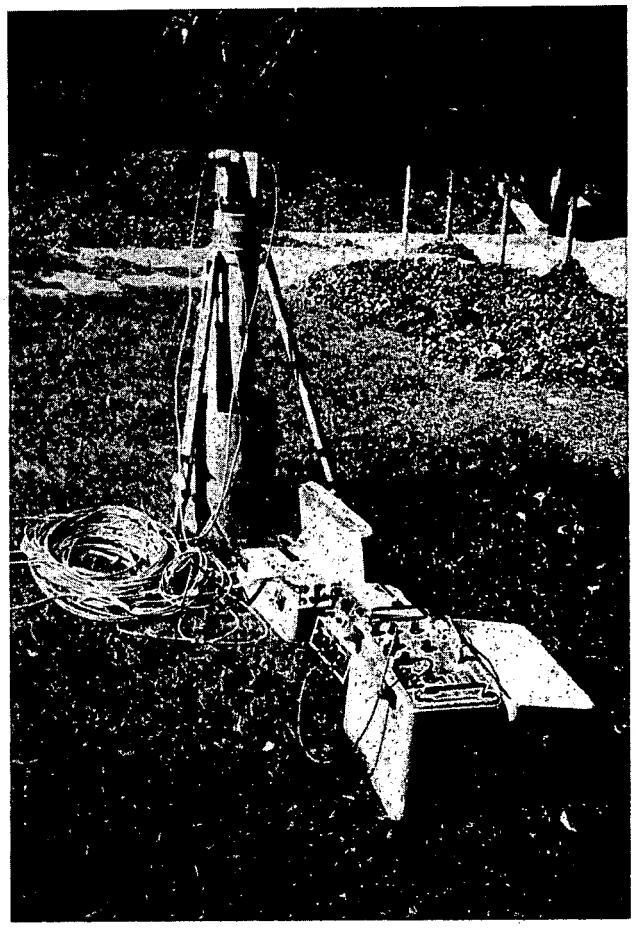

BBC 770-10368

Plate II-1. Photograph of receiving unit.

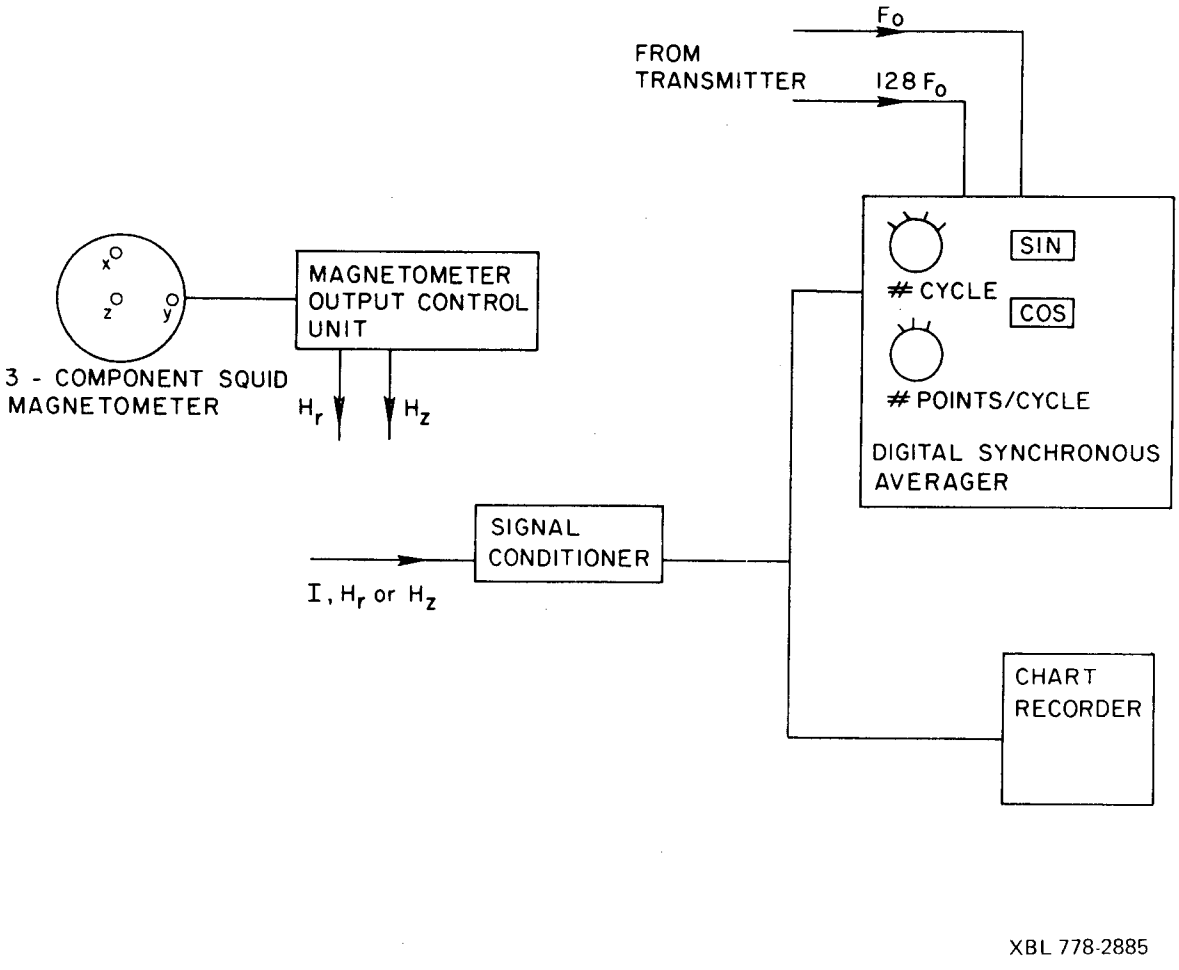

Figure II-9. Schematic of Receiving Unit.

of the magnetometer has a selectable low pass filter and a 60 Hz notch filter, but these were not used in this survey since inserting them would have caused undesirable phase shifts in the output signal.

During the field trial, it was found necessary to provide an aluminum can enclosing the sensors of the magnetometer to cut down high frequency noise (sferics) which, because of their high intensity, were causing the magnetometer to jump frequently out of lock. The can acts like a low pass filter and was designed to have a cut-off frequency at around 120 Hz. The actual effect on the magnetometer response was determined during a calibration check and is reported in Appendix A. A wind cover enclosing the magnetometer was used to reduce wind noise. A photograph of the magnetometer along with the windcover is shown in Plate II-2.

ii) Signal processing unit: The next major subsystem in the receiving unit was the Signal Averager--a preprogrammed digital unit specially designed to retrieve and analyze complex electrical signals. The unit was designed and built by the Engineering Geoscience group of UCB in 1974 as part of signal detection circuit for an airborne electromagnetic system being developed for AMAX Exploration Inc. The unit employs a digital superheterodyne detection algorithm, which mathematically is a process for determining the Fourier Coefficients for a single component of a periodic signal. It provides an accuracy of better than 1 milliradian in phase measurements. A block diagram illustrating this operation is shown on Figure II-10. Though the unit itself is a digital filter, the bandwith of the noise and the dynamic range of the

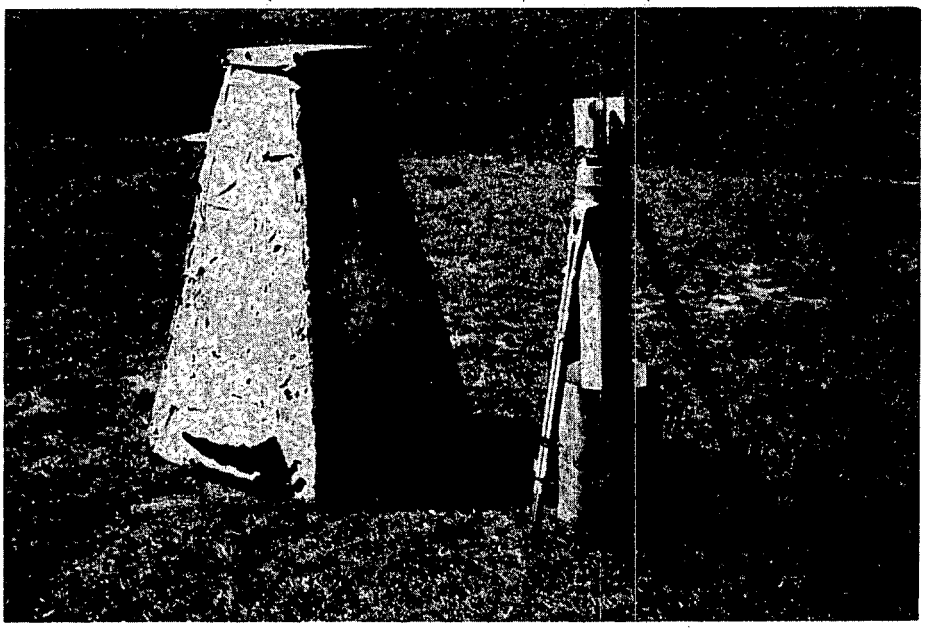

BBC 770-10370

Plate II-2. Photograph showing the Magnetometer and the Windcover.

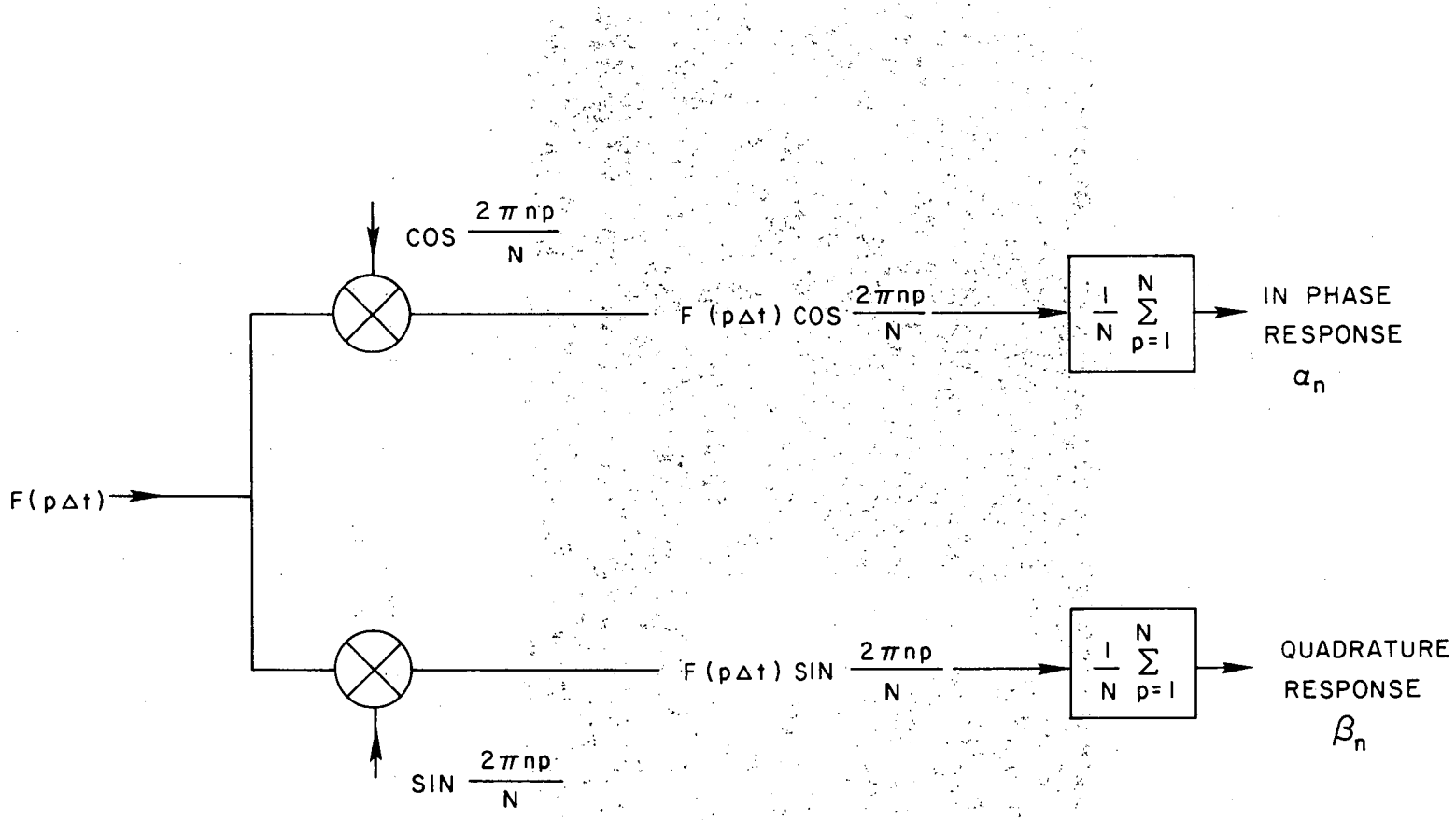

Figure II-10. DIGITAL SUPERHETERODYNE DETECTION ALGORITHM

XBL 778-2882

noise made it necessary to first condition the signal by an analog filter and then process it by the Signal Averager. Use of such an analog filter, however, sacrificed the phase accuracy to some extent, but made it possible to retrieve very weak signals in the natural field noise. A brief description and specifications of the filter used and the Signal Averager is given below.

a) Filter: The filter used to condition the signal was an ITHACO filter-amplifier model 4211. In this filter independently tuned high-pass and low-pass sections can be selected. Each section possesses a maximally flat amplitude using a 4 pole Butterworth filter giving 24 db/octave attenuation. The frequency range of the high-pass section is from .01 Hz to 1 KHz, and of the low-pass from .01 Hz to 10 KHz. Ten equally spaced frequency settings per decade (1.0, 1.25, 1.6, 2.0, 2.5, 3.16, 4.0, 6.3, 8.0, 10) are available for both sections. The amplifier provides 0 to 40 db gain in 10 db steps.

For the best utilization of the filter for this experiment the frequency of EM signal was chosen to follow the cut-off frequency settings available on the filter and the filter was used in a band-pass mode with no separation between the low-pass and the high-pass sections. In this mode signals were attenuated by 6 db, but this improved the signal to noise ratio considerably.

b) Signal Averager: The Signal Averager is a complete analyzing and computing unit incorporating input, process-

ing and display facilities all in a single box. The unit runs on rechargeable batteries and weighs approximately 30 lbs. and is therefore a very convenient field instrument. A photograph of the unit is shown on Plate II-3 and block schematic is presented in Figure II-11.

The actual operation of the Signal Averager can be described by considering its 4 units: i) analog unit, ii) S/H (Sample and Hold) and A/D (Analog to Digital Conversion) unit, iii) logic and memory unit, and iv) data display unit.

i) Analog Unit: The analog unit consists of an input signal level detector, low-pass filter and an amplifier. The maximum allowable input level is ±10 volts, and the device is protected by a diode clamp. If the signal exceeds the voltage limit, a warning light comes on. It also has a selectable low-pass filter and an amplifier with selectable gains of 1, 10, 100 or 1000.

ii) S/H and A/D unit: The analog signal is sampled by sample and hold circuit (DATEL Model SHM-CM) and digitized by an analog to digital converter (DATEL Model ADC-CM 12B) with a precision of 12 bits. The sampling rate is selectable at 16, 32, 64, or 128 points/cycle. The aperture delay for the S/H circuit is 20 n seconds, and aperture time for the A/D converter (the time the A/D converter takes from start to finish for a single A to D conversion) is 350 μ seconds. A warning light comes on if the data rate is too fast for A/D conversion.

iii) Logic and memory unit: The logic and memory unit

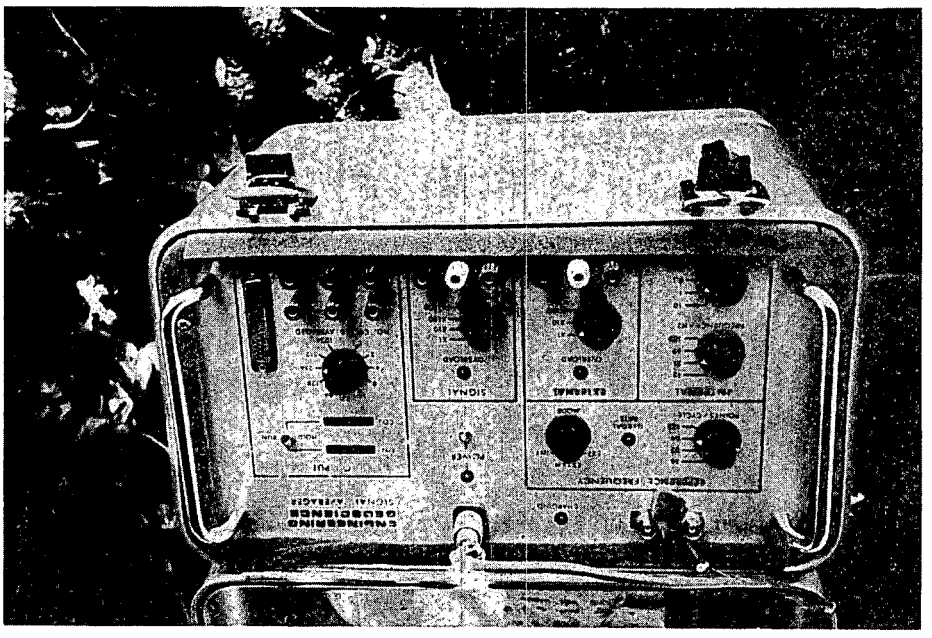

BBC 770-10366

Plate II-3. Photograph showing the Signal Averager.

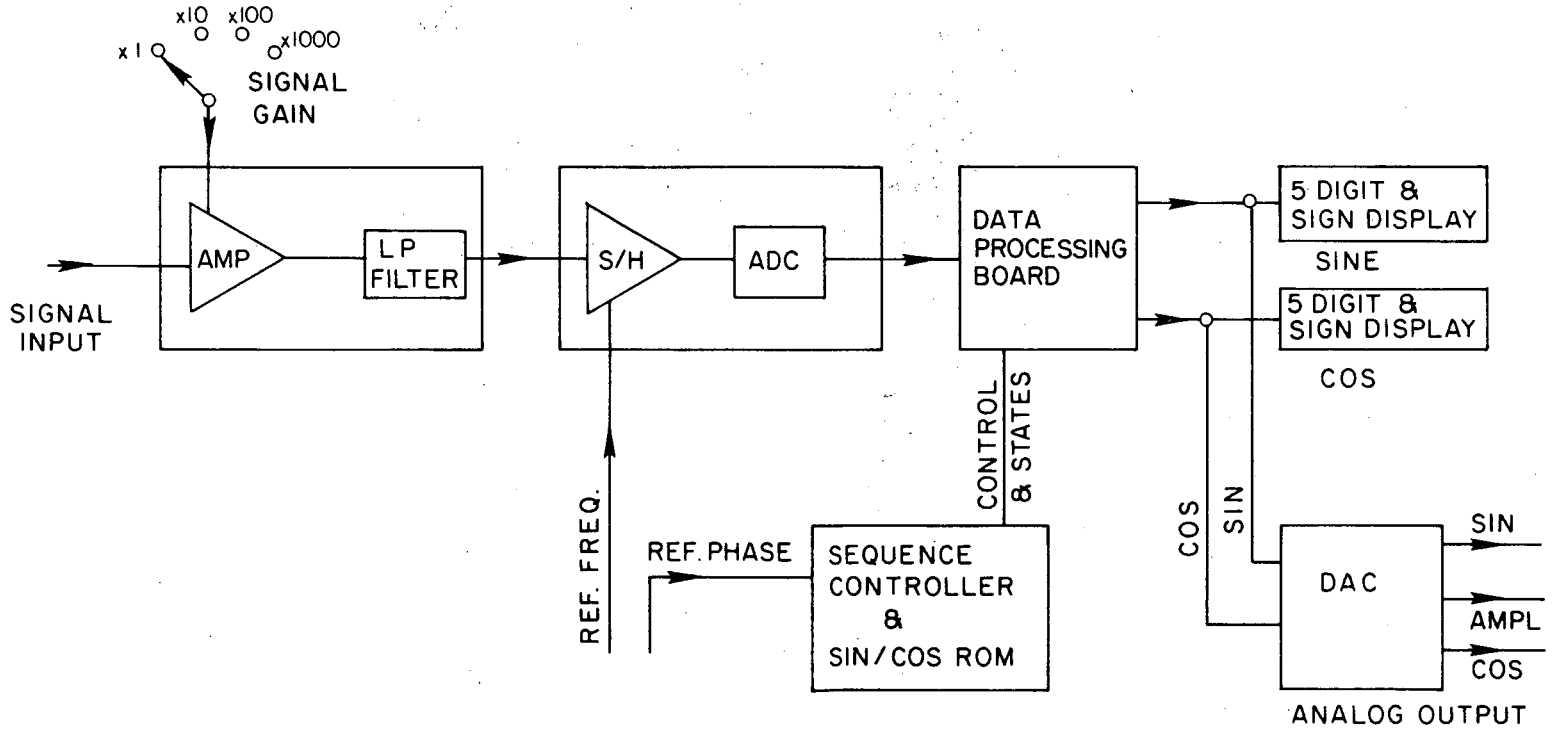

Figure II-11. SYSTEM BLOCK DIAGRAM OF ENGINEERING GEOSCIENCE SIGNAL AVERAGER

XBL 778-2883

does all the logical and mathematical computations. Thirty-two equispaced sine values from 0° to 90° are stored in a ROM with a precision of 16 bits. The digitized signal is multiplied with sine and cosine for one period and the result is averaged (stacked) over a number of cycles. The number of cycles averaged per reading are preselectable and are in steps of power of 2 from 2^0 to 2^{10} (1 cycle to 1024 cycles).

iv) Data display unit: The fourth section of the Signal Averager is a data display system for the average amplitudes of inphase and quadrature components of the processed signal. The data are displayed as five digit numbers, with sign, on a LED panel. It also has a digital to analog converter (10 bit) to give an analog recording of inphase and quadrature amplitudes of the processed signal.

The Signal Averager does not have an internal clock, but rather uses the $128F_0$ signal generated by the function generator (which has been described earlier) as the master clock. Since the function generator is kept at the transmitter site, the clock signal is transmitted to the receiver site through a pair of telephone wires. Such an arrangement proved to be adequate during this survey. However, considering the effort in laying out the wires between transmitter and receiver sites, a telemetry system for future surveys is highly recommended.

The maximum frequency of the signal which the Signal

Averager is capable of processing is dependent upon the number of points selected to be digitized in each cycle of the analog signal. Table II-2 lists the maximum frequency of the signal which can be processed by the Signal Averager for the fixed rate of 16, 32, 64, or 128 points per cycle of the analog signal.

Number of data points/cycle	Maximum signal frequency (Hz)
128	13
64	26
32	52
16	104

Table II-2. Signal frequency and digitization rate specifications for the Signal Averager.

6. Field Set-up

Two transmitter and nine receiver sites were occupied during the test survey (Figure II-6). From a single transmitter location, a minimum of four sounding results were obtained: two each on either side of the transmitter, in a line, with transmitter-receiver separations of 1 and 2 km. Receiver site 5W was the common receiver position for both transmitter locations, thus providing a continuous profile coverage for the line surveyed. Another receiver site, 3N, was located at a distance of 1 km on a perpendicular off-set line from transmitter position 3W, and was used in order to check the assumption of isotropic subsurface layers.

Two vans, one at the transmitter site and one at the receiver site, and a jeep, were used for the survey. The power supply for the transmitter was mounted on a trailer. The jeep was primarily used for laying out the reference wires between the transmitter and the receiver. Two men were sufficient for the survey, one to control the transmitter and one to collect the data at the receiver. In a typical day, two receiver stations were covered and at each station, data were collected at 14 discrete frequencies covering the frequency band of .01to 100 Hz.

At each frequency three sets of measurements, one each for H_z, H_r, and I (shunt voltage), with a common phase reference were made. Shunt voltage and phase reference signals were brought to the receiver site through two pairs of telephone wires. It should be pointed out that the phase and amplitude of current flowing into the transmitter coil changes at each frequency because of the change in load impedance of the transmitter loop. Therefore, the current has to be measured with the same precision in order to calculate accurately the phases and ampli-

tudes of H_r and H_z with respect to the current flowing in the transmitter. Maximum shift in the phase of the current due to transmission delay would be .24° (calculated for signal frequency of 100 Hz and transmitter-receiver separation of 2 km) and such phase delays were accounted for during data reduction.

Ideally one should measure the shunt voltage and the magnetic field simultaneously in order to eliminate the effects of any change in the current in the loop. This, however, was not possible during this survey because the prototype signal averager had only one channel. Thus, at each frequency, the signals H_z, I, and H_r were measured separately. The current was measured at the beginning and at the end of each run and if any current drift was observed the measurement was repeated. Precautionary measures were taken to ensure that the transmitter controls were not changed during a run. In practice the current was found to be very stable.

Each signal was averaged over a number of cycles and readings of in-phase and out-of-phase components, as given by the Signal Averager, were recorded. Readings were repeated at least five times in order to reduce the error in the data. From this set of readings, average phase and amplitude of the measured component were computed. By subtracting the magnetic field phases from the current phase, one obtains the phases of H_z and H_r with respect to the current flowing into the coil. Similarly, by dividing the magnetic field amplitude by the product NIA, one can find the magnetic field per unit transmitter moment.

The main problem faced during the data gathering has been the rather poor signal to noise ratio as visualized in Figure II-12. The amplitudes of signals shown in the figure are the theoretical values of

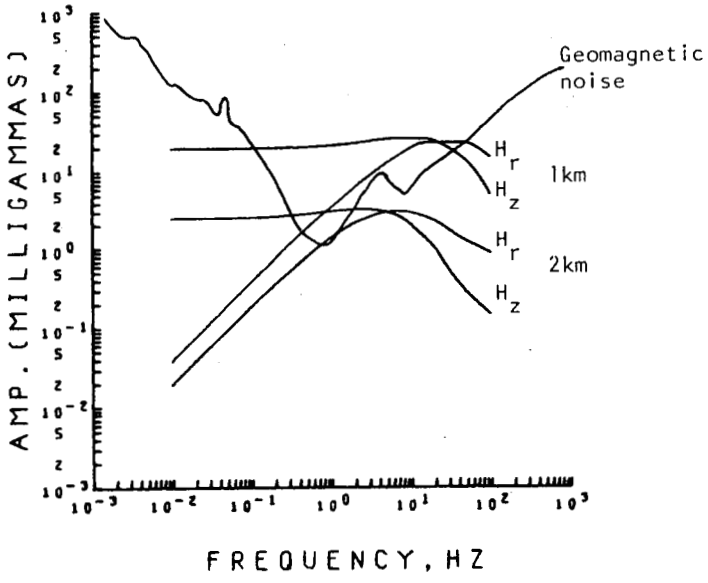

Figure II-12. Approximate levels of signal and noise as encountered in Grass Valley Survey.

H_r and H_z which would be observed over a 10 Ω-m half-space for a dipole moment of 2×10^5 M.K.S.A. units (the maximum moment available in this survey) at transmitter-receiver spacings of 1 and 2 kilometers. The noise level shown in this figure is that given by Keller and Frischknect (1966) and it fairly represents the level of noise observed in this survey. The sources of such noise has been discussed in detail by Keller and Frischknecht (1966). It should be pointed out that the noise level shown is for the vertical field component (H_z) and the noise level in horizontal direction is considerably larger, as much as a factor of ten. Considerable improvement in signal to noise ratio during the field measurement was achieved by averaging the signal over a long period of time. Even so, accurate measurement of H_r and H_z component was difficult below 1 Hz and .1 Hz, respectively.

7. Interpretation of the Results

General

The interpretation of electromagnetic sounding data is accomplished through a comparison of measured responses with those calculated for some mathematical models. Such a comparison then requires that various mathematical models be examined in order to select the best fit model. Calculations of EM response, other than for a simple layered earth model, is complex and requires considerable computation time; interpretation of the Grass Valley data has been attempted in terms of layered earth models only. In such an interpretation the basic assumption has been made that the earth can be represented by plane layers, each with uniform, homogeneous, isotropic, electrical properties. Considerable difficulties in the interpretation of data are expected since this assumption is unlikely to be met in a real field situation. However, the results at eight out of nine soundings closely resemble the response due to a layered half-space. The sounding result for T3-R1 does not resemble the response due to a layered model and in this case the receiver is very close to a major fault as seen from Figure II-6.

Method of Interpretation

Until recently, interpretation of electromagnetic sounding data has been done by trial and error or curve-matching techniques. The main disadvantage of such a method is that large numbers of master-curves are required. Consideration of more than two layers for a proper interpretation becomes very difficult as the number of variable parameters (thicknesses and conductivities) involved becomes prohibitively large. For these reasons, curve-matching techniques have now been replaced with

direct inversion methods. In such methods an initial guess about the model parameters is made and then the parameters are automatically adjusted till a best-fit between the observed data and the model predicted data is found. Besides being automatic, the main advantage of this method lies in the fact that it not only provides a statistically best fitting model but also gives a basis to estimate the uncertainities of the model parameters. Grass Valley sounding data has been interpreted using such an inverse method. The application of these techniques in electrical exploration has been described by Wu (1968), Parker (1970), Glenn et al. (1973), Inman et al. (1973), Inman (1975), Jupp and Vozoff (1975), Vozoff and Jupp (1975), Glenn and Ward (1976), and Ward et al. (1976).

Inversion Problem

The general problem of inverse interpretation is stated mathematically as:

$$\phi = \sum_{i=1}^{N} W_i^2 \, (y_i - f(\underset{\sim}{b}^\circ, x_i))^2 \qquad \text{(II-1)}$$

where

N is the total number of observed data

W_i is the weighing factor for i^{th} data point

y_i is the i^{th} observed data (i.e. amplitude or phase in the EM case)

b° is an initial estimate of M model parameters (e.g. resistivity and thickness)

x_i is the known dependent variables (e.g. frequency and

geometric variables)

f is the non-linear mathematical function of phase or amplitude.

The problem is to find an estimate $\underset{\sim}{b}$ of $\underset{\sim}{b}^{\circ}$ for which the weighted sum of squares ϕ is a minimum.

The values of b_j that minimize this expression are given by the solution to equations

$$\frac{\partial \phi}{\partial b_j} = 0, \quad j = 1, \ldots M. \tag{II-2}$$

which may be written in the form

$$\sum_{i=1}^{N} W_i^2 f_i \frac{\partial f_i}{\partial b_j} = \sum_{i=1}^{N} W_i^2 y_i \frac{\partial f_i}{\partial b_j}, \quad j = 1, \ldots M. \tag{II-3}$$

where $f_i = f(\underset{\sim}{b}, \underset{\sim}{x}_i)$. If the function $f(\underset{\sim}{b}, \underset{\sim}{x})$ depends linearly on the parameters b_j then the derivatives $\frac{\partial f_i}{\partial b_j}$ will be constants and the system of equations is readily solved for the unknown b_j. However, since the function $f(\underset{\sim}{b}, \underset{\sim}{x})$ depends non-linearly on the b_j, the system is not solvable in closed form and, in practice, it is easier to minimize ϕ directly by an iterative technique.

There are many methods published in mathematical journals for minimizing sum of squares of a nonlinear function. Two such methods which have commonly been used in electrical exploration problems are Newton-Raphson method (e.g. Glenn, et al., 1973; Inman, et al., 1973) and Marquardt's (1963) method (e.g. Inman, 1975). Inman (1975) has discussed the superiority of Marquardt's method over Newton-Raphson

method in solving electrical resistivity problems. The basic minimization algorithm used for the Grass Valley electromagnetic sounding data interpretation is named SPIRAL which has originally been developed by Shell Reasearch Limited. This method searches roughly the same area as does Marquardt's, but here the search point is generated by vector addition rather than by matrix inversion and thus considerable computation time is saved. In our experiments, this algorithm is found to solve electromagnetic or resistivity sounding problems very effectively, reaching an acceptable minimum in a maximum of 6 to 7 iterations.

The basic principle of Spiral algorithm has been discussed in detail in a paper by Jones (1969). Only a brief description of this algorithm is presented in the following.

Spiral Algorithm

In the Spiral algorithm, the first search point is generated with the least squares method (Newton-Raphson method). The model (the non-linear function $f(\underset{\sim}{b}^\circ, x_i)$ in equation (II-1)) is expanded in a Taylor Series about the current estimate, $\underset{\sim}{b}^\circ$, retaining only the first order terms. This leads to an improved estimate $\underset{\sim}{b}(=\underset{\sim}{b}^\circ+\underset{\sim}{t})$ for the linearized model, where $\underset{\sim}{t}$ is the solution of

$$[A]\ \underset{\sim}{t} = \underset{\sim}{g} \qquad \text{(II-4)}$$

where

$$[A] = [P']\ [Q]\ [P]$$

and $$\underset{\sim}{g} = [P']\ [Q]\ [y-f_o]$$

P being the (N x M) matrix with elements $\left.\frac{\partial f_i}{\partial b_j}\right|_{b=b_o}$

and Q is the weight matrix.

If the sum of squares at the new point $\underset{\sim}{b}$ is smaller than the sum of squares at the point $\underset{\sim}{b}_o$, then the search procedure is repeated. If the sum of squares is not smaller, then a spiral search procedure is adopted.

The basic idea behind the spiral search is that a reduced sum of squares can always be found in the plane defined by Taylor Series point and the line of steepest descent at the base point (the direction of steepest descent is given by vector $\underset{\sim}{d}$, where $\underset{\sim}{d} = -\underset{\sim}{g}$). In Figure II-13, which is drawn on this plane, O is the base point, T is the Taylor Series point and OD is the direction of steepest descent; the point D being so chosen that the distance OT and OD are equal. The minimum is searched by moving along a spiral OTS, which moves out from T at an angle β into the area OTD and moves back into O tangentially to OD. The equation for this spiral (expressed in polar coordinates with O as the origin) is given as

$$r = r_o \left(1 - \theta \cot\beta - (1 - \gamma \cot\beta)(\theta/\gamma)^2\right) \qquad \text{(II-5)}$$

where r is the distance OS and r_o is the distance OT.

The sequence of points, S, on the spiral to be investigated is computed from a sequence of points, L, generated on the line TD such that L divides TD in the ratio $\mu : (1-\mu)$. The successive values of μ are computed from the recurrent relation

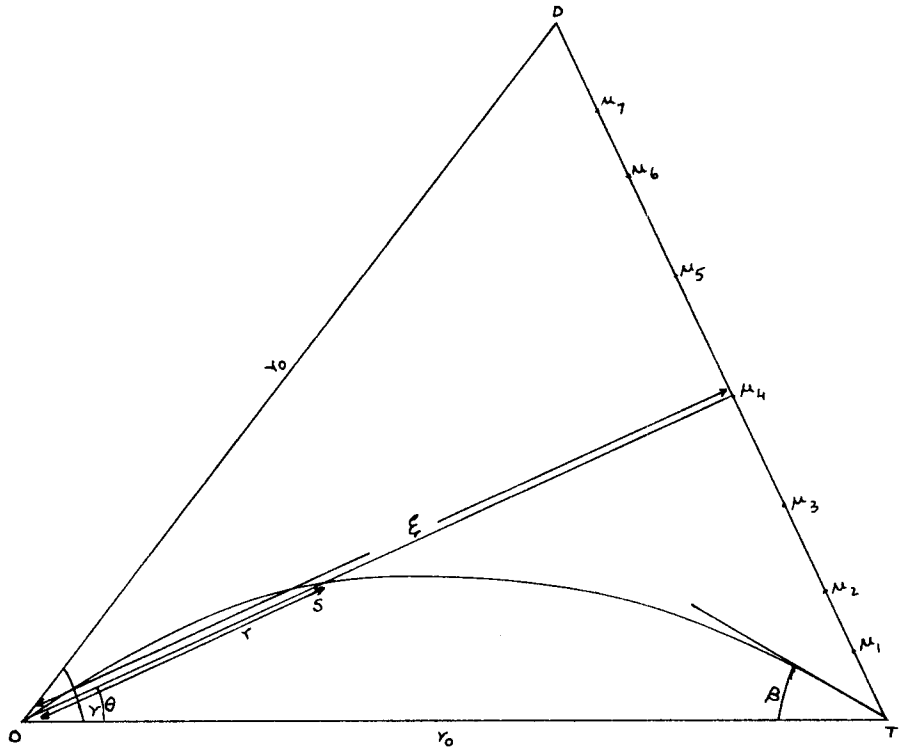

XBL 784-8045

Figure II-13. Geometry of Spiral Algorithm.

$$\mu_{n+1} = 2\mu_n/(1 + \mu_n) \qquad \text{(II-6)}$$

which has been chosen to ensure that the points become closer together as they approach, D.

The coordinates of the search point, S, with reference to O as origin are given in terms of t, the coordinates of T, and d, the coordinates of D, by the relation

$$S = \frac{r}{\xi}\{\mu \underset{\sim}{d} + (1-\mu)\underset{\sim}{t}\} \qquad \text{(II-7)}$$

where

$$\xi = \frac{r_o \mu \sin \gamma}{\sin \theta}$$

and $$\tan \theta = \frac{\mu \sin \gamma}{1-\mu + \mu \cos \gamma}$$

Once a minimum is found in such a spiral search, the corresponding parameter values are taken as the base point for a new search area. This iteration process is assumed to have converged when the search area becomes small i.e. when all the values of t_i are small relative to the corresponding b_i.

Numerical Considerations

Function Evaluation

In the electromagnetic sounding problems, the function f in equation (II-1) represents the vertical (H_z) or horizontal (H_r) component of the magnetic field over a layered half-space due to a

vertical magnetic dipole source. H_z and H_r are expressed as (Ward, 1967)

$$H_z(b_o, x) = \frac{m}{4\pi} \int_0^\infty R(\lambda, b_o, x)\, J_0(\lambda r)\, \lambda^2\, d\lambda \quad \text{(II-8)}$$

and

$$H_r(b_o, x) = \frac{m}{4\pi} \int_0^\infty R(\lambda, b_o, x)\, J_1(\lambda r)\, \lambda^2\, d\lambda \quad \text{(II-9)}$$

Where

m is the dipole moment

r is transmitter-receiver separation

and R is the kernel of the integral.

The method used here in the evaluation of the above function is to integrate numerically between zeros of the appropriate Bessel function and then sum the resulting terms which form an alternating series. An Euler's transformation is applied, if the resulting series are too slow to converge. In the above calculations, an accuracy of better than .1% has been maintained.

The calculation of partial derivatives, $\frac{\delta f}{\delta b}$, which are the elements of P matrix has been done by a 2-point forward difference approximation

$$\frac{\delta f}{\delta b} \simeq \frac{\Delta f}{\Delta b}$$

where $\Delta f = f(b + \Delta b) - f(b)$.

Typically, a value of 1% for the ratio of $\Delta b/b$ has worked satisfactorily in the above estimation of derivatives.

Weighting

There are many choices that can be made in selecting the weighting factor, W_i in equation (II-1). Logically, it should be selected as the inverse of the data errors at each data point, i.e. let $W_i = \frac{1}{\sigma_i}$, where σ_i is the standard deviation of the i^{th} data point. In this way, the residual for each data point is compared with its expected error. Inclusion of such a weighting factor $(\frac{1}{\sigma_i})$ in the minimization problem is also necessary, as then only the parameter set $\underset{\sim}{b}$ found at the minimum would be the maximum likelihood estimate of the true parent function (Bevington, 1969).

The weighting matrix, Q, to be used in the inversion problem is then given as (assuming errors at different data points are uncorrelated)

$$Q = \begin{vmatrix} \frac{1}{\sigma_1^2} & 0 & \cdot & \cdot & 0 \\ 0 & \frac{1}{\sigma_2^2} & & & \cdot \\ \cdot & & \cdot & & \cdot \\ 0 & 0 & & & \frac{1}{\sigma_N^2} \end{vmatrix} \qquad \text{(II-10)}$$

It can be immediately realized that by including such a weighting matrix in the minimization problem, the dimension of the data is effectively removed. Thus different independent sets of data, which may have different measurement units (for example, phase and amplitude) can be combined together for a joint inversion.

To include the weighting matrix Q in the inversion problem, then

one needs to know the absolute values of errors at each data point. In many sounding surveys, the absolute values of data errors may be unknown but it may be possible to estimate the relative errors σ_{r_i} between each data point. In such a case, equation (II-10) is redefined as

$$Q = \frac{1}{\sigma^2} \begin{vmatrix} \frac{1}{\sigma_{r_1}^2} & 0 & \cdot & \cdot & 0 \\ 0 & \frac{1}{\sigma_{r_2}^2} & & & \cdot \\ \cdot & & & \cdot & \cdot \\ 0 & 0 & \cdot & \cdot & \frac{1}{\sigma_{r_N}^2} \end{vmatrix} \qquad \text{(II-11)}$$

where σ is some scalar factor called the problem standard deviation. This weighting matrix is then used in the minimization scheme (σ, the problem standard deviation is assumed to be equal to 1). An estimate of the true problem standard deviation, $\hat{\sigma}$, then may be obtained from the reduced chi-square given as (Bevington, 1969)

$$\hat{\sigma}^2 = \frac{[y-f_o]^T [Q]_{\sigma=1} [y-f_o]}{N-M} \qquad \text{(II-12)}$$

$$= \frac{\phi_{min}}{N-M} \qquad \text{(II-13)}$$

Electromagnetic sounding data generally consists of two types of

measurements: phase (or tilt angle) and amplitude (or ellipticity). The errors in phase data are generally assumed to be constant, i.e. regarded as equal at all data points and thus the elements of the weight matrix for inversion of such a set of data would be unity. The errors in the amplitude measurements, however, are expressed as a fixed percentage of each measurement and thus the weight matrix for the inversion of such a set of data would consist of elements which are inversely proportioned to the magnitude of the data. A similar consideration also applies to the resistivity data, since the errors are again expressed as a percentage of the measured apparent resistivity values.

What happens when a unity weight matrix is used in the inversion of amplitude data, i.e. a weight of 1 is assigned to all measured amplitude values as in the case when a ordinary least squares method is used? Such a method of weighting has often been used (e.g. Glenn et al., 1973; Inman et al., 1973) with the intention of assigning equal importance to the various data points. However, if we closely examined such a weighting scheme, we would discover that an unintentional bias is introduced in the minimization scheme, i.e. data points with larger numerical values are heavily favored in comparison to the data points with smaller numerical values resulting in a biased interpretation result. To illustrate this point, let us consider a resistivity sounding curve which has been obtained over a two layered earth, the resistivity of the upper layer being 1 ohm-m and that of the lower half space being 1000 ohm-m. The two data points at the two asymptotic parts of this curve would be 1 ohm-m (at smaller spacing) and 1000 ohm-m (at larger spacing), respectively. If we initiate the

inversion process with an assumed earth model with resistivity values of 2 ohm-m (upper layer) and 2000 ohm-m (lower layer), the parameter errors being 100%, the residual values (the difference between ovserved data and model data) at the two points may be found to be 1 and 1000 respectively. The minimization scheme basically reacts to these residual values and would try to alter the earth parameter so that these residual values are minimized. In such a process, however, the basement resistivity would be corrected more since it is contributing the largest residual error. Finally, we may obtain an earth model which leaves residual errors of say .1 and 1 at the two data points i.e. the resistivities of the two layers may be determined to be 1.1 and 999 ohm-m respectively. It can then be immediately realized that the error in the estimated resistivity of upper layer is 10%, whereas the same error is only .1% for the lower layer resistivity i.e. the lower layer resistivity has been determined much more accurately. This example clearly demonstrates how a minimization scheme may be biased simply due to the numerical differences among the data. Such a biasing then must be removed in the inversion problems. It can easily be seen that if the data in the example considered were weighted according to the equal percentage error criterion, the noted bias in the estimation of earth's parameters is effectively removed.

The above noted biasing in the inversion problem, introduced due to the incorrect weighting of amplitude data, i.e. weighting of the data by 1 instead of equal percentage error criteria, has gone unnoticed in some of the earlier papers and has caused some of the results presented in these papers to be inaccurate. An example of such a result is given and dicussed below.

Figure II-14 shows the eigenvalues and eigenvectors as presented by Inman et al. (1973) for a 3 layer earth model, Model A (ρ_1 = 10 ohm-m, ρ_2 = 50 ohm-m, ρ_3 = 150 ohm-m, t_1 = 20m and t_2 = 100m). In calculating these eigenvalues and eigenvectors, a weight of 1 has been used for all the data points. The chief advantage of studying the eigenvalues and eigenvectors of a model is that a relationship between the data points and the earth's parameters can be readily visualized. The data eigenvectros which point chiefly in the direction of associated parameter eigenvectors are the data points which have the miximum effect in the resolution of the particular parameter or the combination of parameters. One such relationship between the parameter eigenvector and the data eigenvector can be visualized in Figure II-14 for the parameter ρ_3 (λ = 2.03), as the associated data eigenvector are seen to be pointing chiefly in the direction of the largest spacings. Such a relationship is to be expected as ρ_3 is determined by the asymptotic values measured at the largest data spacings. Most conspicuously, however, a similar relationship between ρ_1 and data eigenvectors at the smallest spacing are noted to be missing in Figure II-14. Inman et al. have offered no explanation for such strange behaviour of the eigenvectors.

Figure II-15 again shows the eigenvalues and eigenvectors for the same model (Model A). In these calculations, however, a proper weight matrix with elements inversely proportional to the magnitude of data (equal percentage error criteria) has been included. As can be noted from this figure, association of ρ_1 (λ = 22.2) and ρ_3 (λ = 1.57) with smallest and largest data eigenvector respectively is clearly demonstrated as expected from theoretical considerations.

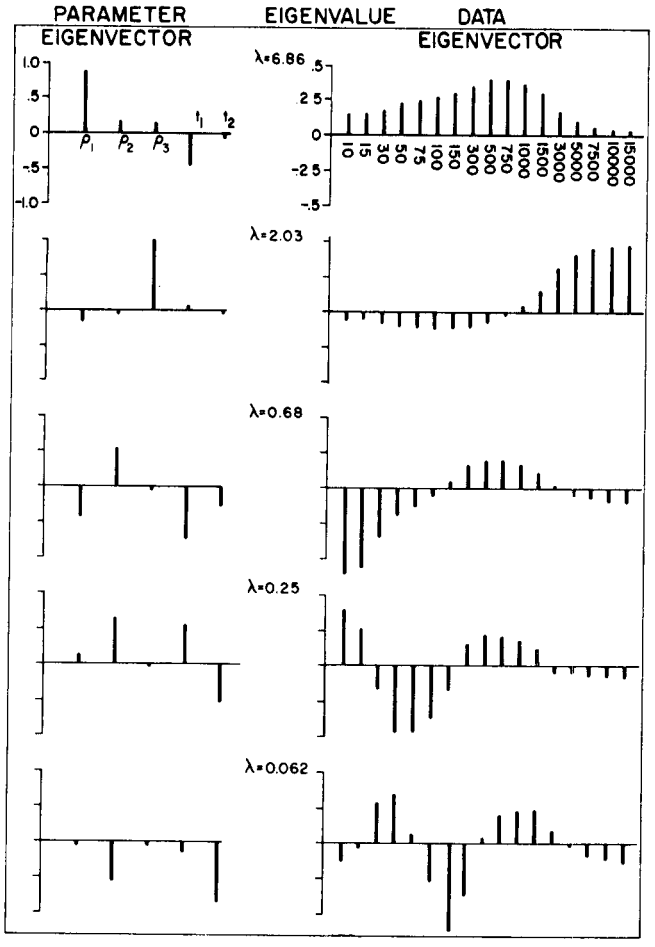

Figure II-14. Eigenvalues and eigenvectors for model A as presented by Inman et al.(1973).

XBL 784-8054

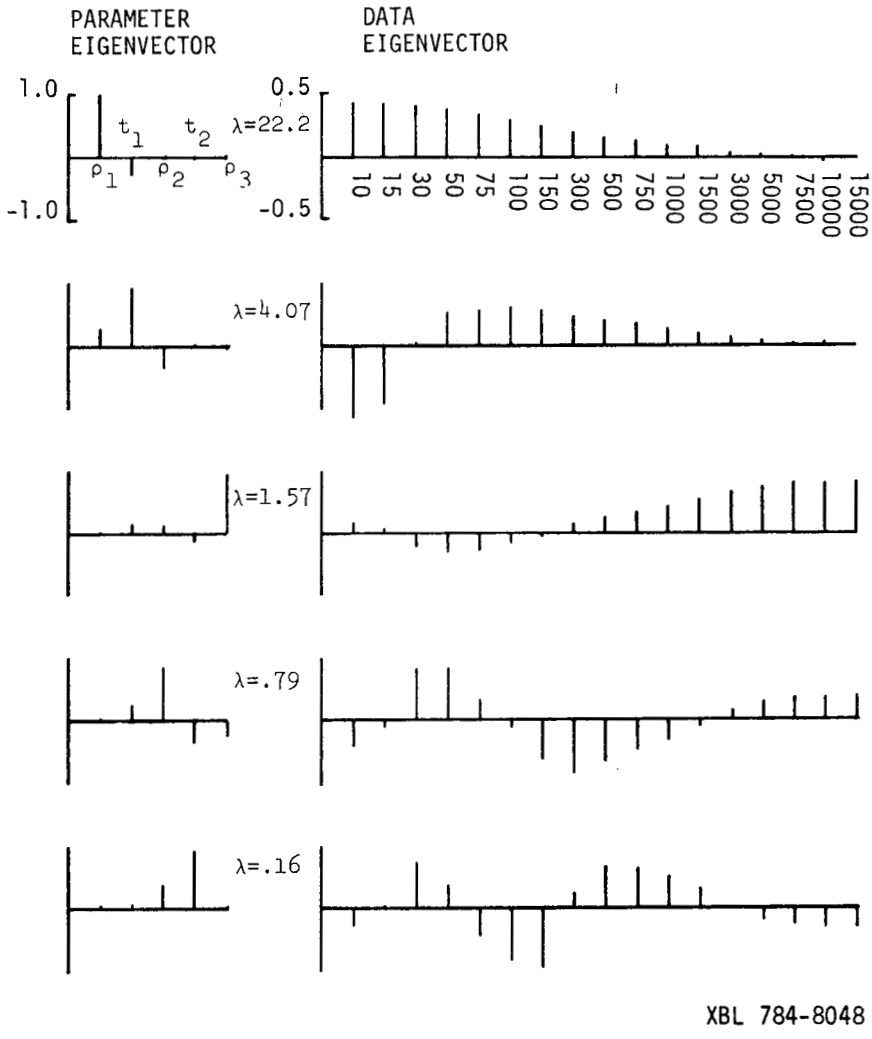

Figure II-15. Recalculated eigenvalues and eigenvectors for model A.

The above examples illustrate the need to include a proper weighting matrix in solving the interpretation problems by inversion methods.

Statistical Evaluation of the Interpreted Model

Once a solution to the inversion problem is found i.e. a model has been determined which best fits the data in the least-squares sense, the next step is to determine its adequacy in fitting the data and calculate the uncertainties in the estimation of model parameters. Here it is useful to consider briefly such an evaluation of the estimated model parameters, the statistical basis for which are described in detail by Bevington (1969). Inman (1975) and Glenn and Ward (1976) have also presented excellent discussion on the application of these statistics in resistivity and electromagnetic sounding problems, repectively.

Adequacy of model interpretation: The adequacy of the model interpretation in describing the data is determined through the use of a chi-squared test (Bevington, 1969) described as follows. The condition that a given set of model parameters is good approximation to the true earth parameters is written as

$$\left(\chi_F^2 \right)_{1-\alpha} \geqslant \left(\chi_F^2 \right)_o \qquad \text{(II-14)}$$

Where $\left(\chi_F^2 \right)_{1-\alpha}$ is the chi-square value at the $(1-\alpha)$ confidence level with $F\,(=N-M)$ degrees of freedom. The experimental or observed value of the chi-square is given by

$$\left(\chi^2_F \right)_o = \frac{\hat{\sigma}^2}{\sigma^2} \qquad \text{(II-15)}$$

Thus when the condition given by equation (II-14) is true, the model parameters are adequate for describing the data. If the condition given by equation (II-14) is violated, either the data have not been fully explained by the theorized model i.e. fit could be improved (resulting in a smaller $\hat{\sigma}^2$) if tried with a more complex model or σ^2 is underestimated.

Model error estimation: The uncertainity in the estimation of model parameters, i.e. the parameter variance, is given as (Bevington, 1969)

$$\sigma^2_{b_j} = \sigma^2 \, (\text{cov}(P)_{jj}) \qquad \text{(II-16)}$$

Where, the parameter covariance matrix, cov(P), is written as

$$\text{cov}(P) = \{ [P]^T [Q]_{\sigma=1} [P] \}^{-1} \qquad \text{(II-17)}$$

Equation (II-16), is the definition for parameter variance for linear solutions only, although it could be taken as an approximate definition for non-linear solutions as well (Bevington, 1969).

The linear dependency between the model parameters, $\text{corr}(b_{ij})$, is given as

$$\text{corr}(b_{ij}) = \frac{\text{cov}(P)_{ij}}{[\text{cov}(P)_{ii}] \, [\text{cov}(P)_{jj}]} \qquad \text{(II-18)}$$

If the value of $corr(b_{ij})$, is near unity, then the parameters b_i and b_j are strongly correlated and nearly linearly dependent. In such a case the individual parameters are not well determined, rather their ratio (if correlation coefficient is +1) or product (if correlation coefficient is -1) can be determined from the data.

Combined Data Interpretation

In an electromagnetic sounding survey, in general, many field quantities are measured for each transmitter-receiver location, i.e. more than one sounding curve is obtained corresponding to $|H_r|$, $|H_z|$, H_r phase and H_z phase field quantities. Each of these sounding curves then can be inverted individually and four independent estimates of earth parameters can be obtained. A much better estimate of earth parameters, however, would be obtained from the joint inversion of these four sounding sets; in such a combined data sample the signal to noise ratio would be greatly enhanced.

Such an improvement in the quality of information contained in the combined data sample can be visualized by examining the relative distribution of information regarding the model parameters in individual sounding sets. Figures II-17 through II-20 give the eigenvalues and associated eigenvectors (the concepts of which have been discussed in detail by Inman et al. (1973)) for the model in Figure II-16 for $|H_r|$, $|H_z|$, H_r phase and H_z phase sounding sets respectively. It should be noted that the model chosen for this study is generally descriptive of the geology of the Grass Valley area. The data eigenvectors which point chiefly in the direction of associated parameter eigenvectors are the data points (frequencies) which have the

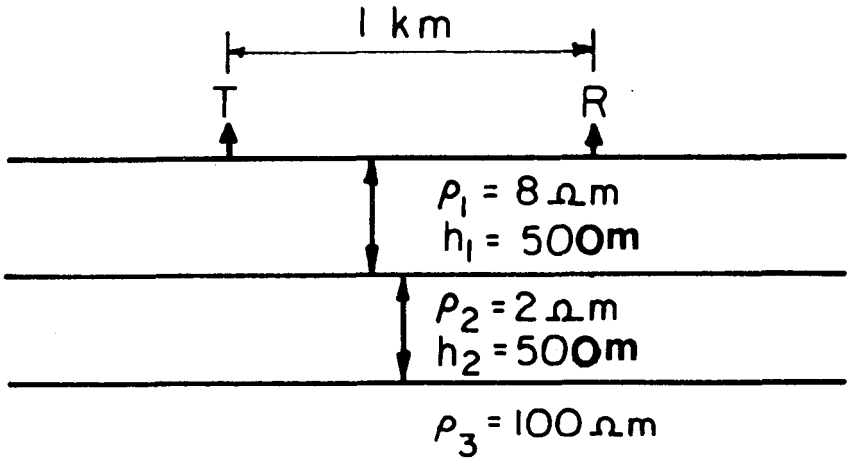

XBL 784-8041

Figure II-16. Three layer earth model used for combined inversion studies.

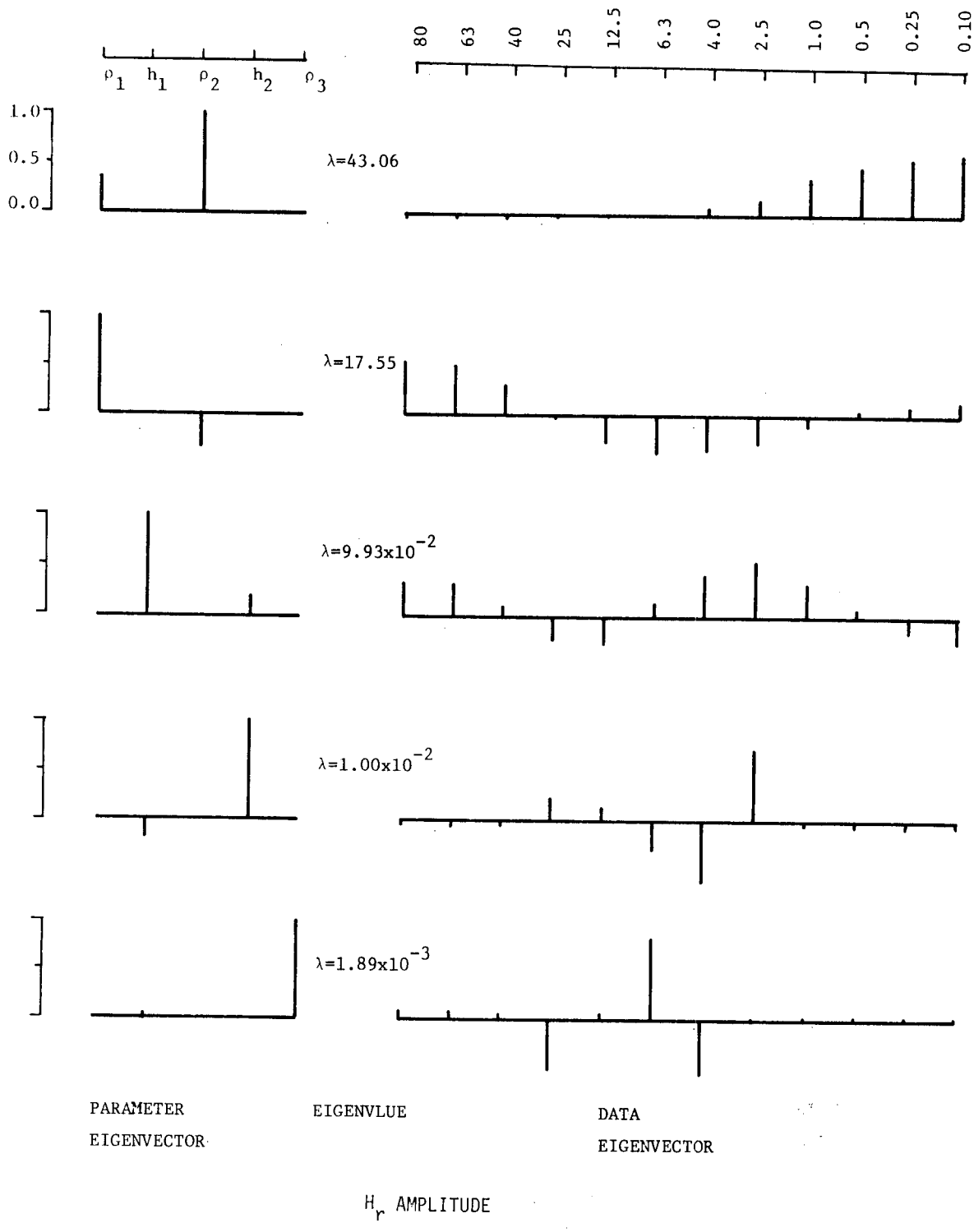

Figure II-17. Eigenvalues and eigenvectors for $|H_r|$ data.

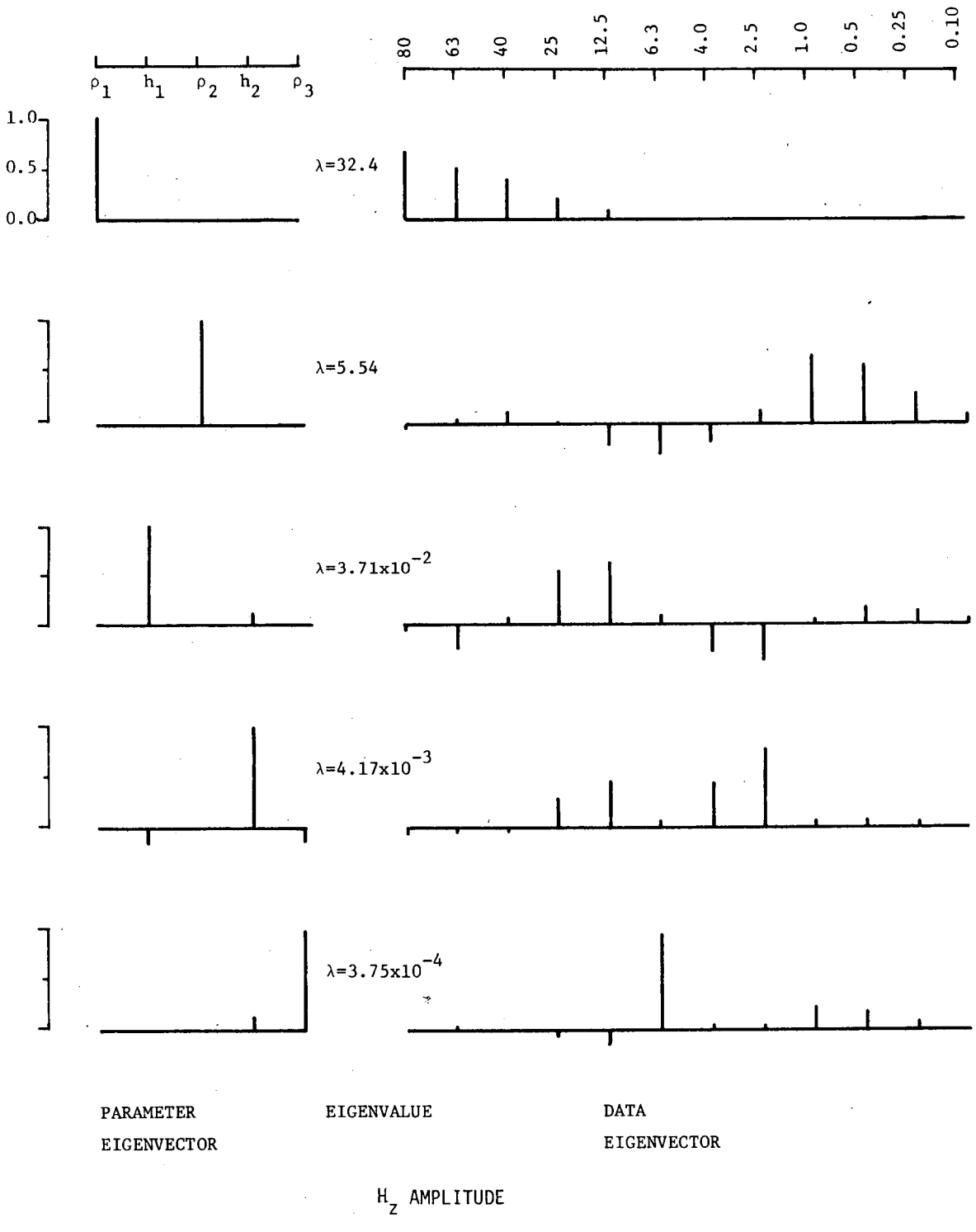

Figure II-18. Eigenvalues and eigenvectors for $|H_z|$ data.

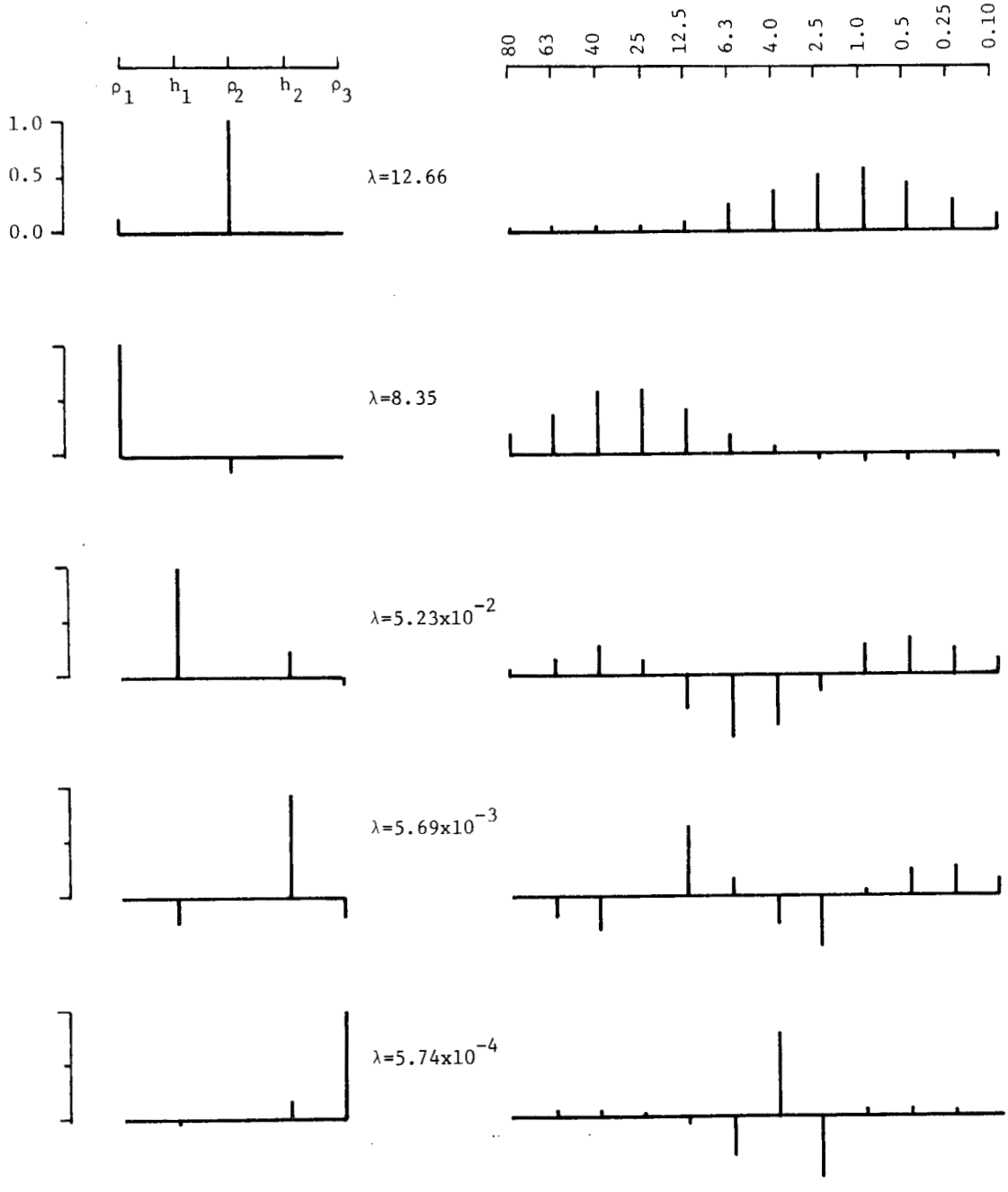

XBL 7712-10980

Figure II-19. Eigenvalues and eigenvectors for H_r phase data.

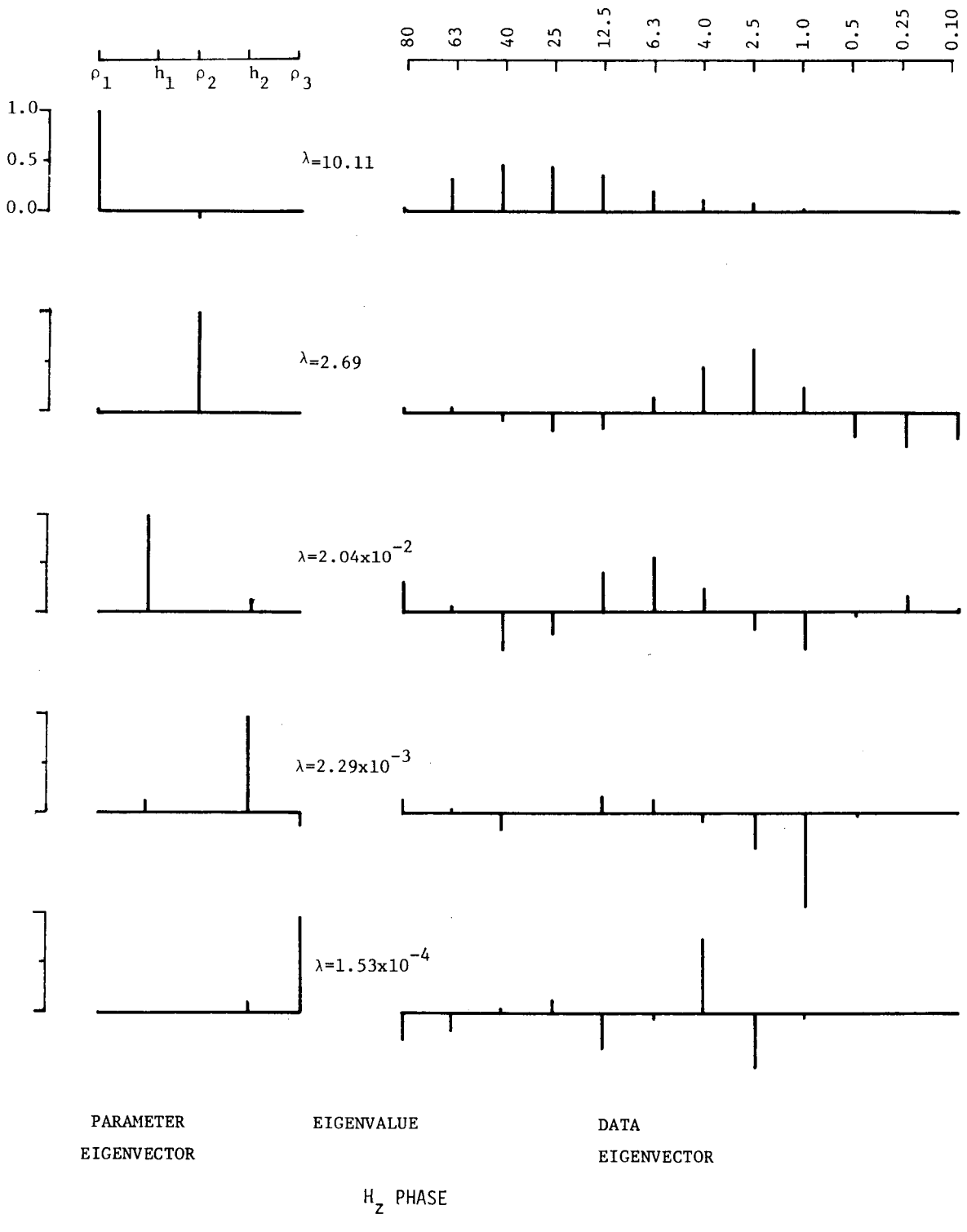

XBL 7712-10981

Figure II-20. Eigenvalues and eigenvectors for H_z phase data.

maximum effect in the resolution of the particular parameter or the combination of parameters. Such a relationship between the data points and the earth's parameters in sounding curves is readily apparent in these figures, e.g. ρ_2 can be seen to be associated with data samples at lower frequencies whereas ρ_1 is assiciated with data samples at higher frequencies. Such a relationship is to be expected from skin depth considerations.

There are many important observations that can be made from the comparative study of the eigenvalues and eigenvectors of the four sounding curves. One of the feature to note from these figures is that the parameter associated with the largest eigenvalue is ρ_2 for horizontal field measurements (Figures II-17 and II-19) whereas it is ρ_1 for vertical field measurements (Figures II-18 and II-20). The parameters associated with the largest eigenvalue are the ones which are found most accurately and determined most quickly by the inversion process (Inman et al., 1973). The advantage of a combined data inversion is most obvious here; in such a data sample ρ_1 and ρ_2 both would be associated with the largest eigenvalue and hence would be determined more accurately than would be possible from individual sounding inversion.

The other important feature to note in this comparative study is that the information about a specific earth parameter is centered around different data points (frequencies) and its spread is different for different sounding curves. So, if for some reason there was large noise in a particular frequency band, its effect would be felt strongly in a particular sounding curve. Effect of such noise, however, would be smoothed out in a combined inversion as the parameter

eigenvector is determined by a least squares fit to many more data points than in an individual inversion.

The above analysis suggests that the earth parameters would be statistically better resolved by a joint inversion of various sounding curves. One of the problem faced in such a combined data inversion, however, is to find a proper weighting matrix to effectively combine the phase and amplitude sets of data for an unbiased inversion. The problem is then to determine the relative error, σ_{r_i}, between two such sets of data. One of the approaches, that can be used to determine such relative errors is outlined below.

At each frequency, the actual quantities measured are the real (x) and imaginary (y) part of the magnetic field and from such measurements, the amplitude (A) and phase (θ) values are calculated from the relations given below

$$A = \sqrt{x^2 + y^2} \qquad \text{(II-19)}$$

and

$$\theta = \tan^{-1} \frac{y}{x} \qquad \text{(II-20)}$$

Hence, if we estimate the errors in the measurement of x and y, the corresponding errors in A and θ can be calculated from the propagation of error analysis.

If σ_x and σ_y are the respective errors in the measurement of x and y then the respective errors σ_A and σ_θ in the amplitude and phase data are given as (Bevington, 1969)

$$\sigma_A^2 = \sigma_x^2 \left(\frac{\delta A}{\delta x}\right)^2 + \sigma_y^2 \left(\frac{\delta A}{\delta y}\right)^2 \qquad \text{(II-21)}$$

and

$$\sigma_\theta^2 = \sigma_x^2 \left(\frac{\delta \theta}{\delta x}\right)^2 + \sigma_y^2 \left(\frac{\delta \theta}{\delta y}\right)^2 \qquad \text{(II-22)}$$

Substituting the values of partial derivatives in the above equations, we get

$$\sigma_A^2 = \sigma_x^2 \cos^2\theta + \sigma_y^2 \sin^2\theta \qquad \text{(II-23)}$$

and

$$\sigma_\theta^2 = \frac{1}{A^2}\left(\sigma_x^2 \sin^2\theta + \sigma_y^2 \cos^2\theta\right) \qquad \text{(II-24)}$$

If we assume accuracies of 1% in the measurements of x and y i.e. $\sigma_x = .01x$ and $\sigma_y = .01y$, then the maximum (at $\theta = 45°$) errors in amplitude and phase values are calculated to be

$$\sigma_A = .01A \qquad \text{(II-25)}$$

and

$$\sigma_\theta = .4° \qquad \text{(II-26)}$$

Thus, if the errors in the measurement of real and imaginary part of the data are assumed to be equal, the corresponding relative errors in the transformed data i.e. in phase and amplitude data would be .4° and 1% respectively. Such an error relationship between the phase and amplitude sets of data then can conveniently be used in forming the weight matrix for the joint inversion. A similar analysis

for the determination of relative error between tilt angle and ellipticity data must be persued, if two such sets of data are to be jointly interpreted.

Grass Valley Results

Data Inversion

Line EE', along which the electromagnetic sounding survey is made, extends across Grass Valley from southeast to northwest, passing about 1km NW of Leach Hot Springs (Figure II-5). The line is oriented at approximately 45° to the strike of the local basin and range structure. The general bedrock topography along the line can be inferred from both the gravity and P-Wave profile data in Figure II-21. The electromagnetic sounding data is confined from 2W to 9W along this line.

The observed field data for eight of the sounding stations occupied in this survey are tabulated in Appendix B and are illustrated in Figures II-22 through II-29. The transmitter and receiver locations are noted at the top of these figures (e.g. T3-R4 indicates transmitter location at 3W and receiver location at 4W). The vertical bars displayed in these figures span ±1 standard deviation around the mean value of the data. The error and the mean value of the data have been calculated from the repeated set of readings taken at each frequency, as explained earlier. These errors then represent the sferic noise in the data.

As was advocated earlier, the four sets of observed sounding data have been inverted simultaneously to obtain a "best-fit" model. The observed errors of the data constituted the weighting matrix for

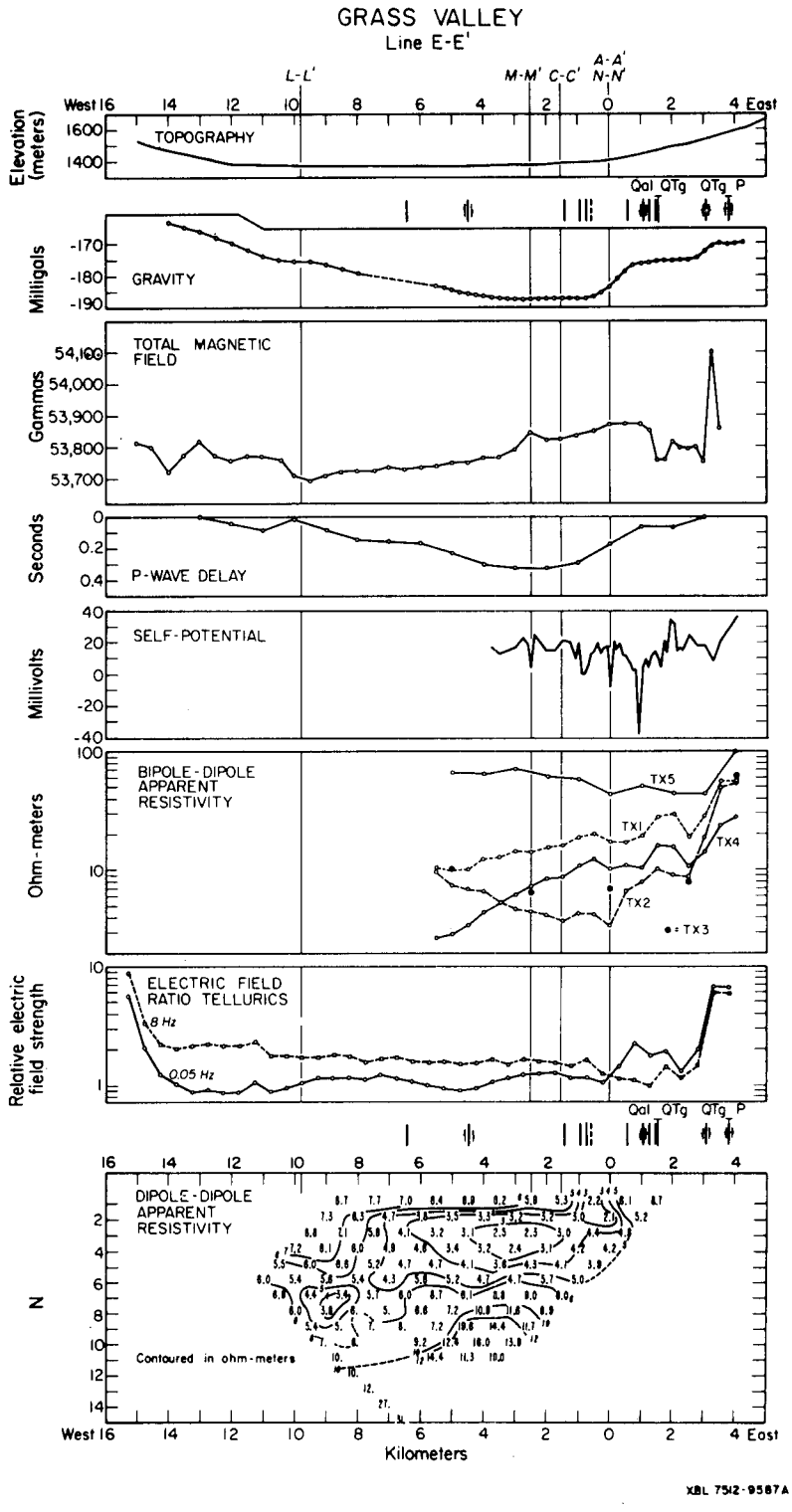

Figure II-21. Geophysical data profile composite for Line E-E' (After Beyer et al., 1976).

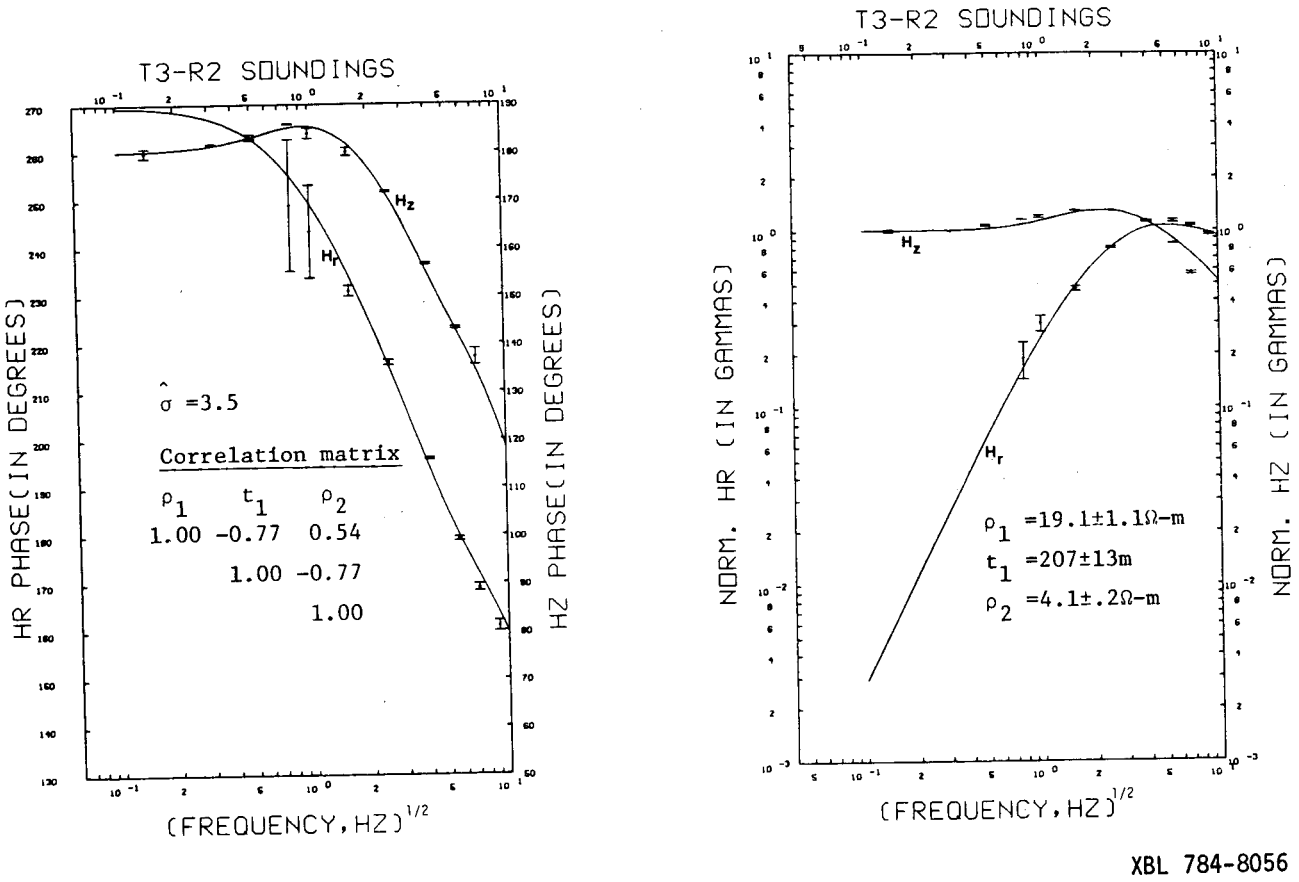

Figure II-22. T3-R2 sounding data and interpreted earth model.

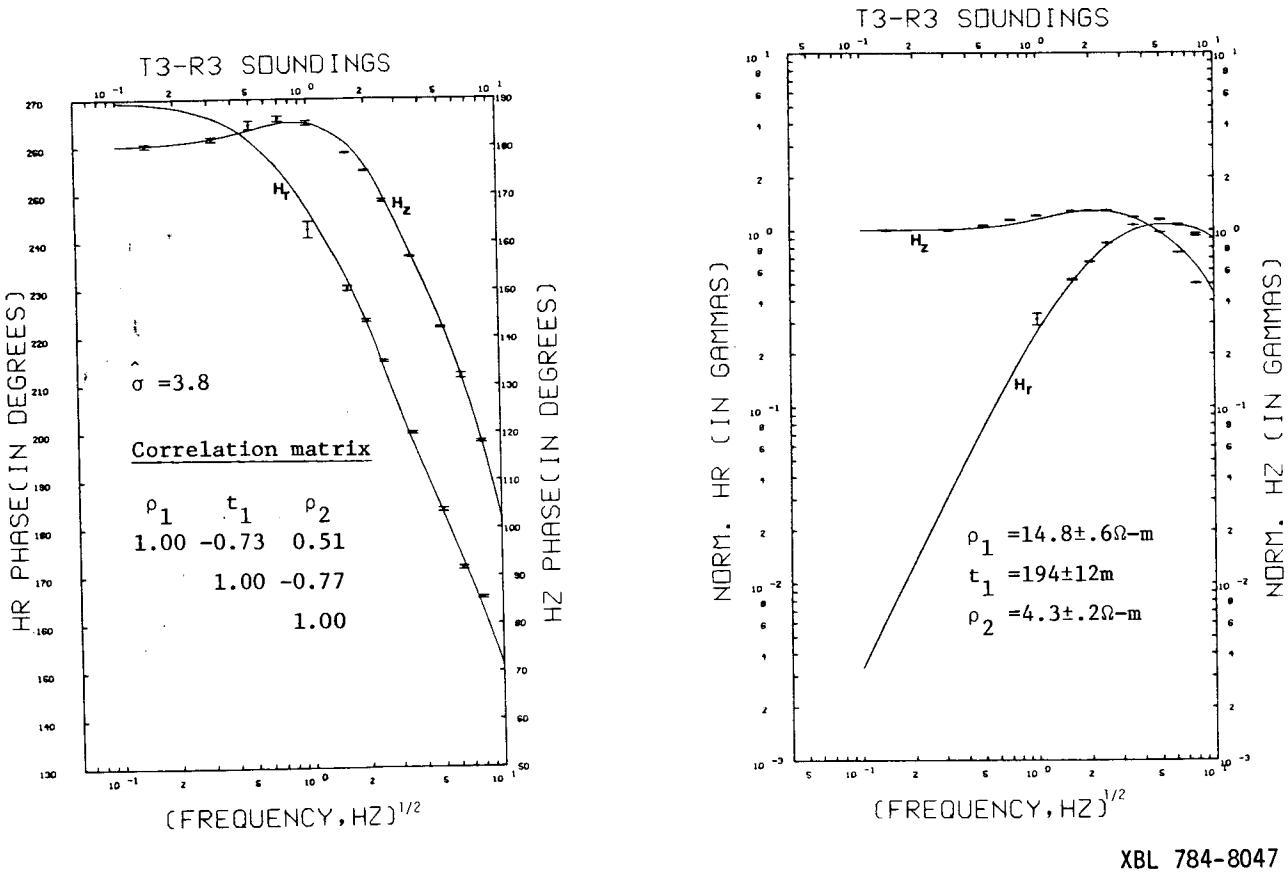

Figure II-23. T3-R3' sounding data and interpreted earth model.

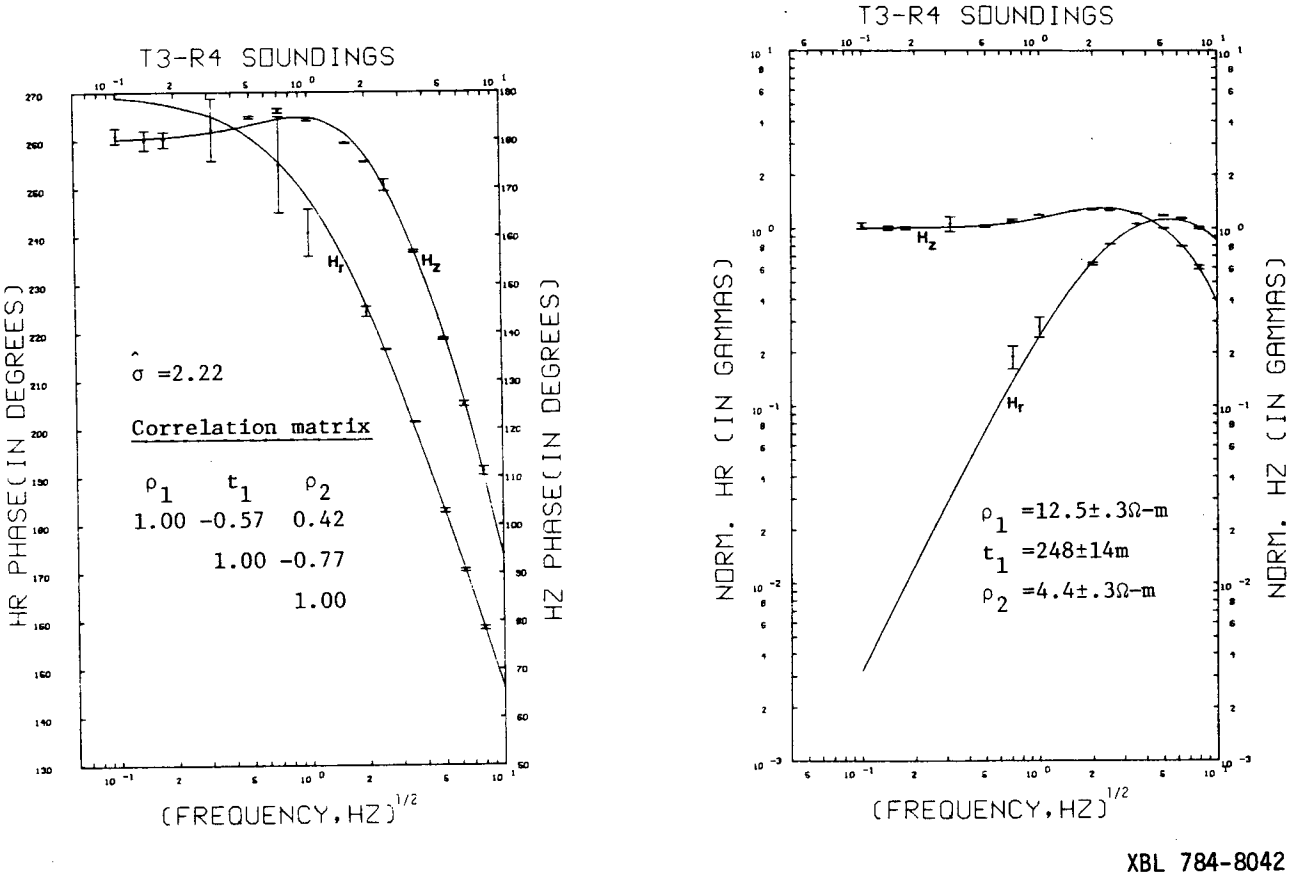

Figure II-24. T3-R4 sounding data and interpreted earth model.

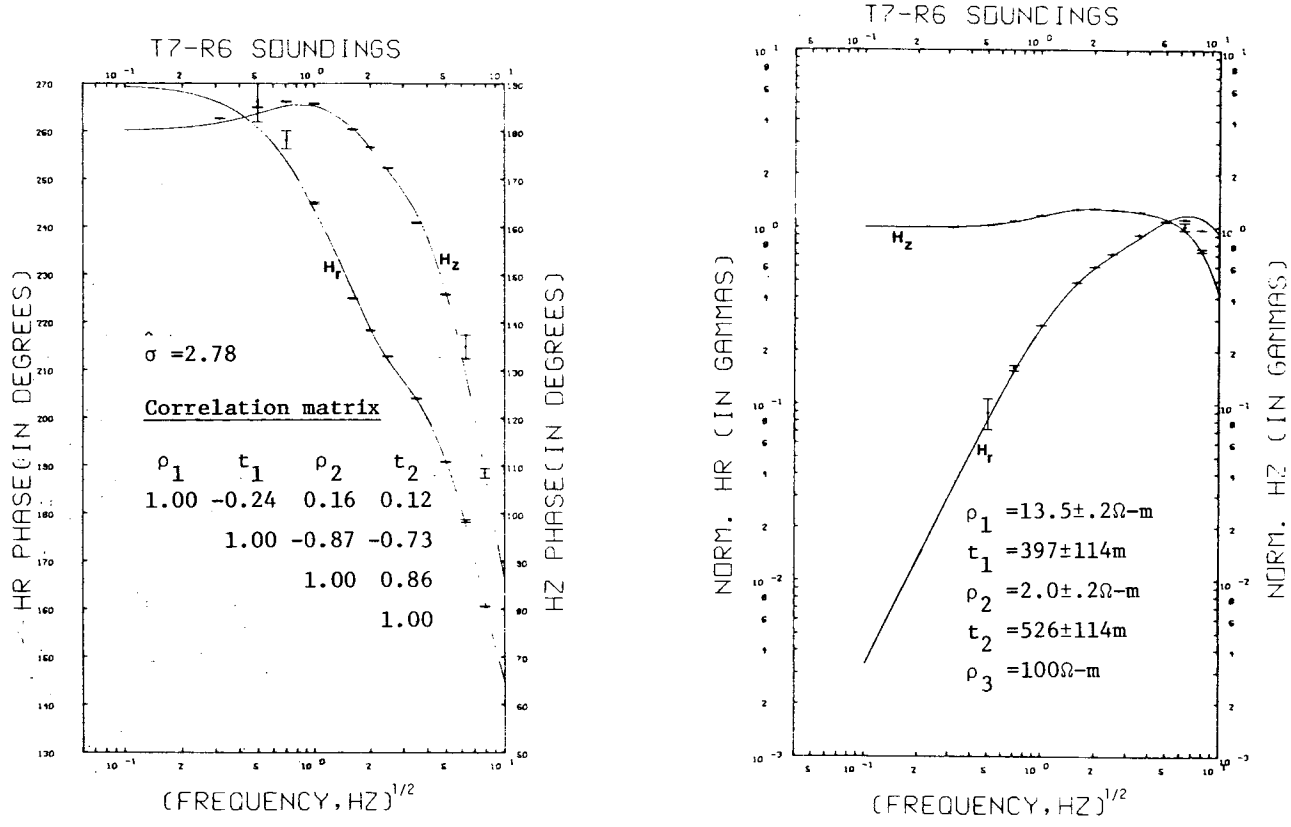

Figure II-25. T7-R6 sounding data and interpreted earth model.

XBL 784-8044

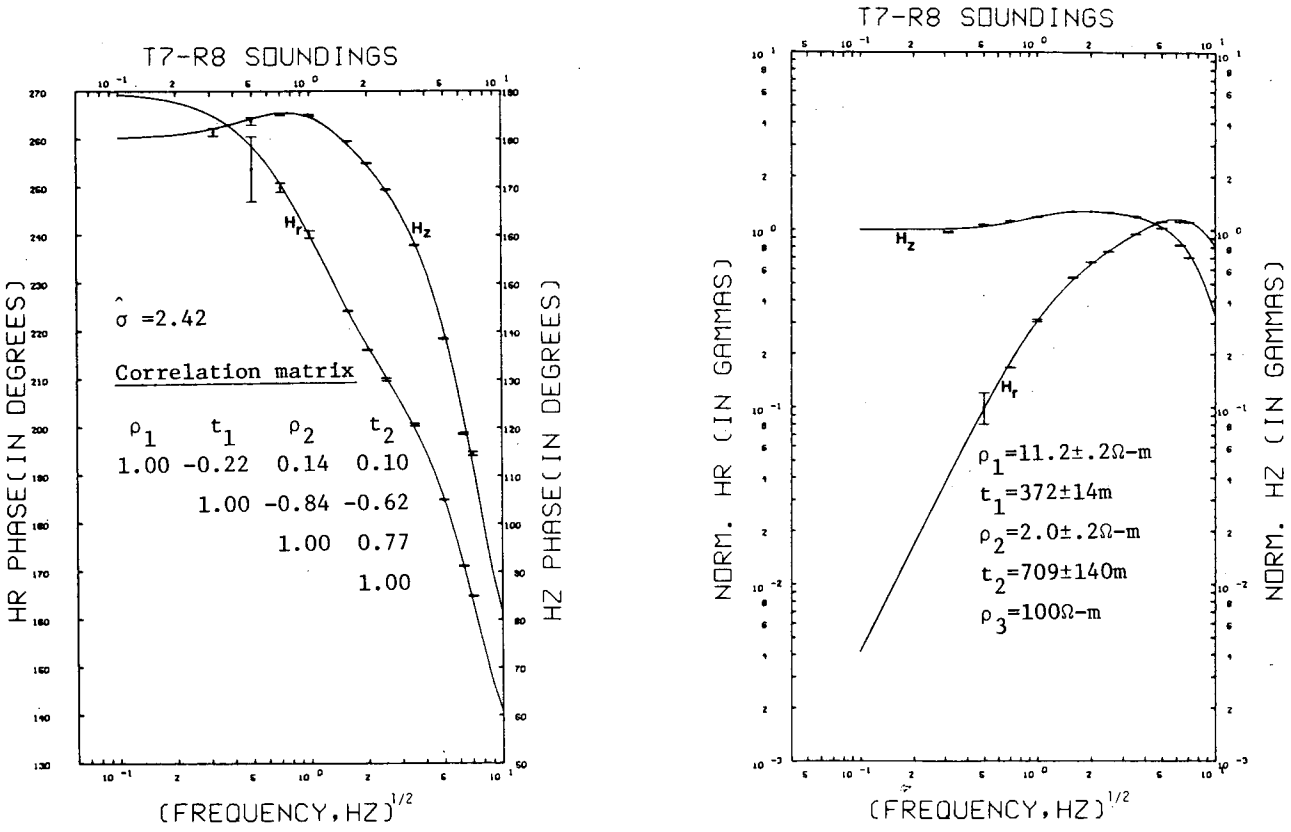

XBL 784-8036

Figure II-26. T7-R8 sounding data and interpreted earth model.

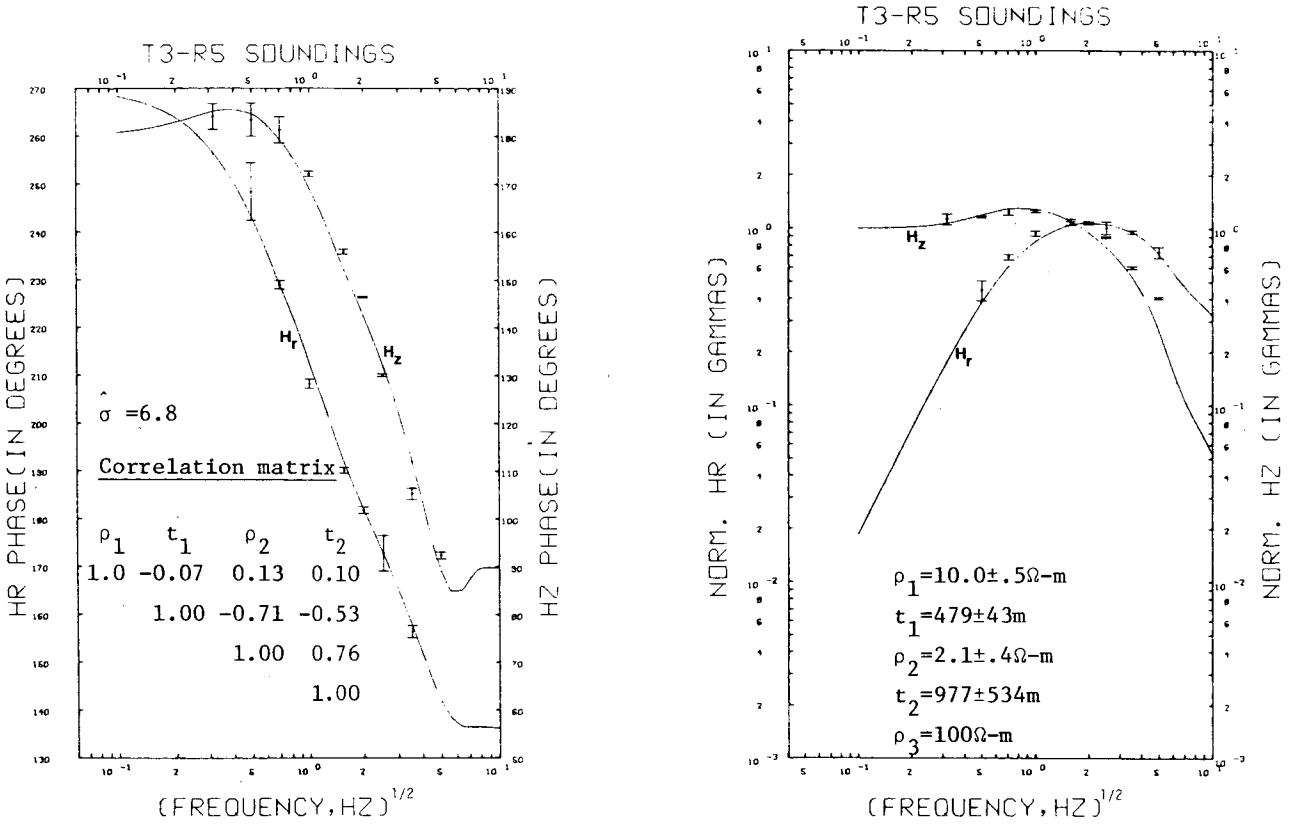

XBL 784-8037

Figure II-27. T3-R5 sounding data and interpreted earth model.

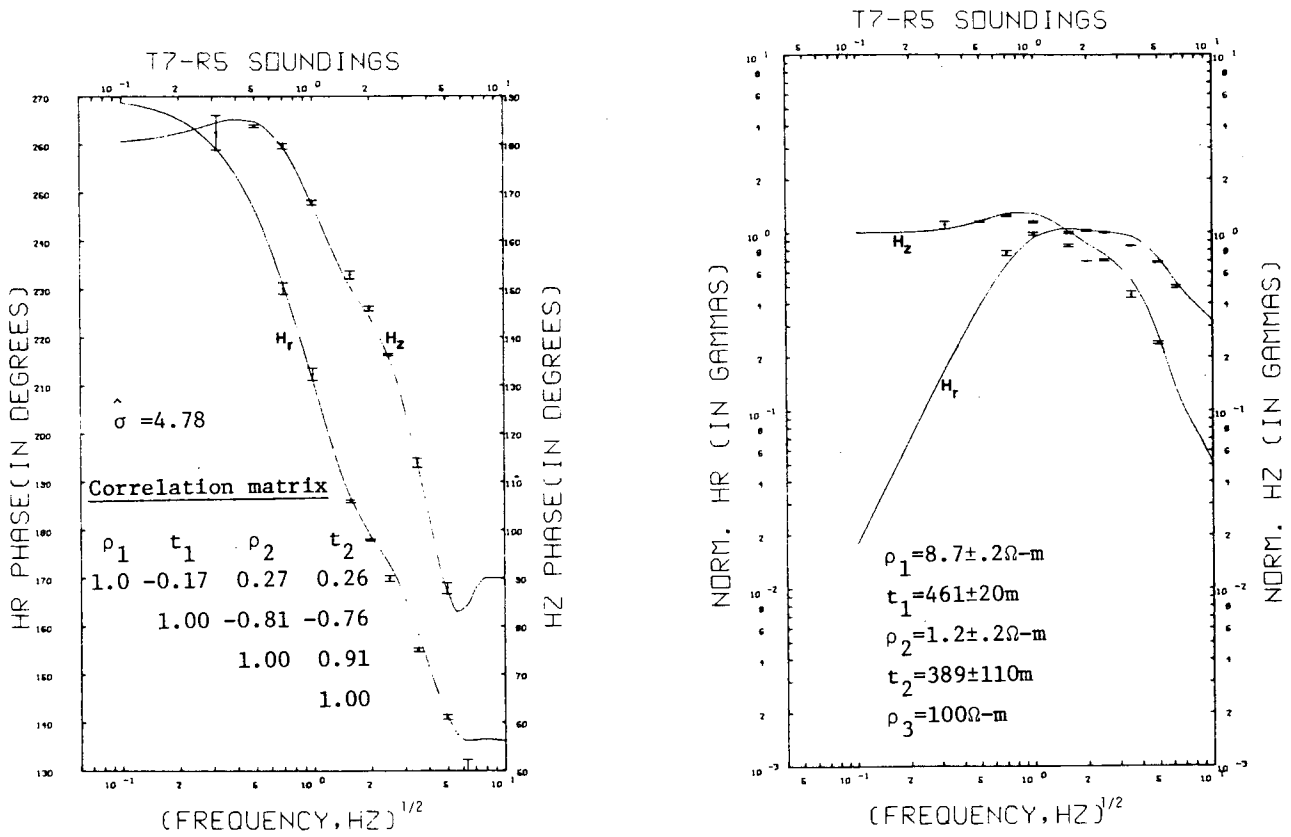

Figure II-28. T7-R5 sounding data and interpreted earth model.

XBL 784-8032

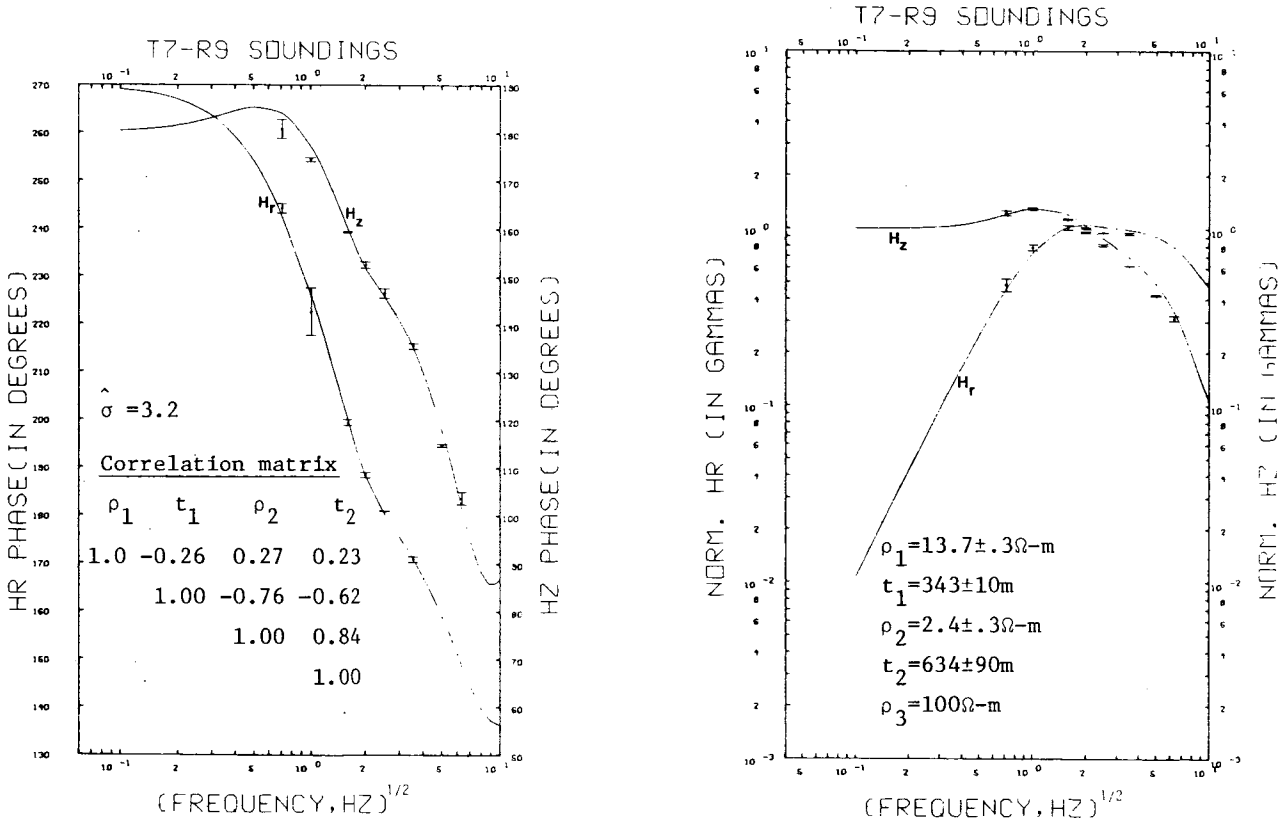

Figure II-29. T7-R9' sounding data and interpreted earth model.

XBL 784-8046

the inversion problem. Some of the poor data points (with rather large noise) were excluded from the data set as inclusion of them only degrades the calculated statistical confidence on the parameters without helping much in resolving them.

The first task in the inverse interpretation of a set of data is to select an initial estimate of the earth model to start the inversion process. The models here were selected from consideration of the geology of the area. Some preliminary curve matching and the available resistivity data aided such a model selection. The data clearly indicated presence of a thick conducting layer overlying and underlying more resistive layers. Such a three layer model was then initially tried to fit each set of sounding data. From the preliminary inversion results, it became apparent that the basement resistivity could not be well resolved from the data. In such a situation, it is best to remove the parameter from the list of unknown variables (model parameters) as it otherwise slows down the convergence rate considerably. So, in the three layered inversion, the basement resistivity was fixed at a 100 ohm-m value and a minimum solution was obtained. An examination of the resulting parameter statistics indicated that the thickness of the second layer was not well resolved by some of the sounding data. These sounding data then were interpreted in terms of a two layered model only. Starting with different initial estimates of the models confirmed that the interpreted models were indeed the minimum solution.

The theoretical response curves for the interpreted earth models are drawn as solid lines in Figures II-22 through II-29. The values

of the interpreted model parameters along with their estimated accuracies (1 standard deviation) and the parameter correlation matrix are noted in these figures. The problem standard deviation $\hat{\sigma}$, which is a measure of goodness of fit of the model with the data, is also shown in these figures. Ideally, if the model describes the data perfectly, the value of $\hat{\sigma}$ would be close to 1 for the weighted least squares solution. The calculated value of $\hat{\sigma}$, here, however are seen to be larger than 1 for all the interpretations. These large values of $\hat{\sigma}$ suggest that the data may also have been contaminated with noises from other sources (e.g. misorientation of coils, error in spacing measurement etc.) rather then just the sferic noises as assumed in the solution here. Effects of these noises on the interpretation, however, are not examined here. The large value of $\hat{\sigma}$ could also be attributed to the lateral changes in the geology.

In general, the fit between the observed and the model data, as visualized in Figures II-22 through II-29 seems to be fairly good except for T3-R5 (Figure II-27) and T7-R5 (Figure II-28) data. The rather poor fit for T3-R5 and T7-R5 data indicates the inadequacy of the 3-layered model interpretation attempted here. Attempts to improve the fit with more complex model (more than 3 layers) were unsuccessful for lack of enough data points. The gross misfit between the observed data and the model response in these two cases, however, may also be attributed to the fact that the structure is not one-dimensional. A fault is suspected to be located near station 5W; layered interpretation may be an inaccurate approximation to the true subsurface structure.

The calculated parameter uncertainities, as noted in the inter-

pretation results presented here, are generally small indicating good resolution of model paremeters from the sounding data. In placing confidence on the calculated parameter standard deviations, one should always examine the parameter correlation matrix. If two parameters are strongly correlated (correlation coefficient > .97) then the standard deviation given by equation (II-16) will be larger than the actual uncertainities. In such a case, it may then be necessary to put a bound on one of the parameters from some added information (e.g. some other geophysical data) which then would restrict the possible range of other parameter. A more detailed discussion on this topic has been presented by Inman (1975). The correlation matrix for the Grass Valley interpreted model indicate that no two parameters are strongly correlated, thus the parameter standard deviations shown in Figures II-22 through II-29 may be taken to be reasonably accurate.

Resistivity Profile

The resistivity profiles of line EE' as obtained from the interpretation of 1km and 2km (spacing between the transmitter and receiver) combined ($|Hr|$, $|Hz|$, H_r phase and H_z phase) parametric sounding data, are shown in Figures II-30A and II-30B respectively. The interpreted model parameters and their estimated errors(± 1 standard deviation) are illustrated in these figures. The two transmitter positions occupied in the survey are located at 3W and 7W respectively.

As is seen from the resistivity sections, a massive conductive zone underlies a more resistive surface layer. A comparision with the geological section of the area (Figure II-3) indicates that the upper resistive layer is likely to be correlated with Quaternary

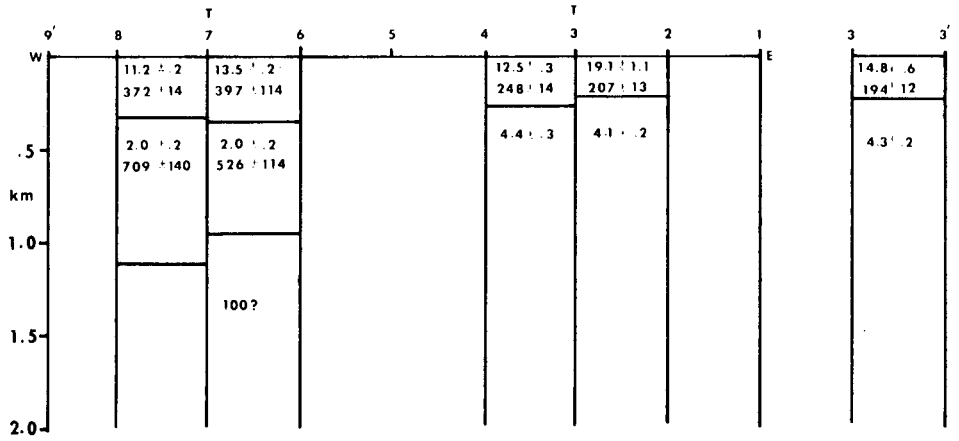

Figure II-30A. Resistivity section along Line E-E' obtained from interpretation of 1km sounding data.

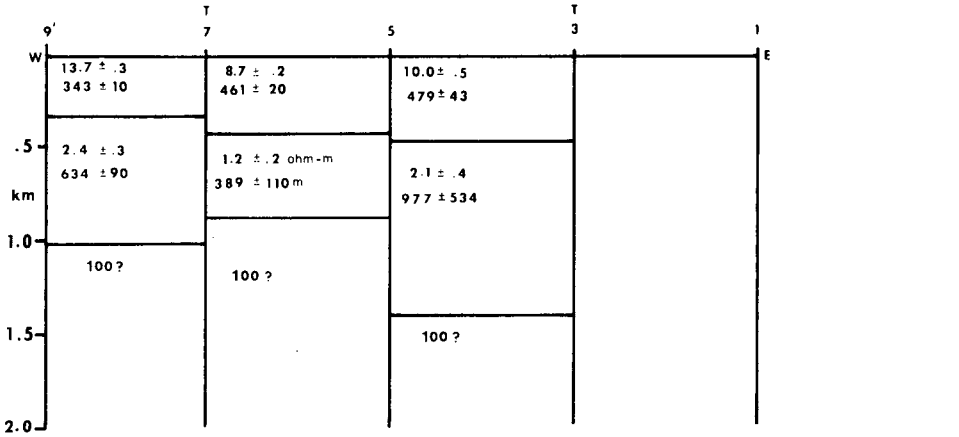

XBL 784-8029

Figure II-30B. Resistivity section along Line E-E' obtained from interpretation of 2km sounding data.

alluviums, the middle conductive layer is likely to be correlated with Tertiary sediments and the resistive basement may correspond to the Paleozoic bed rocks.

Electromagnetic soundings are more sensitive to the presence of deep, a horizontal boundary, if the data is taken at a separation (between transmitter and receiver) large in comparison to the depth of that boundary. This point is obvious when we compare the two interpreted sections obtained with the 1km and 2km spacings. In the western section (west of 5W), where the depth to the basement is on the order of 1 km, both 1km and 2km sounding data are able to resolve this boundary. In the eartern section, on the other hand, only 2km sounding data is able to resolve this depth, which is presumably on the order of 1.5 km.

Electromagnetic sounding is not sensitive to the resistivity of basement rocks lying beneath a more conductive sendimentary section. The relative fit between the observed data and the theoretical model data does not change, even if a basement resistivity of 10 ohm-m is used at greater depths. The fit however deteriorates for values less than 10 ohm-m, indicating that the resistivity of the basement rock is at least 10 ohm-m or greater. Such a difficulty in estimating the true resistivity of a layer lying underneath a more conductive section comes from the fact that the induced current tend to concentrate in the more conductive region. To effectively force the current into the resistive basement i.e. to see a larger effect on the data, a transmitter-receiver spacing many times the depth to the basement would be required. Similar problems in estimating the resistivity

of a resistive basement using the dipole-dipole method has been noted by Beyer (1977). In surveying over the same line, a dipole separation of even 10km was not sufficient to get a good estimate of the resistivity of this relatively resistive basement. Spacings of this order were also required to estimate the thickness of the overlying conductor using the dipole-dipole method. With the electromegnetic technique, this thickness was as well resolved as with resistivity but the transmitter-receiver separation had only to be 2km.

Discussion and Comparison of Results

In electromegnetic sounding interpretation, the subsurface structure is assumed to be isotropic and horizontally layered, whereas in reality this seldom is the case. The resistivity section thus obtained represents an "average" value of resistivities and thicknesses of the subsurface structure between the transmitter and receiver locations. Such an averaging aspect is apparant in the two resistivity sections presented earlier (Figures II-30A and II-30B) which are obtained with two different spacings. The two sections are not significantly different, but they do have different values of resistivities and thicknesses over a common area (e.g. between 3W-4W and 3W-5W) and these are the result of lateral changes in the geology. From the comparison of the two sections, the following qualitative interpretation can be made.

a) The surface layer is most conductive and thick around the center of the section (around station 5W) and it gradually thins out and becomes more resistive on either side.

b) The middle layer is also most conductive around the center of

the section and the resistivity of this layer gradually increases away from the center. A sharp change in the thickness of the second layer around station 5W would be indicative of an easterly dipping fault, causing the basement to slip down to the east of 5W. The presence of this fault could also explain the low resistivity of the second layer noted around station 5W.

Such an interpretation of the surveyed area is in general agreement with other geophysical data summarized in Figure II-21. The telluric data clearly shows low resistivity around station 5W. The dipole-dipole resistivity data is shown in Figure II-31 and a 2D-interpreted model is shown in Figure II-32. From the comparison of Figure II-30 and Figure II-32, the resistivity sections obtained from electromagnetic sounding data are very similar to those in the direct current resistivity interpreted model.

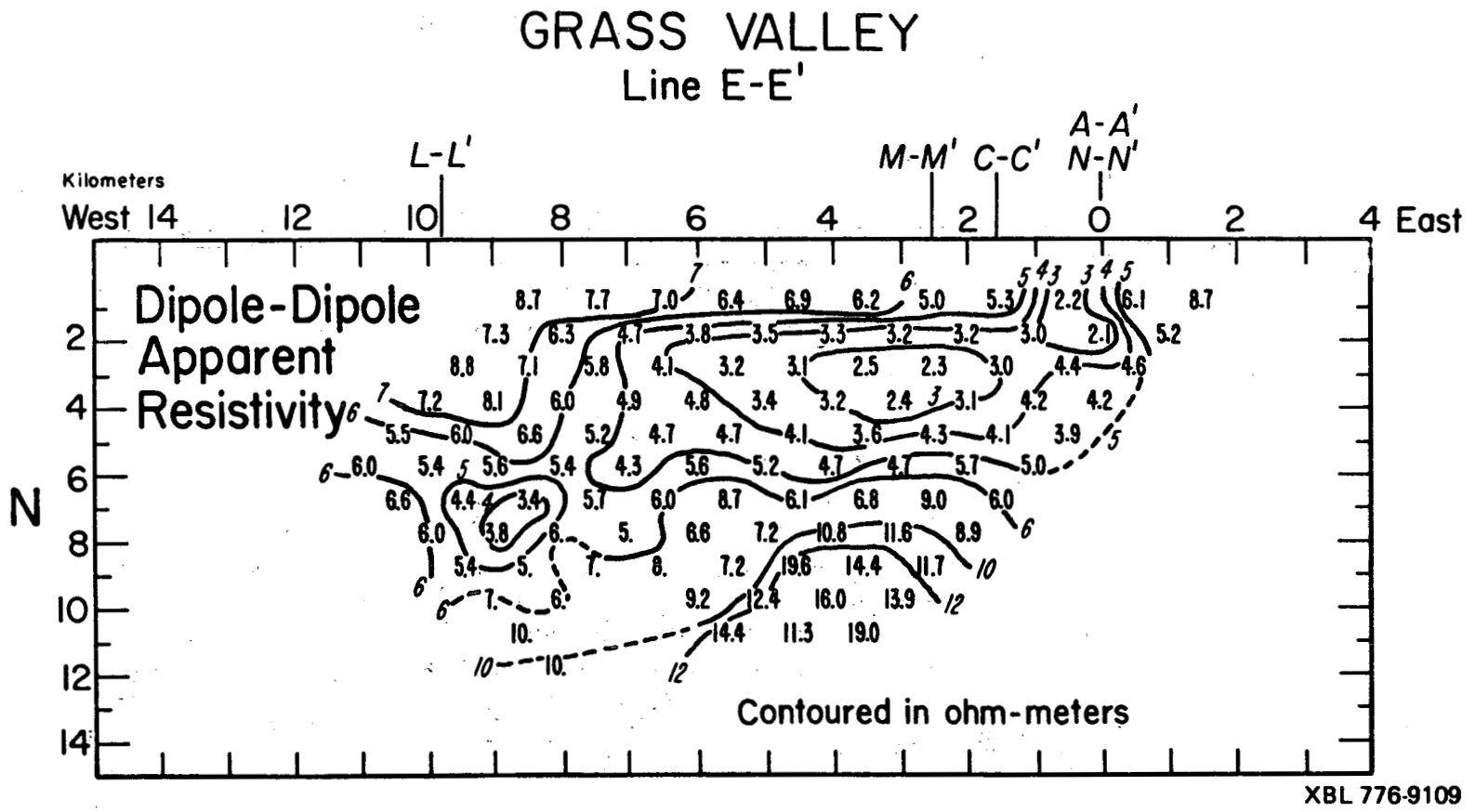

Figure II-31. Field data dipole-dipole apparent resistivity pseudo-section for 1km dipoles along Line E-E' (After Beyer et al., 1976).

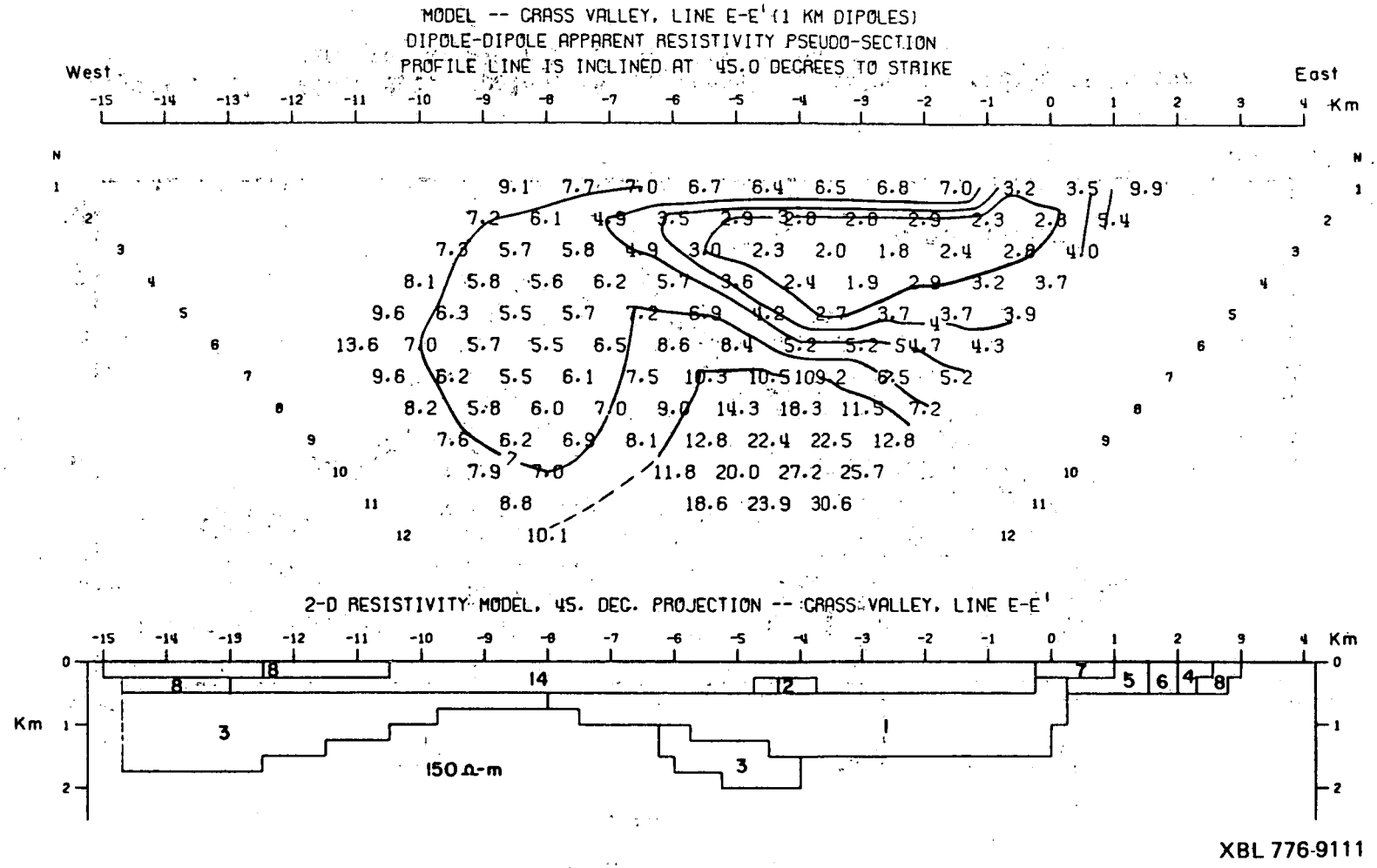

XBL 776-9111

Figure II-32. Two-dimensional resistivity model and resultant dipole-dipole apparent resistivity pseudo-section along Line E-E' (After Beyer et al., 1976).

8. Summary and Conclusions

The objective of the present study has been to investigate the capability of an electromagnetic sounding system in mapping the resistivity structure of conductive sedimentary basins. For this purpose, a prototype electromagnetic sounding system was designed and built and a depth sounding survey was carried out in Grass Valley, Neveda. A current carrying loop, with a moment of the order of 10^5 MKS units was used as a transmitter and a 3-component SQUID magnetometer was used as a receiver. The amplitude and phase of horizontal and vertical components of the magnetic fields were recorded in the survey. The signals were stacked and analyzed in the field by a preprogrammed digital complex signal analyzer. Telephone wire links were provided to carry the phase reference from the transmitter to the receiver. Measurements were made at several descrete frequencies covering a frequency band of 0.01 Hz to 100 Hz. Spacings of 1 and 2 km were used for the depth soundings and a continuous coverage along a survey line, 8 km long, was made.

An automated inversion technique was used to interpret the sounding curves in terms of multi-layered earth model. In general, the fit between the observed data and the computed data was found to be fairly good. The interpreted resistivity profile of the surveyed line is in general agreement with the geology of the area and it matches very will the interpreted dipole-dipole resistivity model.

The results of this experimental survey clearly indicate that inductive electromagnetic depth sounding systems are as capable of mapping resistivity structure as the conventional resistivity systems.

This survey also demonstrated the fact that a much lower transmitter-receiver spacing is needed in an electromagnetic depth sounding survey than in a conventional dipole-dipole resistivity survey for the same effective depth of exploration. A smaller spacing not only reduces the source power requirement, but it also makes electromagnetic data less subject to noise caused by lateral inhomogeneities that add considerable complexity in a comparable resistivity sounding. This Loop-source electromagnetic survey was also conducted without the need of implanting electrodes and with very low power requirement (~72 watts).

REFERENCES

Becker, A., 1967, Design Formulas for Electromagnetic Sensing Coils: Geoexploration, v.5, p. 81-88.

Birch, F., 1943, Elasticity of igneous rocks at high temperatures and pressures: Geol. Soc. America Bull., v. 54, p. 263-286.

Birch, F., and Clark H., 1940, The thermal conductivity of rocks and its dependence upon temperature and composition: Am. Jour. Sci., v. 238, p. 529-558 and p. 613-635.

Bevington, P. R., 1969, Data reduction and error analysis for the physical sciences: McGraw Hill Book Company, Inc., New York.

Beyer, J. H., 1977, Telluric and d.c. resistivity techniques applied to the geophysical investigation of Basin and Range Geothermal Systems: Ph. D. thesis, University of California, Berkeley.

Beyer, H., Dey, A., Liaw, A., Majer, E., McEvilly, T.V., Morrison,H. F., and Wollenberg, H., 1976, Preliminary open file report: geological and geophysical studies in Grass Valley, Nevada, LBL-5262.

Beyer, H., Morrison, H. F., and Dey, A., 1975, Electrical exploration of geothermal systems in Basin and Range Valleys of Nevada: Proceedings: Second U.N. Symposium on the Development and use of Geothermal Resources, May 1975, p. 889-894.

Clarke, J., 1974, Josephson Junction Detectors: Science, v. 184, p. 1235.

Combs, J., and Wilt, M., 1975, Telluric mapping, Telluric profiling, and self-potential survey of the Dunes Geothermal Anomely, Imperial Valley, California: Proceedings: Second U.N. Symposium on the Development and use of Geothermal Resources, May 1975, p. 917-928.

Cormy, Gerard and Muse, Louis, 1975, Utilization of MT-5-EX in Geothermal Exploration: Proceedings: Second U.N. Symposium on the Development and use of Geothermal Resources, May 1975, p. 933-936.

Garcia, D.S., 1975, Geoelecric study of the Cerro Prieto Geothermal area, Baja, California, Mexico: Second U.N. Symposium on the Development and use of Geothermal resources, May 1975, p. 1009-1011.

Ghosh, M. K., and Hallof, G. 1973, Loop-loop EM depth sounding method for delineating geothermal and permafrost zones: Abstract: Geophysics, v. 38, p. 1201.

Glenn, W. E., Ryu, J.,Ward, S.H., peeples, J. J., and Phillips, R. J., 1973, The inversion of vertical magnetic dipole sounding data: Geophysics, v.38, p. 1109-1129.

Glenn, W. E., and Ward, S. H., 1976, statistical evaluation of electrical sounding methods. Part I: Experiment design: Geophysics, v.41, p. 1207-1221.

Grant, F. S., and West, G. F., 1965, Interpretation Theory in Applied Geophysics: McGraw Hill Book Co., Inc., New York.

Gupta, M. L., Singh, S. B., and Rao, G. V., 1975, Studies of Direct Current Resistivity in the Puga Geothermal Field, Himalayas, India: Proceedings: Second U.N. Symposium on the Development and use of Geothermal Resources, May 1975, p. 1029-1036.

Harthill, N., 1976, Time domain Electromagnetic sounding: IEEE Trans. on Geoscience Electronics, v.GE-14, p. 256-260.

Hermance, J. F., Thayer, R. E., and Bjornsson, A., 1975, The Telluric-Magnetotelluric Method in the Regional Assessment of Geothermal Potential: Proceedings: Second U.N. Symposium on the Development and use of Geothermal Resourses, May 1975, p. 1037-1048.

Hochstein, M. P., 1975, Geophysical Exploration of the Kawah Kamojang Geothermal Field, West Java: Proceedings: Second U.N. Symposium on the Development and Utilization of Geothermal Resources, Pisa, Proceedings (Geothermics, Special Issue 2), v.2, pt. 1, p. 487-491.

Hoover, D. B., and Long, C. L., 1975, Audio-Magnetotelluric Methods in Reconnaissance Geothermal Exploration: Proceedings: Second U.N. Symposium on the Development and use of Geothermal Resources, May, 1975, p. 1059-1064.

Inman, J. R., 1975, Resistivity inversion with Ridge regression: Geophysics, v.40, p. 798-817.

Inman, J. R., Ryu, J. and Ward, S. H., 1973, Resistivity inversion: Geophysics, v.38, p. 1088-1108.

Jackson, D. B., and Keller, G. V., 1972, An Electromagnetic sounding survey of the summit of Kilauea Volcano, Hawaii: J. G. R. v.77, p. 4957-4967.

Jiracek, G. R., Smith, C., and Dorn, G. A., 1975, Deep Geothermal Exploration in New Mexico using Electrical Resistivity: Proceedings: Second U.N. Symposium on the Development and use of Geothermal Resources, May, 1975, p. 1095-1102.

Jones, A., 1969, Spiral - A new algorithm for non-linear parameter estimation using least squares: The Computer Journal, v.12, p. 301-308.

Jupp, D. L. B., and Vozoff, K., 1975, Stable interative methods for the inversion of geophysical data: Geophys. J. R. astr. Soc., v.42, p. 957-976.

Keller, G. V., 1970, Induction method in prospecting for hot water: Geothermics-Special Issue 2.

Keller, G. V., and Frischknecht, 1966, Electrical Methods in Geophysical Prospecting: Pergamon Press, New York.

Keller, G. V., Furgerson, R., Lee, C. Y., Harthill, N. and Jacobson, J., 1975, The dipole Mapping Method: Geophysics, v.40, p. 451-472.

Keller, G. V., and Rapolla, A., 1976, A comparison of two electromagnetic probing technique: IEEE Trans. on Geoscience Electronics, v. GE-14, p. 250-256.

Marquadt, D. W., 1963, An algorithm for least squares estimation of non-linear parameters: Journal of the society for Industrial and Applied Mathematics, v.2, p. 431.

McNitt, J. R., 1975, Summary of United Nations geothermal exploration experience, 1965 to 1975: Proceedings: Second U.N. Symposium on the Development and use of Geothermal Resources, May 1975, p. 1127-1134.

Murase, T. and McBirney, A. R., 1973, Properties of some common igneous rocks and their melts at high temperatures: Goel. Soc. America Bull., v. 84, p. 3563-3592.

Noble, D. C., 1975, Geological history and geothermal potential of the Leach Hot Springs Area, Pershing County, Nevada: a preliminary report to the Lawrence Berkeley Laboratory.

Parker, R. L., 1970, The inverse problem of electrical conductivity in the mantle: Geophys. J. R. astr. Soc., v.22, p. 121-138.

Risk, G. F., 1975, Monitoring the Boundary of the Broadlands Geothermal Field, New Zealand: Proceedings: Second U.N. Symposium on the Development and use of Geothermal Resources, May 1975, p. 1185-1190.

Ryu, J., Morrison, H. F., and Ward, S. H., 1970, Electromagnetic fields about a loop source of current: Geophysics, v.35, p. 862-896.

Sass, J. H., Lachenbruch, A. H., Muroe, R. J., Greene, G. W. and Moses, T. H., 1971, Heat flow in the Western United States: J. G. R., v. 67, p. 6376-6413.

Spencer, J. W., Jr., and Nur, A. M., 1976, The effects of pressure, temperature, and pore water on velocities in westerly granite: Jour. Geophys. Reasearch, v.81, p. 899-904.

Vozoff, K., and Jupp, D. L. B., 1975, Joint inversion of geophysical data: Geophys. J. R. astr. Soc. v.42, p. 977-991.

Wait, J. R., 1962, Electromagnetic Waves in Stratified Media: Pergamon Press, New York.

Ward, S. H., 1977, A report on "Workshop on Electrical Methods in Geothermal Exploration": Geophysics, v.42, p. 664-666.

Whiteford, P. C., 1975, Assessment of the Audio-Magnetotelluric Method for Geothermal Resistivity Surveying: Proceedings: Second U.N. Symposium on the Development and use of Geothermal Resources, May 1975, p. 1255-1262.

Wu, F. T., 1968, The Inverse Problem of Magnetotelluric Sounding: Geophysics, v. 35, p. 972-979.

Zimmerman, J. E., and Campbell, W. H., 1975, Tests of cryogenic SQUID for Geomagnetic field measurements: Geophysics, v.40, p. 269-284.

APPENDIX - A

Magnetometer Calibration Results

The magnetic field detector used in this experimental survey was a 3-axis SQUID magnetometer (Develco Model 8230). It has a sensitivity of $10^{-5}\gamma/\sqrt{Hz}$ and a flat frequency response from D.C. to several KHz. To make measurements in the low frequency range, it was found necessary to provide a conducting shield around the magnetometer to cut down high frequency noise (sferics). The conducting shield was provided by an aluminum can(40 mil thick, 12" in diameter and 18" in height with open ends) enclosing the sensors of the magnetometer.

Theoretically, the effect of such a shield on the magnetometer response would be similar to that of placing a single pole low pass RC filter in series with the magnetometer input. To evaluate the actual response of such a shield on the magnetometer and also to find the absolute conversion factor for each of the magnetometer outputs, a calibration test was run in the field.

A small multiturned calibration coil (NA = 21.92 turn meter^2), placed 5 meters away from the shielded magnetometer, was used as a magnetic dipole source and measurements were made at several discrete frequencies in the frequency band of 10 Hz to 100 Hz. The current flowing in the calibration coil and the magnetometer outputs were carefully monitored with the Signal Averager which provided the necessary phase and amplitude information at each frequency.

The observed response of the shield was found to be in close

agreement with that of a low-pass RC filter. The phase and amplitude responses of a low-pass RC filter are given by

$$\theta(\omega) = -\tan^{-1}(\omega\tau)$$

and

$$A(\omega) = \frac{1}{\sqrt{1 + \omega^2 \tau^2}}$$

where ω is angular frequency and τ is RC time constant in seconds. By matching the observed response to that of low pass filter, time constant for the effect of the shield on each component was calculated. Thus by knowing τ, amplitude and phase correction can be easily calculated from the above formulae for any frequency. Figures A1 through A6 are plots of observed response (phase and amplitude) plotted along with that of RC filter with proper τ for each component. Absolute conversion factor and calculated τ along with cut-off frequency (F_c) are listed below for each component.

x-Axis

Absolute conversion factor = 20.85γ/volt (error < .5%)

τ = .00123 seconds

F_c = 129.6 Hz

y-Axis

Absolute conversion factor = 21.08γ/volt (error < .5%)

τ = .0010 seconds

F_c = 144.7 Hz

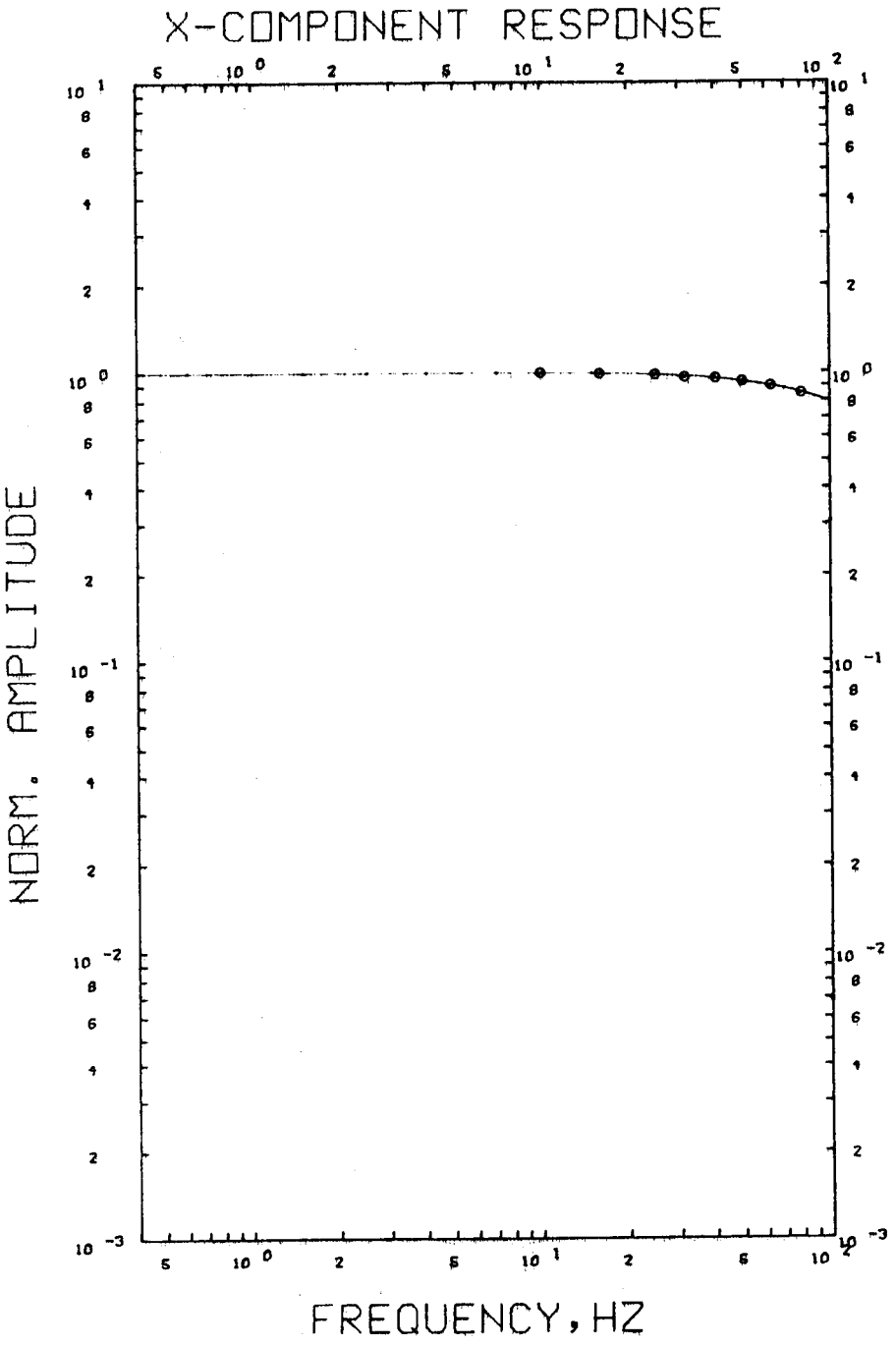

Figure A1. Amplitude response of x-component of the shielded magnetometer.

XBL 784-8034

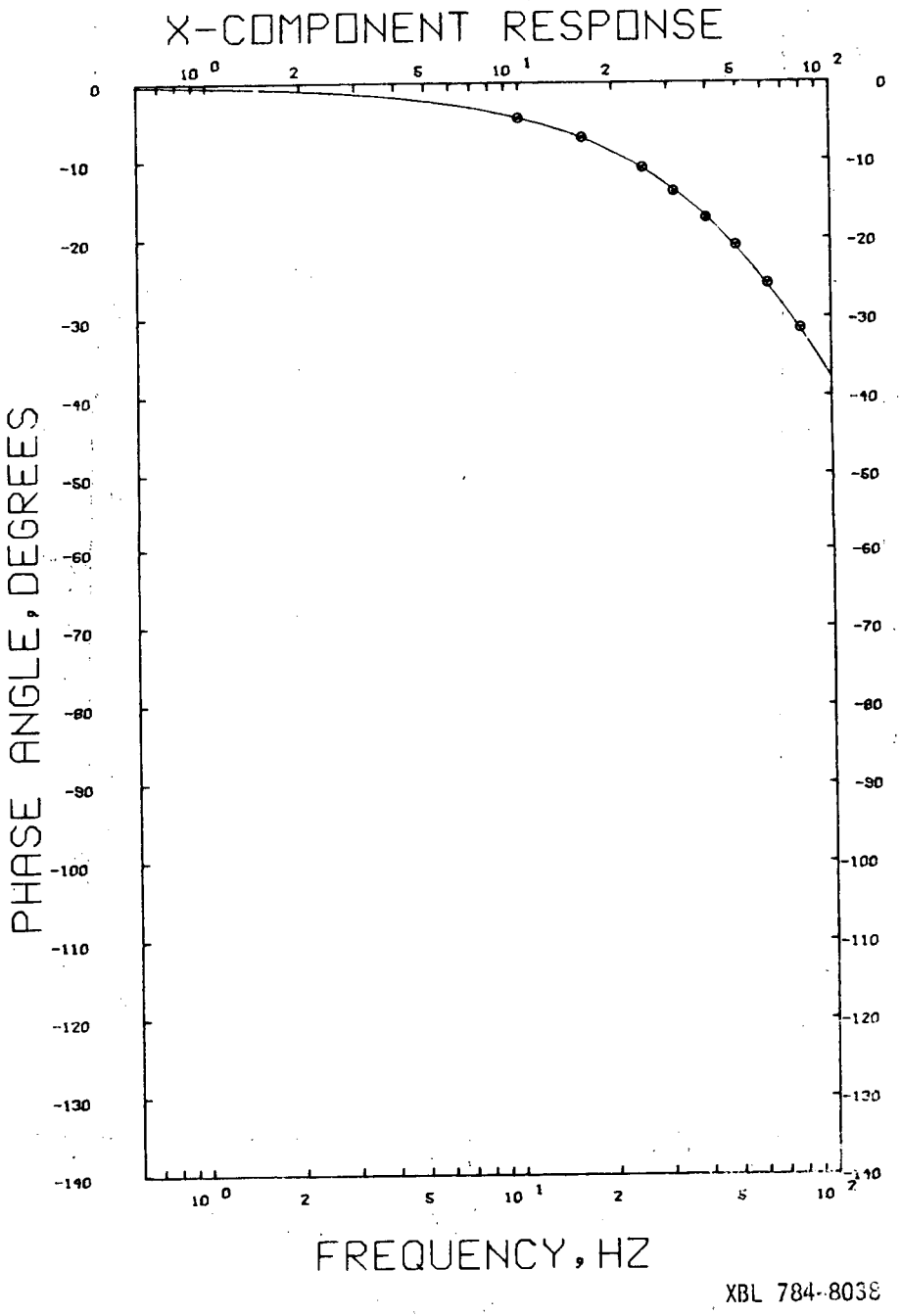

Figure A2. Phase response of x-component of the shielded magnetometer.

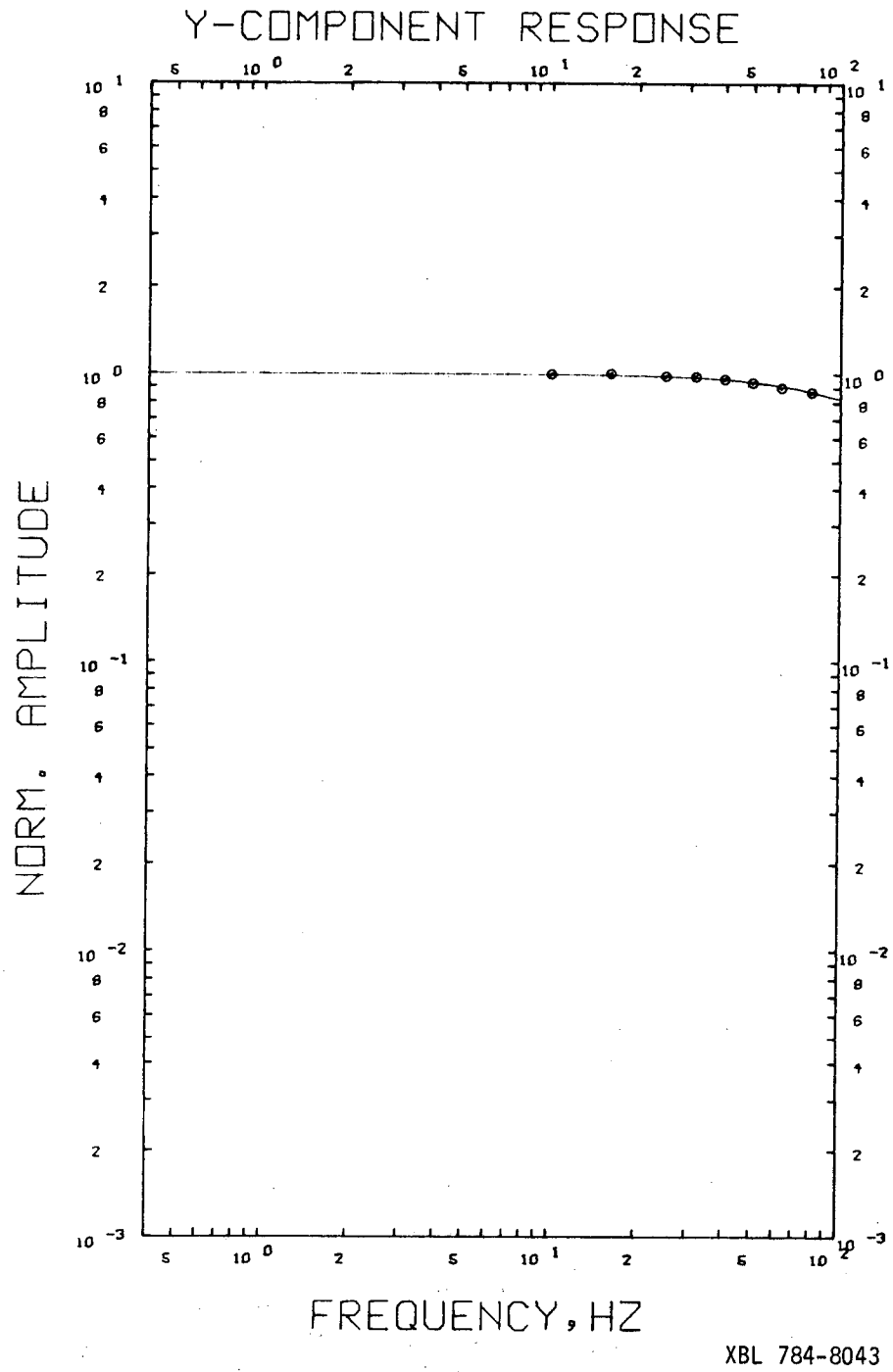

Figure A3. Amplitude response of y-component of the shielded magnetometer.

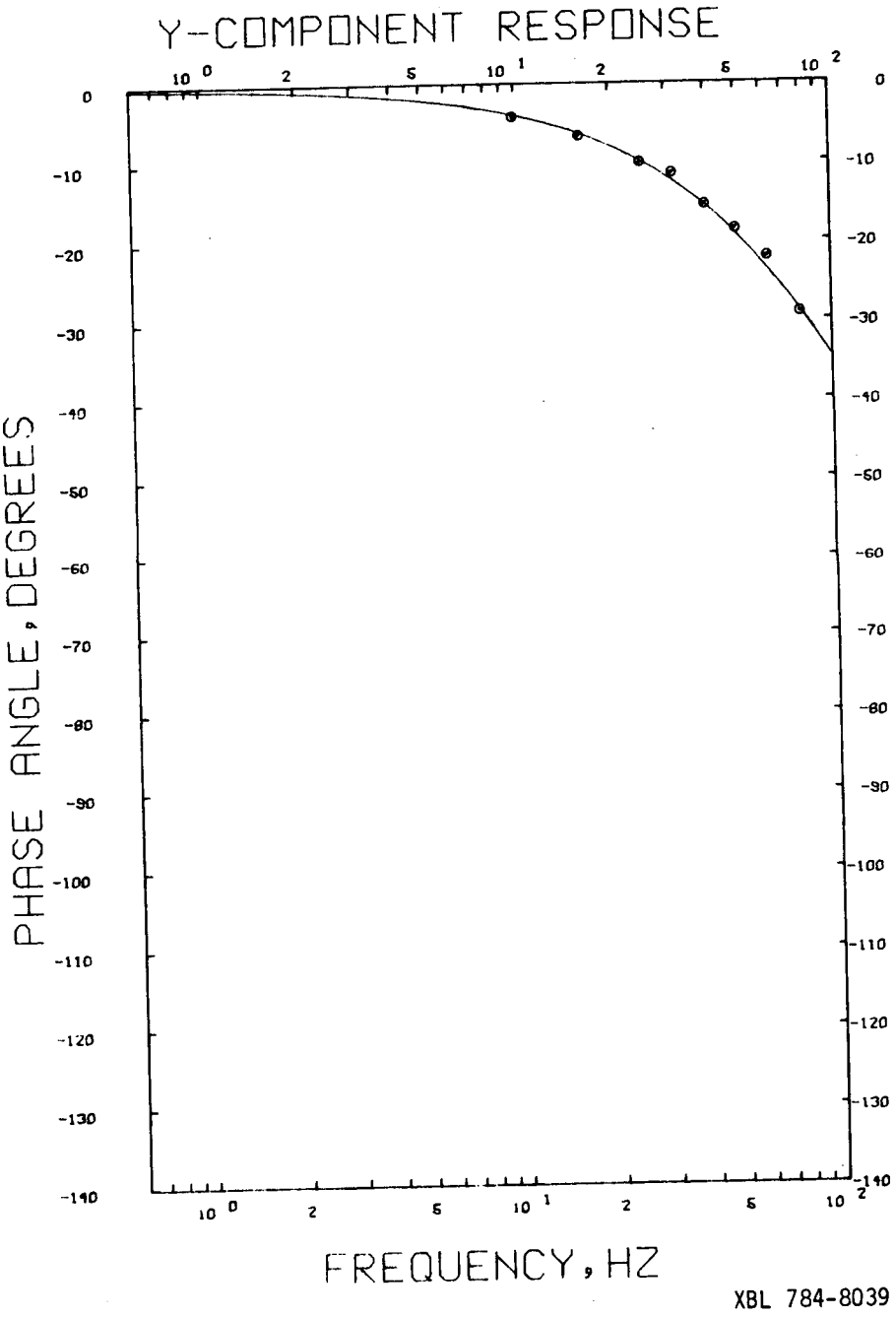

Figure A4. Phase response of y-component of the shielded magnetometer.

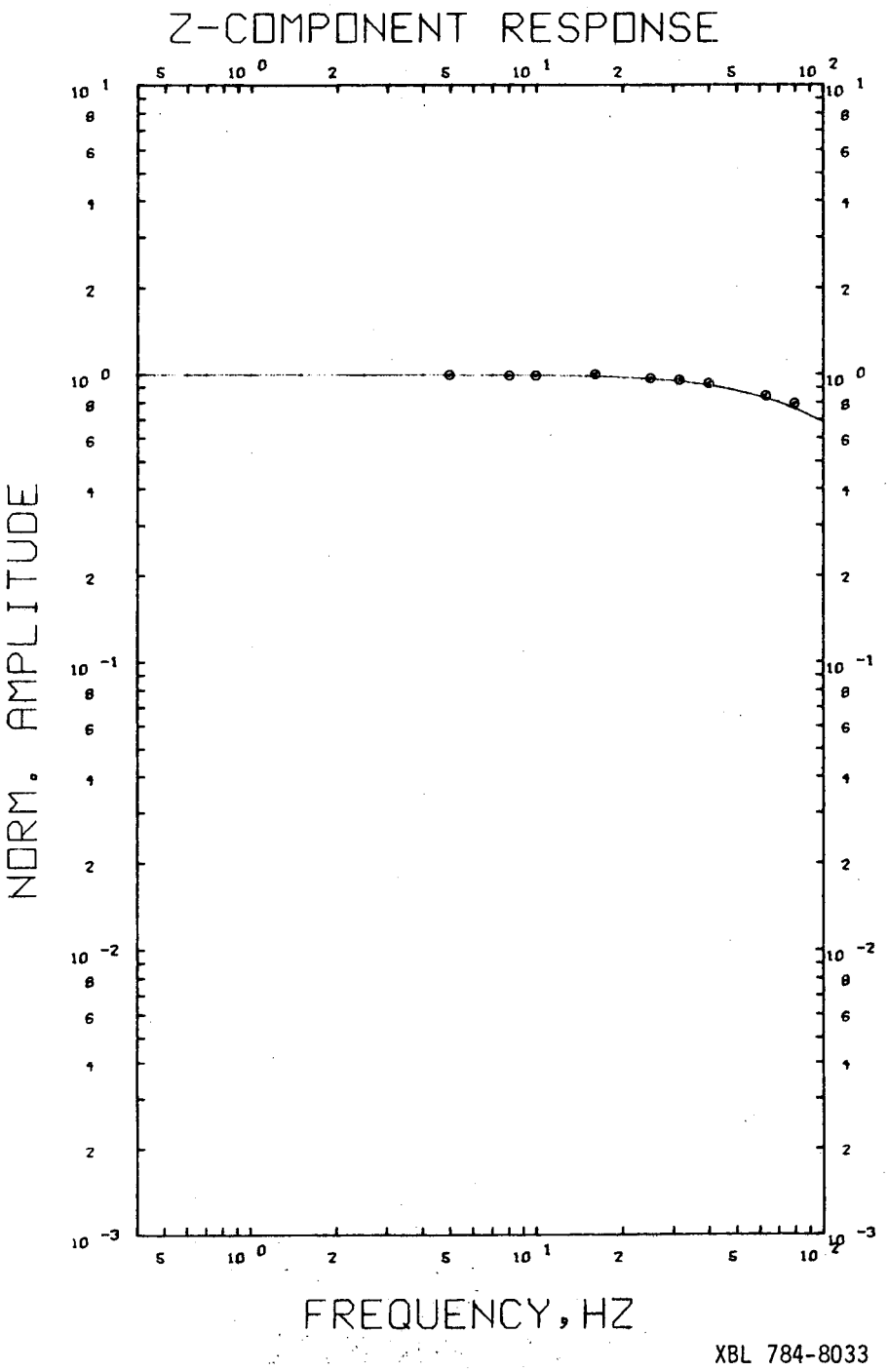

Figure A5. Amplitude response of z-component of the shielded magnetometer.

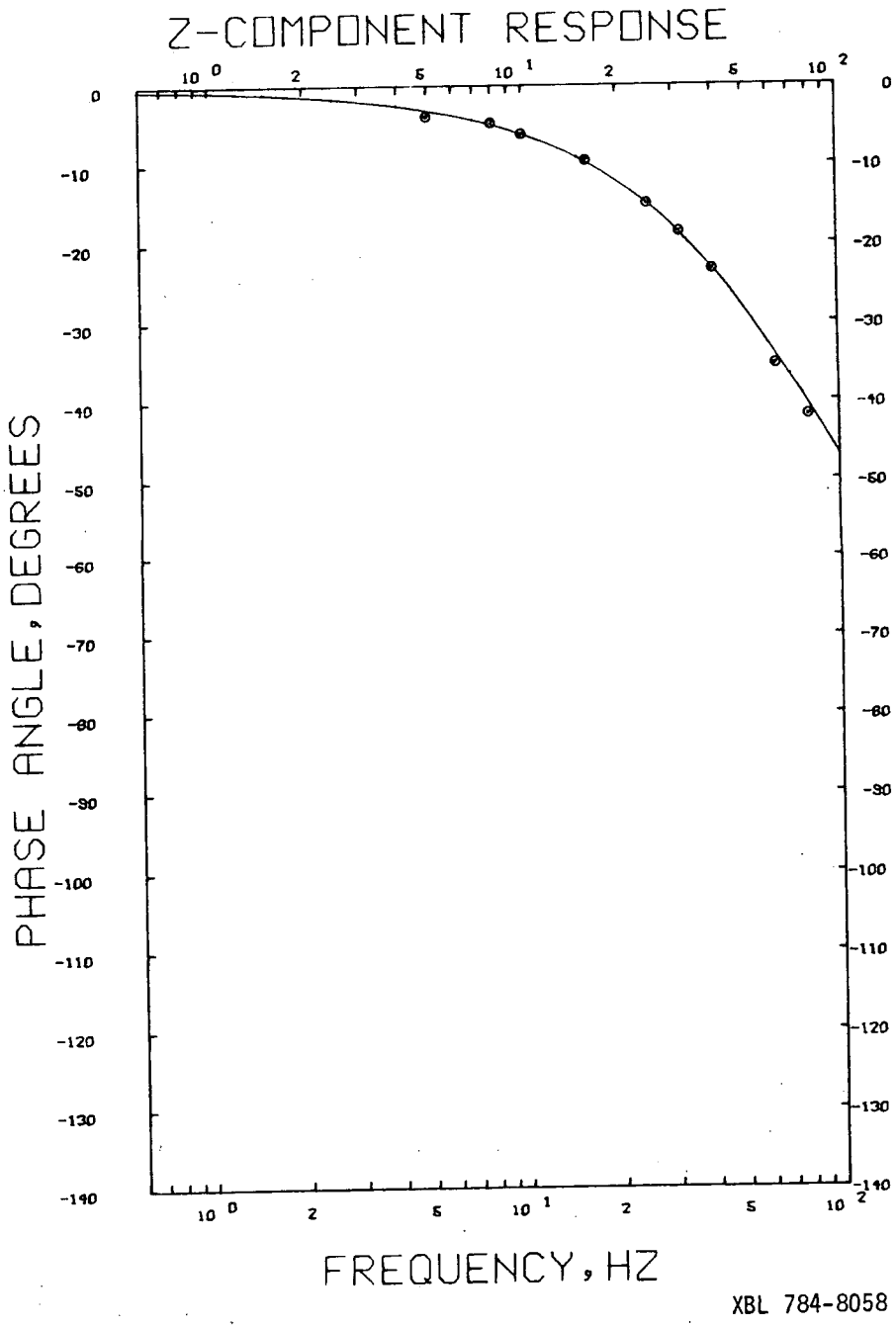

Figure A6. Phase response of z-component of the shielded magnetometer.

z-Axis

Absolute conversion factor = 22.20γ/volt (error < .5%)

τ = .0017 seconds

F_c = 93.6 Hz

APPENDIX - B

GRASS VALLEY SOUNDING DATA

T3-R2 Sounding Data

Frequency (Hz)	Normalized Field		Phase in Degrees	
	H_r	H_z	H_r	H_z
80.0	0.94±1.5%	-	161.0±1.1	-
50.0	1.06±1.0%	0.57±1.5%	169.0±0.7	137.2±1.7
31.6	1.12±2.0%	0.84±1.0%	179.2±0.4	143.2±0.4
16.0	1.11±1.0%	1.13±1.0%	196.0±0.4	156.6±0.4
6.3	0.80±1.0%	1.29±1.0%	216.1±0.6	171.8±0.4
2.5	0.47±3.0%	1.29±1.0%	231.1±1.1	180.1±0.9
1.0	0.30±10.%	1.20±1.5%	243.5±9.7	184.1±1.1
0.63	0.19±24.%	1.16±1.1%	249.0±14.	186.0±0.4
0.25	-	1.07±1.0%	-	182.8±0.4
0.10	-	1.00±0.9%	-	181.9±0.4
0.02	-	1.00±1.8%	-	180.0±1.0

T3-R3' Sounding Data

Frequency (Hz)	Normalized Field		Phase in Degrees	
	H_r	H_z	H_r	H_z
63.0	0.94±1.5%	0.50±1.0%	165.4±0.4	118.1±0.4
40.0	1.07±1.0%	0.75±1.0%	171.7±0.4	131.9±0.5
25.0	1.15±1.0%	0.97±1.0%	183.8±0.4	142.1±0.4
12.5	1.07±1.0%	1.19±1.0%	200.0±0.4	157.0±0.4
6.3	0.85±1.0%	1.30±1.1%	215.1±0.4	168.7±0.4
4.0	0.66±1.0%	1.29±1.0%	223.5±0.4	175.0±0.4
2.5	0.53±1.0%	1.29±1.2%	230.3±0.5	178.8±0.4
1.0	0.32±8.0%	1.22±1.0%	242.7±1.7	185.0±0.5
0.5	-	1.15±1.0%	-	186.0±0.6
0.25	-	1.06±1.0%	-	184.6±0.9
0.10	-	1.0 ±1.1%	-	181.7±0.5
0.02	-	1.0 ±1.0%	-	180.4±0.5

T3-R4 Sounding Data

Frequency (Hz)	Normalized Field		Phase in Degrees	
	H_r	H_z	H_r	H_z
63.0	1.00±1.2%	0.60±2.5%	158.4±0.4	111.1±0.9
40.0	1.13±1.0%	0.79±1.0%	170.5±0.4	125.1±0.5
25.0	1.18±1.0%	0.99±1.0%	182.9±0.4	138.7±0.4
12.5	1.06±1.0%	1.21±1.0%	201.4±0.4	156.8±0.4
6.3	0.81±1.0%	1.27±1.0%	216.5±0.4	170.6±1.2
4.0	0.63±1.7%	1.27±1.2%	224.4±1.1	175.5±0.4
2.5	-	1.25±1.1%	-	179.4±0.4
1.0	0.28±13.%	1.19±1.0%	240.8±4.9	184.3±0.4
0.5	0.19±15.%	1.11±1.0%	255.0±10.	186.2±0.5
0.25	-	1.03±1.5%	-	184.8±0.5
0.10	-	1.06±10.%	-	182.2±6.5
0.03	-	1.00±2.0%	-	180.2±1.6
0.02	-	1.00±2.5%	-	180.0±2.0
0.01	-	1.00±4.0%	-	181.0±1.6

T7-R6 Sounding Data

Frequency (Hz)	Normalized Field		Phase in Degrees	
	H_r	H_z	H_r	H_z
63.0	0.97±1.0%	0.74±2.0%	160.6±0.4	108.5±1.0
40.0	1.11±1.0%	1.01±5.0%	178.5±0.4	135.0±2.5
25.0	1.09±1.0%	1.08±1.0%	190.9±0.4	146.0±0.4
12.5	0.91±1.0%	1.22±1.0%	204.2±0.4	161.0±0.4
6.3	0.71±1.0%	1.26±1.0%	213.0±0.4	172.4±0.4
4.0	0.60±1.0%	1.28±1.0%	218.4±0.4	176.7±0.4
2.5	0.49±1.0%	1.27±1.0%	225.1±0.4	180.4±0.4
1.0	0.28±1.0%	1.17±1.0%	245.1±0.4	185.8±0.4
0.5	0.16±3.5%	1.09±1.0%	258.3±1.9	186.3±0.4
0.25	0.09±20.%	1.03±1.0%	266.3±4.4	185.1±0.4
0.10	-	1.00±1.0%	-	182.7±0.5

T7-R8 Sounding Data

Frequency (Hz)	Normalized Field		Phase in Degrees	
	H_r	H_z	H_r	H_z
50.0	1.11±1.0%	0.70±1.0%	164.9±0.4	114.6±0.4
40.0	1.12±1.1%	0.82±1.0%	171.2±0.4	118.8±0.4
25.0	1.12±0.9%	1.03±1.0%	185.0±0.4	138.5±0.4
12.5	0.95±1.0%	1.19±1.0%	200.6±0.5	158.0±0.4
6.3	0.76±1.1%	1.26±1.2%	210.0±0.5	169.5±0.4
4.0	0.66±0.9%	1.27±1.0%	216.2±0.4	175.0±0.4
2.5	0.54±1.0%	1.27±1.1%	224.3±0.4	179.6±0.4
1.0	0.31±1.5%	1.19±1.2%	240.2±0.8	185.0±0.4
0.5	0.17±1.0%	1.13±1.0%	250.0±1.0	185.2±0.4
0.25	0.10±20.%	1.07±1.2%	253.8±6.8	183.8±0.8
0.10	-	0.97±1.4%	-	181.5±0.8

T3-R5 Sounding Data

Frequency (Hz)	Normalized Field		Phase in Degrees	
	H_r	H_z	H_r	H_z
25.0	-	0.40±1.4%	-	92.4±0.7
12.5	0.96±2.0%	0.60±2.0%	156.5±1.3	105.3±1.2
6.3	1.01±8.0%	0.89±1.0%	172.9±3.7	130.2±0.5
4.0	1.08±2.0%	1.06±1.0%	181.9±0.7	146.5±0.5
2.5	1.07±2.5%	1.13±0.9%	190.2±0.6	156.0±0.5
1.0	0.94±3.0%	1.25±1.0%	208.3±1.0	172.1±0.5
0.5	0.69±4.0%	1.24±4.0%	229.0±0.9	181.4±2.8
0.25	0.45±13.%	1.16±1.0%	248.6±6.0	183.5±3.5
0.1	-	1.13±7.0%	-	184.2±2.7

T7-R5 Sounding Data

Frequency (Hz)	Normalized Field		Phase in Degrees	
	H_r	H_z	H_r	H_z
40.0	0.50±2.0%	-	129.2±3.1	-
25.0	0.68±1.0%	0.24±2.0%	141.1±0.5	87.9±1.2
12.5	0.84±1.0%	0.45±4.0%	155.1±0.4	113.9±1.0
6.3	1.00±1.0%	0.70±1.0%	170.0±0.7	136.4±0.5
4.0	1.03±1.0%	0.69±1.0%	178.0±0.5	146.0±0.5
2.5	1.00±1.0%	0.85±1.5%	186.0±0.5	153.0±0.8
1.0	0.99±2.0%	1.15±1.0%	212.4±1.3	168.0±0.5
0.5	0.77±3.0%	1.25±1.0%	230.2±1.3	179.7±0.6
0.25	-	1.16±1.0%	-	183.8±0.5
0.10	-	1.11±5.0%	-	182.5±3.6

T7-R9' Sounding Data

Frequency (Hz)	Normalized Field		Phase in Degrees	
	H_r	H_z	H_r	H_z
40.0	-	0.31±3.3%	-	103.7±1.3
25.0	-	0.42±1.0%	-	114.7±0.5
12.5	0.94±1.0%	0.62±1.1%	170.9±0.6	135.5±0.6
6.3	0.95±1.1%	0.81±1.5%	181.0±0.5	146.6±1.0
4.0	1.01±1.0%	0.95±1.0%	188.5±0.5	152.5±0.6
2.5	1.02±3.0%	1.13±1.0%	199.5±0.6	159.3±0.5
1.0	0.78±4.0%	1.30±1.5%	222.6±5.0	174.5±0.5
0.5	0.48±8.0%	1.23±3.0%	244.3±1.0	180.9±2.0

This report was done with support from the Department of Energy. Any conclusions or opinions expressed in this report represent solely those of the author(s) and not necessarily those of The Regents of the University of California, the Lawrence Berkeley Laboratory or the Department of Energy.

TECHNICAL INFORMATION DEPARTMENT
LAWRENCE BERKELEY LABORATORY
UNIVERSITY OF CALIFORNIA
BERKELEY, CALIFORNIA 94720